

Methodical Approach for Analyzing Process Parameters and Optimizing Boundary Conditions in Multi-Axis Robot Programs

Methodischer Ansatz zur Analyse von Prozessparametern und Optimierung von Randbedingungen in Multi-Achs-Roboterprogrammen

Scientific work for obtaining the academic degree

Master of Science (M.Sc.)

at the TUM School of Engineering and Design of the Technical University of Munich

| | |
|----------------------|---|
| Supervised by | Prof. Dr.-Ing. Michael Zäh Institute for Machine Tools and Industrial Management (iwb) |
| Submitted by | Jan Nalivaika Lerchenauerstrasse 10 80809 Munich |
| Submitted on | March 15, 2024 in Garching |

Acknowledgment

I would like to take this opportunity to express my heartfelt appreciation to my two supervisors, Marius Breuer and Ludwig Siebert, for their exceptional guidance and unwavering support throughout the entire duration of my master's thesis. Their expertise, dedication, and willingness to share their knowledge have been instrumental in shaping the direction and quality of this research. Their valuable insights and constructive feedback have significantly contributed to the development of this work. I am truly grateful for their availability, as they were always approachable and ready to assist whenever I encountered challenges or needed clarification. Their prompt response and timely feedback were incredibly valuable in ensuring the smooth progress of this thesis. I am deeply thankful for their remarkable contributions and for being outstanding mentors throughout this journey.

Scope of Work

Title of the Master's Thesis:

Methodical Approach for Analyzing Process Parameters and Optimizing Boundary Conditions in Multi-Axis Robot Programs

Titel der Master's Thesis:

Methodischer Ansatz zur Analyse von Prozessparametern und Optimierung von Randbedingungen in Multi-Achs-Roboterprogrammen

Author: Jan Nalivaika

Issue: 02.10.2023

Supervisor: Ludwig Siebert

Submission: 29.03.2024

Motivation:

Computer-aided manufacturing (CAM) is used to automatically generate tool paths for computer numerically controlled machines. The CAM software considers the models of the raw and finished parts, the constraints of the machine, the tools, and the manufacturing technology. Together with user-configurable parameters, tool paths for 3-axis, 5-axis, and robot-based machine tools are generated. The growing demand for flexibility in machine tools, such as the use of multiple manufacturing technologies in one machine or automated loading and unloading, has led to many machine tools being equipped with additional mechanical axes. Examples include robots mounted on linear axes and rotary-tilt tables. The tool paths created in CAM programs are usually defined by five degrees of freedom. The first three are the translational axes X, Y, and Z. The tilting and inclining of the tool are defined by the A- and B-axes. Occasionally, an additional rotation of the tool (C-axis) around the Z-axis (e.g., for dragging a swivel knife) is defined. Machines with more degrees of freedom than those limited by the toolpath often need user-defined constraints. These constraints are necessary to fully specify the movements of the machine axes. An example is the alignment of a part using the rotary-tilt table so that the Z-axis of the tool always points in the direction of gravity. This is helpful in processes like fused deposition modeling (FDM) and wire arc additive manufacturing (WAAM). It is common practice to set the user-defined constraints based on experience. The definition of these constraints does not affect the relative tool path generated by the CAM software. A preliminary literature review indicates that the configuration of

these degrees of freedom has an impact on the energy demand and stability of the process. As such, a methodical approach to optimize these constraints in terms of efficiency, speed, and energy demand of the machine is required. Currently, no literature provides a comprehensive analysis or methodology regarding this global optimization problem.

Objective:

This work aims to attain a methodical approach that analyzes a set of constraints and evaluates the influence of those constraints on a set of defined process variables. It will focus on a 6-axis robot with a rotary-tilt table, whereby the results should also be transferable to other machines. Furthermore, the experiments and validations will be limited to the manufacturing processes of WAAM and milling. First, the influence of the constraints on relevant process variables (energy demand, joint turnover, speed and acceleration peaks, and total joint movements) in a manufacturing process such as WAAM will be assessed. Subsequently, a process evaluation will be elaborated in the CAM software, by means of which the process quality can be determined. Depending on the respective process variables, approximation or machine learning methods will be investigated for the process evaluation. The process quality as a one-dimensional variable will be determined by weighting the process variables. Subsequently, a method for the optimization of the constraints will be elaborated. This task corresponds to an optimization problem in which the process quality will be maximized by selecting suitable constraints.

Procedure and working method:

The following work packages are conducted within this thesis:

- Literature research
- Familiarization with WAAM, milling machines, and CAM software
- Selection of suitable process parameters
- Elaboration of the proposed method in a suitable programming language
- Verification and validation of the elaborated method
- Documentation of the work

Agreement:

Through the supervision of B.Sc. Jan Nalivaika intellectual property of the *iwb* is incorporated in this work. Publication of the work or transfer to third parties requires the permission of the chair holder. I agree to the archiving of the work in the library of the *iwb*, which is only accessible to *iwb* staff, as inventory and in the digital student research project database of the *iwb* as a PDF document.

Garching, 29.03.2024 WHAT DATE GOES HERE ??

Prof. Dr.-Ing.
Michael F. Zäh

B.Sc.
Jan Nalivaika

Abstract

Place your abstract here.

Zusammenfassung

Hier könnte Ihre Kurzzusammenfassung stehen.

Contents

| | |
|---|-----------|
| List of Abbreviations | xi |
| 1 Introduction | 1 |
| 1.1 Motivation | 1 |
| 1.2 Problem Formulation | 2 |
| 1.3 Objective | 4 |
| 2 State of Science and Technology | 5 |
| 2.1 Manufacturing Technologies | 5 |
| 2.1.1 Subtractive Manufacturing | 5 |
| 2.1.2 Additive Manufacturing | 9 |
| 2.1.3 Industrial Robots | 13 |
| 2.2 Computer-Aided Manufacturing | 21 |
| 2.2.1 CAM Software | 21 |
| 2.2.2 Path Planning | 22 |
| 2.3 Optimization Algorithms | 23 |
| 2.4 Comparison of the State of the Art | 25 |
| 2.4.1 Singularity avoidance | 25 |
| 2.4.2 Optimization of Joint Accelerations and Jerk | 27 |
| 2.4.3 Optimization of Stiffness | 27 |
| 2.4.4 Optimization of Energy use | 28 |
| 2.4.5 Summary | 29 |
| 3 Methodology | 31 |
| 3.1 Introduction | 31 |
| 3.2 General Methodology for Process Analysis and Evaluation | 31 |
| 3.2.1 General Methodology | 31 |
| 3.2.2 Process Parameters | 33 |
| 3.3 User-Defined Weights and Score Calculation | 37 |
| 3.3.1 Local Rating and Global Score | 37 |
| 3.3.2 Local Rating Calculation | 38 |
| 3.3.3 Information Extraction from Time-Series Data | 39 |
| 3.4 Information from Angular Position | 40 |
| 3.4.1 Total Joint Travel and Direction Changes | 41 |

| | | |
|----------|---|-----------|
| 3.4.2 | Rotation Limits | 43 |
| 3.4.3 | Velocity, Acceleration and Jerk of the Joints | 44 |
| 3.5 | TCP Coordinates, Velocity and Acceleration | 46 |
| 3.6 | Energy Usage | 47 |
| 3.6.1 | Continuous Energy-Usage | 48 |
| 3.6.2 | Total Energy-Usage | 50 |
| 3.7 | Reach, Singularities and Torch Orientation | 51 |
| 3.7.1 | Reach and Orientation | 51 |
| 3.7.2 | Singularities | 53 |
| 3.7.3 | Torch Orientation in WAAM | 53 |
| 3.8 | Summery for Boundary Condition Evaluation | 55 |
| 3.9 | General Methodology for Process Optimization | 57 |
| 3.9.1 | Optimization Loop without CAM-software | 57 |
| 3.9.2 | Optimization Loop with CAM-software | 59 |
| 4 | Implementation and Validation | 61 |
| 4.1 | Simple Implementation | 61 |
| 4.1.1 | Modeling a 6-DoF robot | 61 |
| 4.1.2 | Modeling a basic Toolpath | 63 |
| 4.1.3 | Extracting process parameters | 65 |
| 4.2 | Testing and Validation | 66 |
| 4.2.1 | Toolpath Evaluation with one Redundant DoF | 66 |
| 4.2.2 | Toolpath Evaluation with two Redundant DoF | 71 |
| 4.2.3 | Boundary Condition Optimization | 75 |
| 4.3 | Analysis and Discussion of the Results | 81 |
| 4.3.1 | Analysis of the Results | 81 |
| 4.3.2 | Discussion of the Results | 83 |
| 5 | Conclusion | 85 |
| 5.1 | Summary | 85 |
| 5.2 | Outlook | 87 |
| | Bibliography | 95 |

List of Abbreviations

| | |
|------|-----------------------------------|
| AI | Artificial Intelligence |
| AM | Additive Manufacturing |
| API | Application Programming Interface |
| CAE | Computer-Aided Engineering |
| CAM | Computer-Aided Manufacturing |
| CAD | Computer-Aided Design |
| CMT | Cold Metal Transfer |
| CNC | Computer Numerical Control |
| DED | Directed Energy Deposition |
| DH | Denavit-Hartenberg |
| DoF | Degrees of Freedom |
| ERP | Enterprise Resource Planning |
| FDM | Fused Deposition Modeling |
| GMAW | Gas Metal Arc Welding |
| ML | Machine Learning |
| PSO | Particle Swarm Optimization |
| RNN | Recurrent Neural Network |
| SLA | Stereolithography |
| SLM | Selective Laser Melting |
| TCP | Tool center point |
| TWA | Twist decomposition approach |
| WAAM | Wire Arc Additive Manufacturing |

Chapter 1

Introduction

1.1 Motivation

In the age of "Industrie 4.0", advanced technologies like digital twins, have greatly transformed industrial manufacturing [0]. A considerable amount of data can be gathered from various processes, like milling or 3D printing. By analyzing this data, it is possible to find new and optimized methods for efficient manufacturing [0]. By doing so, a significant amount of resources, like time and money, can be saved while at the same time increasing the quality of the produced product [0].

Computer-Aided Manufacturing (CAM) has been introduced as a crucial tool to improve productivity and accuracy in creating customized products [0]. CAM systems automate and optimize tasks such as machining, welding, and assembly [0]. One of the key strengths of CAM lies in its precision and consistency, ensuring that intricate components are produced with minimal error. Furthermore, CAM systems contribute to increased efficiency by minimizing material waste and reducing production time [0]. These capabilities play a significant role in achieving a carbon-neutral production process [0]. One of the most important areas of CAM is the calculation of the tool path for Computer Numerical Control (CNC) machines as well as the movement and behavior of multi-axis industrial robots [0].

Manufacturing machines are the backbone of modern industrial processes [0]. These machines encompass a wide range of equipment, from CNC machining centers to 3D printers and automated assembly lines. Their primary ability lies in precision (μm -scale) and efficiency [0]. CNC machines, for instance, can repeatedly produce intricate parts with high accuracy, reducing human error and ensuring consistency [0].

Industrial robots are a dominant part in the area of manufacturing as they can perform multi-axis movements. These capabilities are especially helpful to fulfill the customers wishes for individualized products [0]. They are cheaper to acquire and more flexible compared to CNC milling machines, but have their own set of disadvantages like for example lower stiffness [0]. One of the most important advantages is its wide adaptability. They allow for quick

reconfiguration to produce different components or products, promoting flexibility in manufacturing [0]. Further, advancements in robotics and Artificial Intelligence (AI) have broadened their capabilities, enabling tasks that were once deemed too complex or hazardous for humans [0].

For achieving better efficiency and continuous sustainability in the current fast-changing environment requires a thorough analysis of the interdependent relationships between the manufactured part, process parameters, and boundary conditions that govern multi-axis robot programs [0]. As the companies that work with industrial robots can place a strong emphasis on energy reduction, cycle-time minimization, or precision, optimizing these parameters is essential. CAM enables the simulation of the planned process, thus adapting any boundary conditions to fit the selected goals [0]. This thesis is focused on a methodical approach for analyzing process parameters and optimizing boundary conditions in multi-axis robot programs.

1.2 Problem Formulation

Manufacturing systems that incorporate redundant degrees of freedom (DoF) offer significant advantages in terms of flexibility and adaptability [0]. One example of a system with redundancy is a 6-DoF industrial robot with a rotary tilt table, which brings the system to eight DoF. However, these systems also present various conflict points that need to be carefully managed to ensure optimal performance [0].

One of the critical challenges in manufacturing systems with redundant DoF is singularity avoidance [0]. Singularities occur when the robot manipulator loses control or achieves limited mobility due to certain configurations [0]. These configurations result in the loss of a DoF or make the system highly sensitive to small changes, leading to unstable or unpredictable behavior [0]. Limiting the possible positions by adding artificial constraints can help to avoid this problem [0].

One significant aspect of manufacturing systems with redundant DoF is joint acceleration and jerk, which is the rate of change of acceleration. The robot must allocate accelerations effectively among its joints to achieve smooth and coordinated motion. Failure to do so can result in jerky or erratic movements, which not only compromise precision but also impact the efficiency of the manufacturing process [0]. Rapid changes in acceleration and jerk can cause mechanical stress, decrease system lifespan, and compromise precision. Additionally, the joints can be limited in their ability to keep up with the required speed due to limitations in power [0]. Therefore, advanced control algorithms and motion planning techniques are necessary to optimize joint motion and minimize conflicts in joint acceleration and jerk [0].

Extension control is another critical aspect that needs to be addressed in systems with redundant DoF. Redundant DoF can provide additional extension capabilities to industrial robots, allowing them to reach difficult-to-access areas [0]. However, managing and controlling the extension can be challenging, particularly when precise positioning or maintaining stability is required [0]. The robot must accurately determine the appropriate position for each joint to avoid unnecessary overextension and collisions with the surrounding environment. The robot pose, which is the combination of position and orientation in three-dimensional space, also has a significant effect on robot stiffness [0]. An increased number of joints can introduce more play and reduce overall system stiffness. This can affect precision, accuracy and stability. Robot pose and its DoF must be carefully considered to ensure the desired level of system rigidity [0].

Precision is a crucial element in manufacturing systems, closely tied to its stiffness. The robot needs to have precise control over the movement of each joint to achieve the desired accuracy of position in the manufacturing process. Nevertheless, achieving and maintaining high accuracy and repeatability can be difficult due to the increased complexity and sensitivity to various factors [0]. Frequent changes in direction in the joints are another factor that affects precision. Due to the serial kinematics of industrial robots, the present play in the motor joints can add up the inaccuracies and impede the manufacturing process [0]. Mechanical stress, decreased precision, and increased energy consumption can result from abrupt and frequent direction changes [0].

Furthermore, effectively coordinating the movement of multiple joints to execute rapid direction changes can prove to be a difficult and computationally intensive task [0]. Poor direction changes can result in prolonged and unnecessary movement times, ultimately hampering the overall productivity of the manufacturing process [0]. Minimizing production time is crucial for improving efficiency and throughput. Optimal path planning, motion optimization, and parallel processing techniques can be employed to reduce non-value adding movements while leveraging redundant DoF effectively [0].

Energy use is also a significant concern in manufacturing systems employing redundant DoF [0]. The presence of additional joints and their non-optimal usage can require more power to operate, potentially leading to increased energy consumption. As energy efficiency becomes a priority in modern manufacturing, efficient energy management strategies are necessary to mitigate the increased power demand [0].

While redundant DoF may introduce potential conflicts and require special attention, they can also significantly enhance performance in manufacturing systems [0]. The added DoFs increase flexibility and adaptability, enabling the robot to carry out complex tasks more efficiently. Redundancy enables multiple approaches to achieve a desired end-effector position or orientation. By effectively utilizing the surplus of DoF, manufacturing systems can enhance their performance, increase efficiency, and exhibit greater flexibility in handling diverse tasks [0].

Currently, there is no integrated system that can evaluate a computed tool path based on the chosen objective, such as minimizing movement or maximizing stiffness. Additionally, there is no option to provide an optimal or near-optimal solution for defining the necessary constraints for a specific goal like for example, minimizing energy usage while at the same time reducing joint accelerations.

1.3 Objective

The definition of the redundant constraints, mentioned in chapter 1.2, does not affect the relative tool path as generated by the CAM software. As such, a methodical approach to optimize these constraints without altering the toolpath in terms of efficiency, speed, and energy demand of the machine is required. Currently, no literature provides a comprehensive analysis or methodology regarding this global optimization problem. This work aims to attain a methodical approach that analyzes a set of constraints and evaluates the influence of those constraints on a set of defined process variables. This work is focused on a 6-axis robot with a rotary-tilt table, whereby the results should also be transferable to other machines. Furthermore, the experiments and validations will be limited to the manufacturing processes of Wire Arc Additive Manufacturing (WAAM) and milling.

First, the influence of the constraints on relevant process variables (energy demand, joint turnover, speed and acceleration peaks, total joint movements) in a manufacturing process such as WAAM will be assessed. Subsequently, a process evaluation will be elaborated, by means of which the process quality can be determined. Depending on the respective process variables, approximation methods or machine learning methods will be investigated for the process evaluation. The process quality as a one-dimensional variable will be determined by weighting the process variables. Subsequently, a method for the optimization of the constraints will be elaborated. This task corresponds to an optimization problem in which the process quality will be maximized by selecting suitable constraints.

Chapter 2

State of Science and Technology

The following chapter gives an overview of manufacturing technologies, CAM, and algorithms for optimization problems. Special attention is given to the comparison of optimization problems in manufacturing with redundant degrees of freedom.

2.1 Manufacturing Technologies

Manufacturing technologies encompass a wide range of processes that are used to transform raw materials into finished products. Two major categories within this field are subtractive and additive manufacturing AM [0]. Subtractive manufacturing involves removing material from a workpiece to shape it into the desired form [0]. On the other hand, additive manufacturing, also known as 3D printing, typically involves building up layers of material to create an object. This process offers greater design flexibility and the ability to create complex geometries [0]. Both subtractive and additive manufacturing play crucial roles in various industries, revolutionizing production methods and offering new possibilities for customization and innovation [0].

2.1.1 Subtractive Manufacturing

Subtractive manufacturing, also referred to as subtractive fabrication or machining, is a precise and efficient method utilized in contemporary manufacturing processes [0]. This approach entails the removal of material from a workpiece, resulting in the formation of a desired shape or product [0]. In contrast to additive manufacturing techniques, subtractive manufacturing always relies on material that is removed [0].

Subtractive manufacturing involves various techniques such as milling, turning, drilling, and grinding that are mostly performed by using CNC machines [0]. Such machines are programmed to precisely control the cutting tool movement to clear material from the workpiece based on a predetermined design [0].

The versatility and precision of subtractive manufacturing are two of its significant advantages. A CNC machine can process a diverse array of materials, such as metals, plastics, and composites, with high levels of precision and surface quality, allowing for the creation of intricate and complex components [0]. As a result, it finds applications in industries where precision and quality are critical, such as aerospace, automotive, and medical.

The process of subtractive manufacturing starts with the drafting of the intended component using Computer-Aided Design (CAM) software. Subsequently, CAM software is used to generate instructions that are used to guide the CNC machine (see chapter 2.2 for more details). The machining process begins with the machine operator setting up and securing the work-piece in the machine and starting the execution of the generated instructions [0]. The cutting tools then perform various operations, such as drilling holes, creating pockets or slots, and shaping the external contours of the part, by following the predetermined movements. In a typical 3-axis machine, the degrees of freedom are along the X, Y, and Z axes. In a 5-axis machine, two additional degrees of freedom in form of rotations are present. Additionally, recent research is trying to extend the machines possibilities by adding advanced abilities like constantly monitoring and adjusting the cutting parameters on the fly to ensure the most efficient cutting speed, feed rate, and tool engagement while minimizing errors [0].

Subtractive manufacturing provides numerous advantages over alternative manufacturing techniques. This method allows for the creation of intricate and highly customizable components with tight tolerances and complex geometries [0]. In addition, it results in exceptional surface finish, dimensional accuracy, and consistency, guaranteeing uniform quality across production runs. Moreover, it is cost-effective for small to medium production volumes as it does not necessitate the use of costly molds or part-specific tooling, which makes it a great alternative to produce a multitude of parts [0].

One of the disadvantages of the process is the possibly long cycle time. Particularly for intricate and large-volume designs, the process can result in significant material waste [0]. Furthermore, it may not be appropriate for high hardness or brittle materials, which can lead to excessive tool wear or breakage [0].

Another common issue in CNC machining is tool vibration. Tool vibration, also called chatter, refers to the unwanted oscillation or movement of the cutting tool during the machining operation [0]. This phenomenon can have detrimental effects on the quality of the finished part and can lead to various problems, such as poor surface finish, reduced dimensional accuracy, increased tool wear, and even tool breakage [0]. Several factors contribute to tool vibration in CNC machining. One of the primary factors is the cutting parameters, which include the cutting speed, feed rate, and depth of cut. When these parameters are not optimized, excessive cutting forces can be generated, causing the tool to vibrate. It is crucial to find the right balance between material removal rates and minimizing tool vibration to ensure optimal machining outcomes [0]. The tool holder and spindle system also influence tool vibration. A rigid and stable tool holder and spindle are necessary to minimize vibrations and maintain accuracy during machining [0]. Any play or misalignment in these components

can contribute to tool vibration. Thus, it is paramount to ensure stiffness for high-precision operations. Chapter 2.1.3 gives a more in-depth look regarding the stiffens in machining operations executed with industrial robots.

In summary, subtractive manufacturing offers a wide range of applications but should be carefully considered for each situation. CNC technology, in combination with subtractive manufacturing, has become indispensable across a variety of industries. Nonetheless, it is crucial to evaluate its restrictions and suitability for specific design needs and material characteristics.

Figure 2.1 shows the basic design of a CNC machine. In this design, the workpiece is placed on the worktable and secured using a vice to hold it in place. The worktable has the ability to move in two directions, namely the X and Y directions. This movement allows for precise positioning and maneuvering of the workpiece. On the other hand, the spindle, which is the rotating component responsible for cutting or shaping the workpiece, moves in the Z direction. This vertical movement of the spindle enables it to perform various machining operations at different depths.

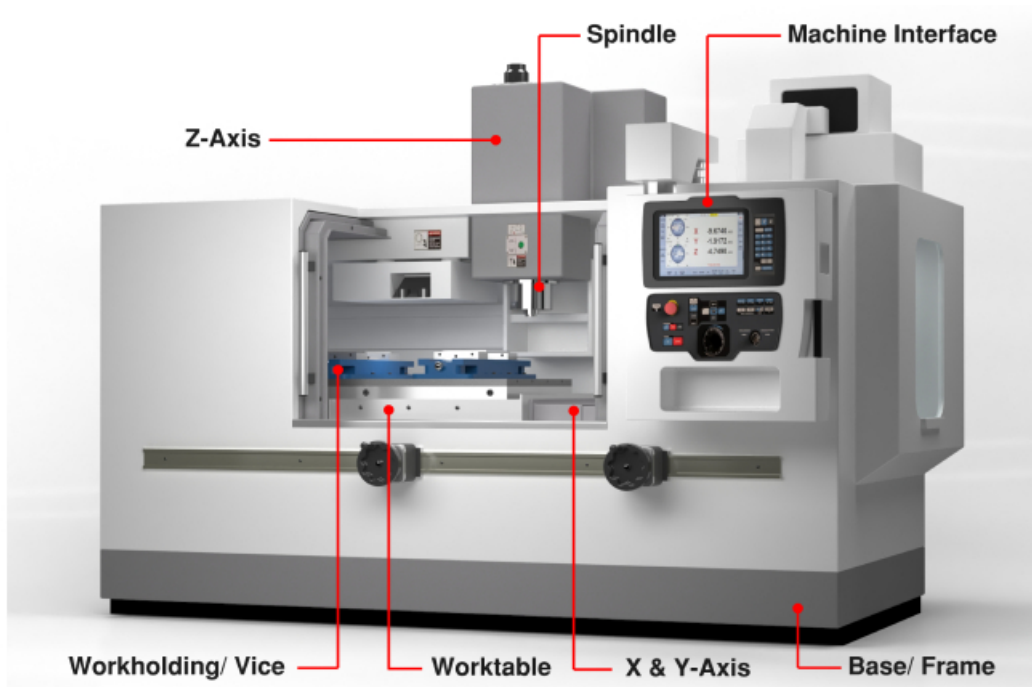


Figure 2.1: 3-Axis CNC Machine [0]

Additionally, the machine interface serves as the control panel for the CNC machine. It provides the user with options to select and load the desired CNC program. By selecting the appropriate program, operators can control the movements and actions of the CNC machine to achieve the desired part.

Figure 2.2 shows the schematic model of a 5-axis CNC machine. In this particular design, the spindle, which is responsible for cutting the workpiece, has the ability to move along three axes, namely the X, Y, and Z axes. This movement allows for precise control over the position and depth of the tool in relation to the workpiece.

In addition to the spindle movement, the machine features a rotary-tilt table that can adjust two additional axes, namely the A and B axes. These axes provide rotational and tilting capabilities to the worktable, allowing for more intricate movements and increased flexibility in part design. By adjusting the A and B axes, the workpiece can be positioned and oriented in different angles, enabling the CNC machine to access and machine complex geometries that would otherwise be difficult or impossible to achieve with fewer axes. The inclusion of these two additional degrees of freedom in the 5-axis CNC machine significantly expands the range of operations that can be performed. It enables the machine to handle more complex and sophisticated machining tasks, such as multi-sided machining, contouring, and simultaneous machining on multiple surfaces. This increased flexibility and versatility make the 5-axis CNC machine a valuable tool in industries that require high precision and intricate part production.

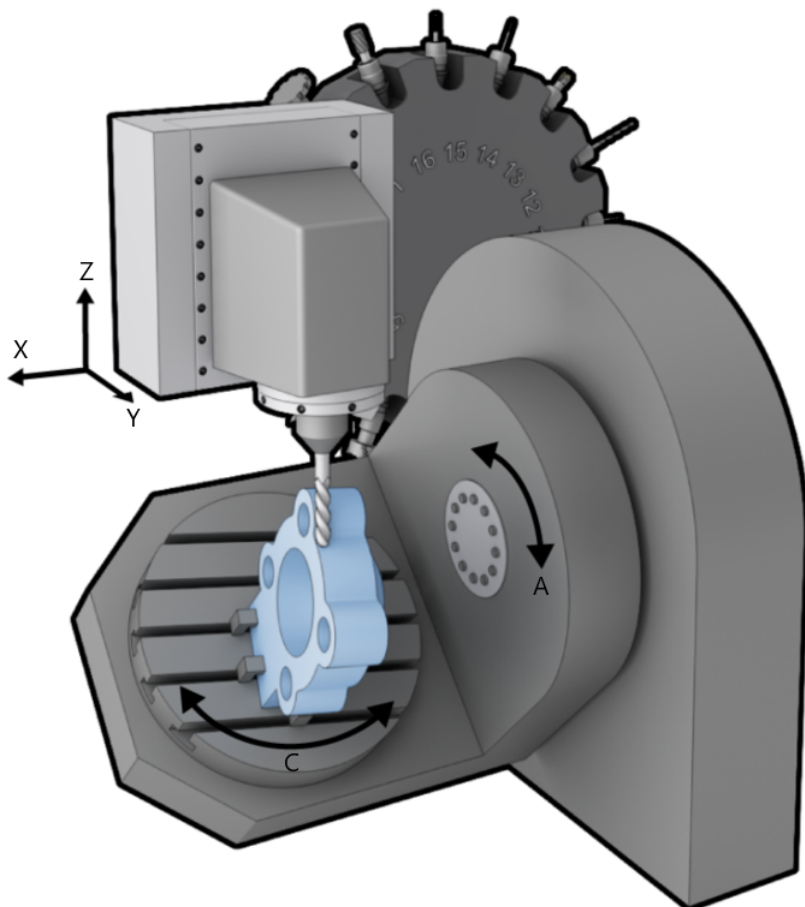


Figure 2.2: 5-Axis CNC Machine [0]

2.1.2 Additive Manufacturing

AM consists of the conversion of digital designs into physical objects by building them layer by layer. This layering approach offers the option for creating complex geometries that would be extremely challenging or impossible to produce using traditional manufacturing methods [0]. This advantage allows to fabricate intricate structures with internal cavities or undercuts, thus opening up new possibilities in engineering and design [0].

Various AM technologies utilize different methods to build the layers. Fused Deposition Modeling (FDM), for example, involves extruding molten thermoplastic filament through a heated nozzle, which solidifies as it cools, creating the desired shape [0]. Stereolithography (SLA) employs a liquid photopolymer resin that is solidified by a UV laser, while Selective Laser Melting (SLM) uses a high-power laser to selectively fuse powdered materials, such as plastics or metals [0].

The compatibility of AM with a wide range of materials is another significant advantage [0]. It enables the production of components with diverse properties, including strength, flexibility, conductivity, and heat resistance. AM can accommodate various plastics, such as ABS, PLA, and nylon, as well as metals like titanium, aluminum, and stainless steel. Additionally, ceramics and even biomaterials, like hydrogels or living cells, can be used in AM processes. New materials specifically tailored for AM are continuously developed, expanding the possibilities for unique applications [0].

The design freedom offered by AM is a significant selection criterion when choosing a manufacturing method. Traditional methods often have design constraints due to limitations in tooling and manufacturing processes. With AM, designers have greater flexibility to create complex and organic shapes, lightweight structures, and intricate internal features. This freedom leads to optimized performance and improved functionality [0].

However, AM also poses scientific challenges. Post-processing requirements, such as smoothing, polishing, or heat treatment, may be necessary to achieve the desired surface finish or material properties [0]. Additionally, certain applications may have limited material options, particularly in terms of high-temperature or high-strength applications. Production speed can also be a constraint for large or complex parts, as AM processes can be time-consuming compared to traditional manufacturing methods [0].

As AM technologies continue to advance, they have the potential to transform supply chains. The concept of distributed manufacturing, where products are produced closer to the point of use, becomes feasible with AM [0]. This reduces transportation costs, lowers carbon emissions, and enables on-demand manufacturing, leading to shorter lead times and increased sustainability [0].

Wire Arc Additive Manufacturing

WAAM is a specific type of additive manufacturing process which is part of Directed Energy Deposition (DED) processes [0]. According to the DIN EN ISO 52900 standard, DED involves using focused thermal energy to melt material during the application process to build up the individual layers [0].

The operating principle of WAAM involves the generation of an arc through electrical discharge between an feed-wire and the workpiece. This arc transfers energy to the workpiece, causing melting in the fusion zone [0]. Additionally, if a welding filler material in the form of a wire is introduced into the arc, it also melts and can be used to deposit additional material onto a metallic substrate [0]. To ensure a continuous weld seam, a wire feed system must be employed [0]. By placing multiple weld seams over each other, the workpiece is formed layer by layer.

The industrial manufacturing of components using WAAM involves a kinematic system that allows movement of the welding torch. This can be achieved using robot-configurations or gantry systems [0]. Alternatively, a spatially fixed welding torch, combined with robotic kinematics or rotary-tilt table, can be used to move the component [0].

WAAM offers several advantages over other additive manufacturing techniques. One major advantage is its high deposition rate, which ranges up to 6 kg/h. This high deposition rate enables the construction of large components in a relatively short amount of time. Components can be produced within a single workday, providing a significant time advantage compared to techniques like SLM, which typically operate at around 0.1 kg/h and thus much slower deposition rates. [0]

Another advantage of WAAM is its capability to construct large components with almost no limitations on part size. The production volume is only constrained by the working range of the kinematics employed. For example, in the case of an articulated-arm robot, the range is defined by its maximum reach. This means that WAAM has the potential to create components of various sizes without compromising its effectiveness [0].

However, it is important to note that WAAM components may have some inherent defects. These include residual stresses and deformations that persist after the production process, as well as relatively low geometric precision and modest surface quality. These limitations should be taken into consideration when utilizing WAAM for manufacturing purposes. [0]

Figure 2.3 shows a schematic representation of the WAAM process. In this process, a wire is fed trough the Gas Metal Arc Welding (GMAW) torch to supply a continuous stream of material. The wire is then subjected to high heat generated by an electric arc. The wire is melted and then deposited onto a substrate plate. The substrate plate serves as the foundation or base on which the material is built. As the molten wire is deposited, it solidifies and fuses with the previous layers, gradually building up the desired 3D object.

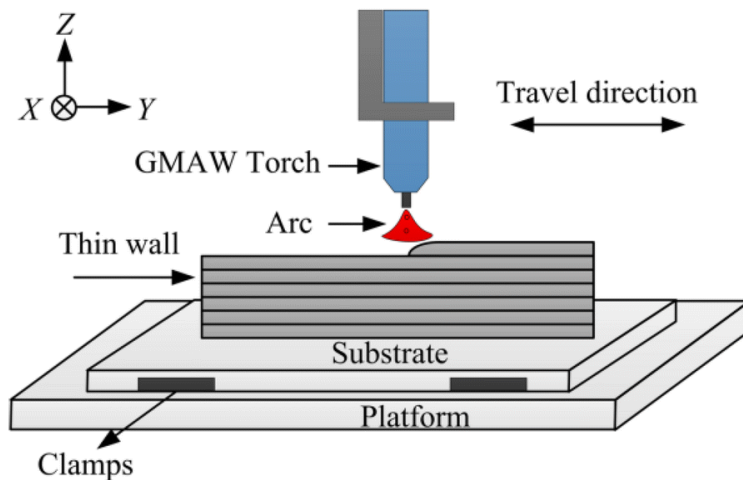


Figure 2.3: Schematic representation of WAAM [0]

Figure 2.4 shows a part produced by WAAM with the addition of a post processing step. The rough surface finish is clearly visible on the non post processed side of the part.

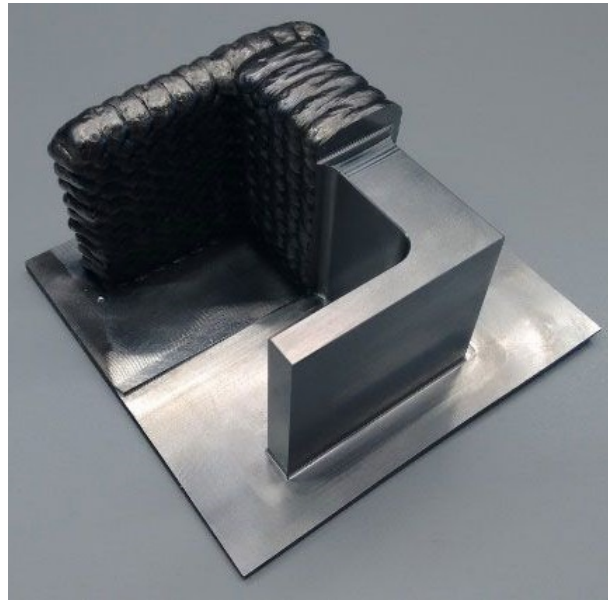


Figure 2.4: Part produced by WAAM with post machining [0]

Cold Metal Transfer

Cold Metal Transfer (CMT) welding is a sophisticated process that merges the advantages of multiple welding techniques [0]. It functions based on the principle of controlled short-circuiting, wherein the welding torch generates a short circuit between the wire and the workpiece. This short circuit triggers the melting of the tip of the wire and subsequent detachment. The detachment is assisted by a retraction of the wire. This process is generating a sequence of droplets that are transferred to the weld pool with high precision [0].

CMT welding provides superior heat control with lower heat input than conventional meth-

ods. The controlled arc and droplet transfer reduce the risk of overheating and distortion, making it suitable for thinner materials and heat-sensitive applications [0]. The process minimizes spatter formation, resulting in cleaner and smoother welds and reducing the requirement for post-weld cleaning [0]. CMT welding is ideal for applications that require the highest weld quality which includes structural fabrication and automotive manufacturing [0].

For dependable weld quality, CMT welding typically integrates advanced process control systems, which utilize adaptive control and real-time monitoring to consistently adjust welding parameters based on sensor feedback. This enhances the precision and dependability of the welding process [0].

A CMT cycle consists of three phases [0]:

1st - pulse phase: A high current pulse leads to the ignition of the arc, which melts the wire electrode. A droplet begins to form at the tip of the wire. The wire is moved forward in the direction of the workpiece.

2nd - arc phase: The arc is kept burning at a lower current. This prevents the melt droplet from detaching early and from detaching prematurely and transferring to the workpiece.

3rd - short-circuit phase: As soon as the wire comes into contact with the substrate, the voltage drops to 0 V and the wire feeder is signaled to withdraw the wire. This supports the droplet detachment from the wire into the molten bath.

Figure 2.5 shows the three Phases of a CMT cycle. The voltage is constant in the first two phases and drops to zero in the short circuit phase. The spike of current is clearly visible in the first phase, which is also the shortest.

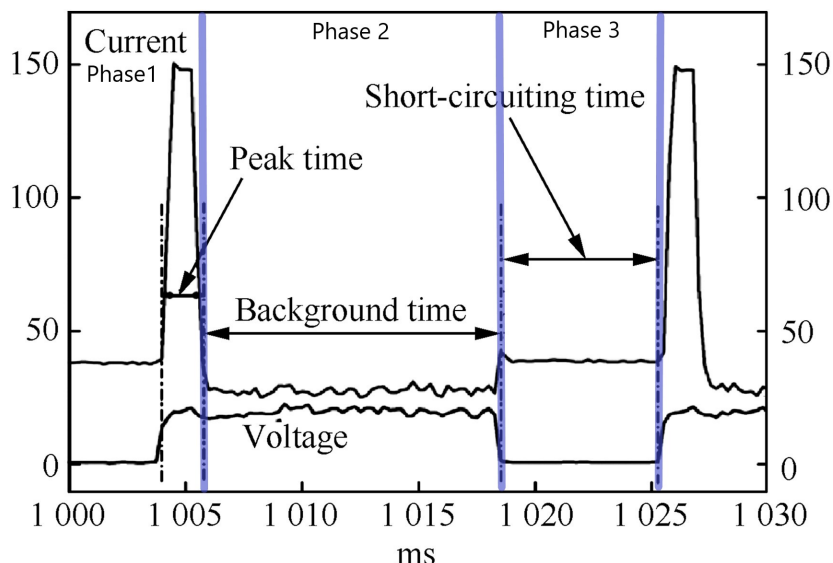


Figure 2.5: Current and Voltage wave forms of a CMT process [0]

Figure 2.6 shows the clearly distinct parts in a CMT cycle. At first an electric arc is formed and melts the wire. After a short circuit is established the wire retracts and detaches from the molten droplet. After that the cycle restarts.

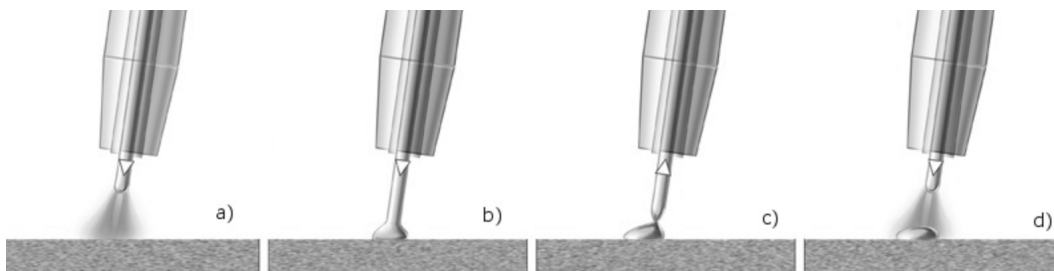


Figure 2.6: Individual sections of a CMT cycle [0]

In summary, WAAM and CMT are highly sophisticated processes that enable the creation of additively manufactured parts with specifically designed parameters. CMT achieves precise welds with low heat input and minimal spatter. It is ideal for thinner materials and applications requiring high weld quality. Advanced process control systems can enhance the reliability of CMT welding [0].

2.1.3 Industrial Robots

Industrial robots are advanced machines designed to perform various tasks in manufacturing and industrial settings. They come in different types, each with its own set of capabilities and advantages. They are crucial to modern manufacturing and automation, transforming production methods and repetitive task performance across diverse industries. Since their inception in the mid-20th century, these machines have undergone significant advancements, evolving into highly adaptive and sophisticated devices that promote productivity, accuracy, and safety within manufacturing processes [0]. At their core, industrial robots are programmable machines designed to execute tasks with a high degree of accuracy and efficiency. They can carry out repetitive actions consistently, which enhances productivity and reduces the risk of human error [0].

One common type of industrial robots are the articulated robots. These robots have rotary joints that allow them to move like a human arm, with multiple links and joints. They can perform a wide range of tasks, such as welding, material handling, or assembly operations [0]. Another type is the Cartesian robot, also known as gantry robots. These robots move along three linear axes (X, Y, and Z) to perform tasks. They are commonly used for pick-and-place operations or in applications that require precise positioning [0]. SCARA robots, shown in figure 2.7, are designed for fast and precise movements in assembly operations. They have a selective compliance assembly robot arm that allows them to move quickly while maintaining accuracy [0]. Delta robots, shown in figure 2.8, robots are used for high-speed pick and place applications, such as packaging or sorting. They are known for their rapid movements and

high throughput [0]. Collaborative robots, or cobots, are designed to work safely alongside humans. They have built-in safety features, such as force sensors or vision systems, that allow them to interact with humans without causing harm. Cobots are often used in tasks that require human-robot collaboration, such as assembly [0].



Figure 2.7: SCARA robot



Figure 2.8: Delta robot

Industrial robots are based on articulated robots and have a wide range of applications across various industries. Depending on the attached tool, they can perform tasks like fastening, welding, or soldering components together. These robots are also commonly used for material handling tasks in warehouses or production lines. Inspection tasks can be automated with robots equipped with sensors or cameras, allowing them to inspect products for defects or perform quality control checks [0].

Industrial robots offer several benefits. Firstly, they increase productivity by working continuously, without breaks or fatigue. This leads to higher production rates and shorter cycle times. Additionally, robots can perform tasks with high precision and accuracy, reducing errors and defects and thereby improving product quality [0]. Safety is another important aspect of industrial robots. They are designed to handle dangerous or hazardous tasks, keeping human workers safe. Robots can work in environments with high temperatures, toxic substances, or heavy loads, minimizing the risk of injury to humans [0]. While the initial investment in industrial robots can be high, they offer long-term cost savings. Robots can reduce labor costs by automating repetitive tasks and increasing efficiency. They also offer flexibility, as they can be reprogrammed or reconfigured to perform different tasks, allowing for greater adaptability in manufacturing processes [0].

When comparing industrial robots to CNC machines, there are a few notable disadvantages for industrial robots. Firstly, industrial robots generally have lower positional accuracy and repeatability compared to CNC machines. CNC machines are purpose-built for precise machining operations and can achieve high levels of accuracy and repeatability [0]. Secondly, industrial robots typically have a longer cycle time compared to CNC machines for similar tasks. The complex movements and computations involved in robot control can result in slower overall operation speeds, which may not be ideal for high-volume production environments [0]. Additionally, industrial robots can be more complex to program and set up than CNC machines. CNC machines follow a predefined set of instructions, whereas pro-

gramming industrial robots often requires more advanced programming skills and can be time-consuming [0]. Lastly, industrial robots may have limitations when it comes to handling heavy loads or performing heavy-duty machining operations. CNC machines are specifically designed for heavy-duty cutting, milling, and drilling tasks, whereas industrial robots are better suited for lighter material handling and assembly operations [0]. These differences should be considered when deciding between industrial robots and CNC machines for specific manufacturing applications.

Industrial robots can be programmed using different methods. One common method is using a teach pendant, where operators manually move the robot to record positions and actions. Offline programming is another approach, where programs are created and simulated on a computer before being transferred to the robot. Sensor-based programming allows robots to respond to sensor inputs or interact with the environment [0].

Serial kinematics is a widely used configuration in industrial robots, where the robot arm is constructed as a sequential chain of joints and links. Each joint provides one DoF, enabling the robot to move and position its end-effector in a controlled manner. The joints can be of various types, including revolute, prismatic, spherical, and cylindrical, providing rotational, linear, and combined movements. The motion of the robot arm is controlled using forward kinematics and inverse kinematics. Forward kinematics calculates the position and orientation of the end-effector based on the joint angles, while inverse kinematics determines the joint angles required to achieve the desired end-effector pose [0].

Figure 2.9 shows the schematic design of a 6-DoF industrial robot with a spindle and force sensor that is used for machining.

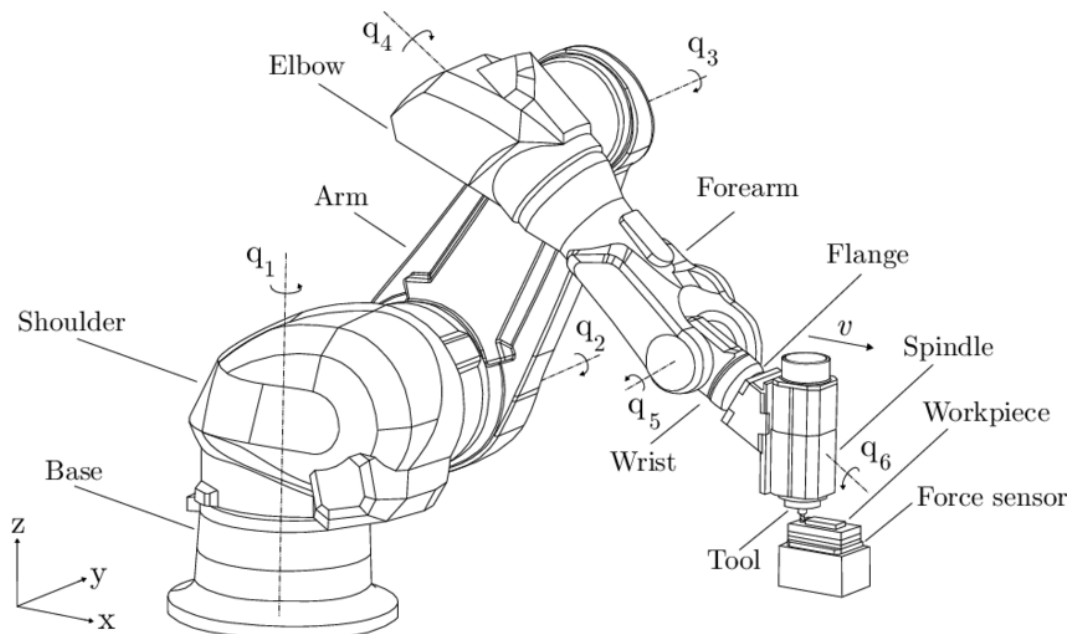


Figure 2.9: 6-DoF industrial robot [0]

In summary, the robots performance relies on sophisticated control algorithms and feedback systems that allow them to adapt to dynamic conditions, adjust movements in real-time, and maintain a consistently high level of accuracy [0]. This improves both the quality of the final product and the safety of the manufacturing process, as robots can navigate complex paths without risking collisions or accidents [0]. As technology continues to advance, industrial robots will play an even more prominent role in shaping the future of manufacturing and automation [0]

Redundancy in robotic systems

Industrial robots with redundant degrees of freedom are robotic systems that have been designed with more DoF than are necessary for a specific task [0]. This extra DoF allows the robots to perform additional joint movements or configurations beyond what is required for basic movement or manipulation.

The primary advantage of these redundant robots is their increased flexibility and adaptability [0]. Robots with more DoF can access a wider range of positions and orientations, making it possible for them to complete complex tasks in constrained environments that would have been difficult or impossible otherwise. With this added flexibility, they can avoid obstacles and work around them without disrupting their duties. In industrial settings, redundant manipulators provide significant advantages. Their additional degrees of freedom enable them to improve accessibility to hard-to-reach areas and enhance overall operational capabilities [0].

Redundancy can take on many different forms in robotic systems. One option is to increase the number of joints in the serial kinematics of an articulated robot [0]. Another approach to redundancy is the addition of a rotary tilt table, which is commonly used in WAAM in combination with a 6-DoF robot [0]. This combined system enables the robot to manipulate the workpiece from various angles, enhancing the manufacturing process. Furthermore, the inclusion of a linear axis that the robot base can traverse on is yet another form of redundant DoF. This additional linear motion provides the robot with extended reach and the capability to access a larger workspace, making it suitable for tasks that require movement along a specific axis [0]. Additionally, redundancy can also be observed when using a generic 6-DoF system for operations that only necessitate 5 or fewer DoF (for example, milling or WAAM) [0]. The system possesses more flexibility than required for the specific task and allows for adaptability and versatility, thus accommodating different operations without the need for reconfiguring the robot.

Figure 2.10 shows two industrial robots from the manufacturer KUKA GmbH that are placed on a linear axis. This enables the robots to use the additional and redundant DoF to optimize the process. Multiple robots can be positioned on one linear unit. Figure 2.11 shows how a 7-DoF robot can have multiple poses reaching the same position. In this case, only six DoF are necessary to achieve the position, while one DoF can be defined manually.



Figure 2.10: Industrial robots with an additional linear axis [0]

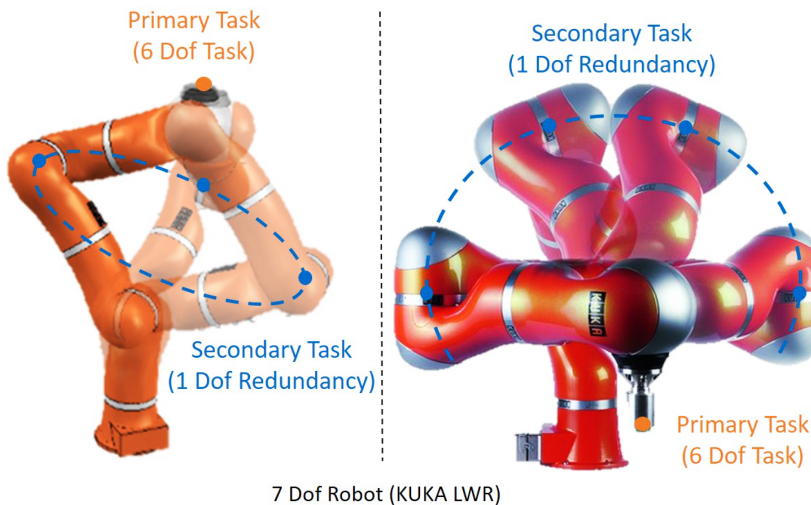


Figure 2.11: 7 DoF robot [0]

In summary, redundancy in robotic systems can be achieved through various means, such as increasing joint numbers, incorporating rotary tilt tables, including linear axes, or using a higher DoF system for tasks that demand fewer DoF. These redundant features enhance the capabilities and versatility of the robot, enabling it to perform a wide range of complex tasks efficiently.

While redundancy in industrial robots can provide increased flexibility and adaptability, it also comes with certain disadvantages. One major drawback is the increased complexity and cost associated with redundant systems [0]. The addition of extra joints, axes, or mechanisms adds to the overall complexity of the robot, requiring more sophisticated control algorithms and hardware [0]. This complexity not only increases the initial cost of the robot but also adds to the maintenance and troubleshooting efforts [0]. Additionally, the presence of redundant DoF can make the robot more susceptible to mechanical failures as more components

are involved. This can result in increased downtime and higher maintenance costs. Moreover, the increased complexity of redundant systems can make programming and calibration more challenging, requiring specialized skills and expertise [0]. Therefore, while redundancy can offer advantages in certain scenarios, careful consideration must be given to the cost, complexity, and maintenance implications before implementing it in industrial robotics applications.

Continuous-path mode

In the context of industrial robotics, continuous paths without abrupt direction or velocity changes of a tool play a crucial role in achieving precise and smooth movements of robotic arms along a defined trajectory [0]. This ensures that the robot can execute complex tasks and movements with accuracy and efficiency. By incorporating continuous path mode into industrial robot programming, manufacturers can optimize production processes and improve the quality of manufactured products [0]. Constant velocity of a tool is especially important in applications like WAAM where the quality of the layer is directly dependent on the feed rate [0]. In CNC machining, discontinuities in velocity, acceleration, and jerk result in non-optimal surface finishes [0].

Continuous path mode refers to a mode of operation in high-speed robotics as well as CNC machines where the goal is to achieve a smooth and uninterrupted movement of the machine along a toolpath. In this mode, the machine is expected to follow a path without any sudden changes in velocity, acceleration, or curvature. The purpose of continuous path mode is to minimize jerk spikes, machine vibrations, and other undesirable effects that can occur when there are discontinuities in the toolpath [0].

Figure 2.12 gives a visual example of a contouring toolpath that is defined with a constant velocity. To maintain a constant velocity along sharp corners or small radii, significant deceleration and acceleration may be needed.

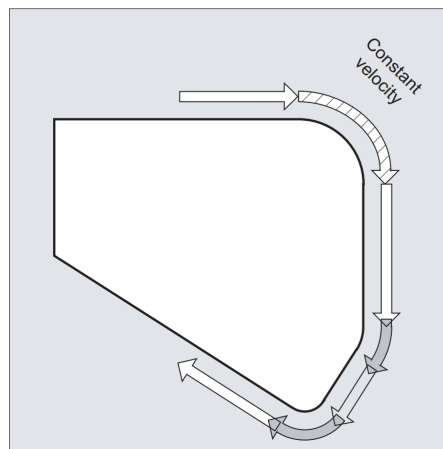


Figure 2.12: Desired path with constant velocity [0]

Figure 2.13 shows how specific G-code commands of the SINUMERIK 840D influence the targeted feedrate. N1 to N12 are the individual G-code lines defining the coordinates with the corresponding orientation, also called waypoints, of the tool center point TCP. When using the G60 command, the points are reached exactly, but the feedrate is reducing to 0 at every waypoint. When implementing the G64 (continuous pathmode) command, the feedrate can be held at the desired value but at the cost of precision.

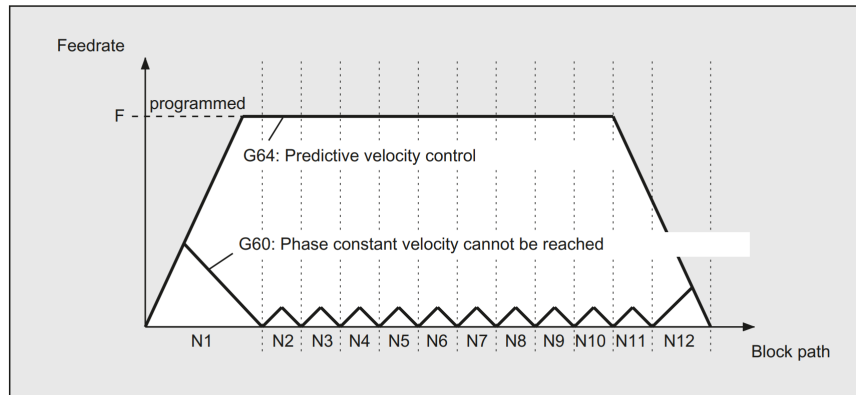


Figure 2.13: Influence of G-Code commands regarding feedrate compliance [0]

The SINUMERIK 840D offer more commands to specify how much deviation is desired. Figure 2.14 shows how the G-code command G641 ADIS=0.5 is influencing the programmed contour. The rounding of the path begins no more than 0.5 mm before the programmed end of the block and must finish 0.5 mm after the end of the block.

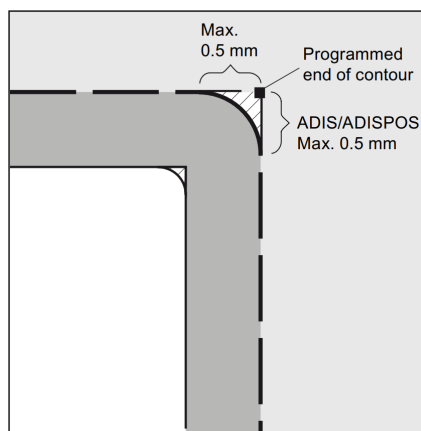


Figure 2.14: Predetermined deviation of the programmed and executed path [0]

It is also possible to define the precision criterion globally instead of individually at every coordinate. For that the commands G601 and G602 can be utilized. Figure 2.15 shows how these two commands influence the executed trajectory. In this case, two different tolerance limits allow the tool to deviate from the programmed path.

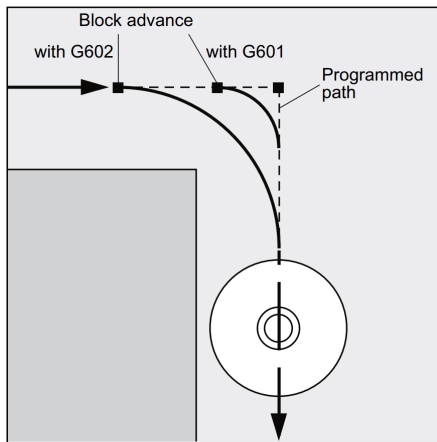


Figure 2.15: Influence of commands G601 and G602 [0]

Continuous-path mode in CNC machining is a crucial aspect when it comes to processing parts with rapidly varied geometric features. These types of components, often found in high-end equipment, pose challenges due to their intricate structures and strict dimensional requirements. The presence of rapidly varied geometric features, coupled with the continuous-path running characteristic, gives rise to trajectory errors during the machining process, which severely hampers the overall machining accuracy of such parts [0]. This becomes even more critical in high-speed machining scenarios, where existing studies struggle to effectively reduce this error without compromising machining efficiency [0].

In CNC machines, toolpaths are typically composed of lines and arcs [0]. At the transition points between these elements, careful consideration is required to ensure that the physical limits of the machine are not exceeded. For example, when the machine is moving at a constant feedrate, a sudden change in velocity can occur when two successive non-tangent linear moves meet. This can lead to undesirable effects on the machine and the quality of the cut [0]. Similar issues arise at transitions between lines and arcs or between two arcs, where curvature discontinuities need to be addressed.

Many path smoothing methods have been proposed in the literature, but most of them are limited to linear toolpaths. However, in high-speed CNC machines and industrial robots, the toolpaths often consist of both lines and arcs. Therefore, there is a need for a path smoothing method that can handle both line-to-line transitions and transitions involving arcs [0]. These errors are caused by factors such as servo lag, dynamics mismatch, external disturbances, and more [0]. Reducing these contouring errors while at the same time allowing high-speed and high-precision machining is essential for improving the performance of CNC motion systems.

To address this issue, various estimation and compensation methods have been proposed for reducing trajectory error. These approaches can be divided into contouring-error estimation and contouring-error reduction approaches [0]. These approaches include the "Moving frame based method", "Analytical method", "Generalized method" or "Servo-tuning approach". It is important to note that these methods for contouring-error estimation and reduction, only offer relative significance. Each algorithm has its own optimal range of applications and may

outperform other methods within that range. Additionally, it is important to note that not every approach can be implemented on every system.

Another approach for achieving continuous path mode is by using biclothoid fillets. These fillets are used for corner smoothing and can be fitted between two arcs or a line and an arc. The main advantage of using biclothoid fillets is that they result in a smoother curvature profile compared to other methods, such as Bezier fillets. Especially with tight tolerance values, only a few biclothoid fillets are needed compared to Bezier fillets. Additionally, the biclothoid approach is more suitable in regards to the jerk and acceleration limits of the driving units. This smoother curvature profile allows for higher feedrates and shorter cycle times, ultimately improving the overall performance of the CNC machine [0].

2.2 Computer-Aided Manufacturing

CAM is a technology that uses computer software to automate and optimize manufacturing processes. It involves the use of computer systems to control and operate machinery, such as CNC machines, robots, and 3D printers. CAM software can generate tool paths and instructions for machines based on CAM models, allowing for precise and efficient production. By reducing manual labor, CAM helps improve productivity, accuracy, and consistency in manufacturing. It is widely used in industries like aerospace, automotive, and electronics to streamline production [0].

2.2.1 CAM Software

CAM software enables manufacturers to generate toolpaths and machining instructions for a variety of manufacturing processes, including milling, turning, drilling, and 3D printing [0]. It takes into account factors such as material properties, tool capabilities, and manufacturing constraints to generate the most efficient and accurate instructions for the machines. CAM software can also simulate the machining process to detect any potential collisions or issues before actual production begins, saving time and resources [0].

One of the key features of CAM software is its ability to optimize the machining process. It can automatically optimize toolpaths to minimize machining time, reduce material waste, and improve surface finish. By analyzing the geometry of the part, the software can determine the most efficient toolpath strategies, such as contouring, pocketing, or adaptive machining. It can also optimize tool selection, toolpath sequencing, and cutting parameters to achieve the best possible results [0].

Furthermore, CAM software often integrates with other manufacturing software systems, such as Computer-Aided Engineering (CAE) and enterprise resource planning (ERP) systems [0]. This integration enables seamless data exchange, improves collaboration between

different departments, and ensures that the manufacturing process is aligned with the overall production goals [0]. With features such as optimization, simulation, multi-axis machining, and integration with other systems, CAM software empowers manufacturers to stay competitive in today's fast-paced and complex manufacturing environment [0].

Figure 2.16 shows the interface of Siemens NX, a CAM/CAM software that can be used to design parts and generate machine-specific instructions for manufacturing.

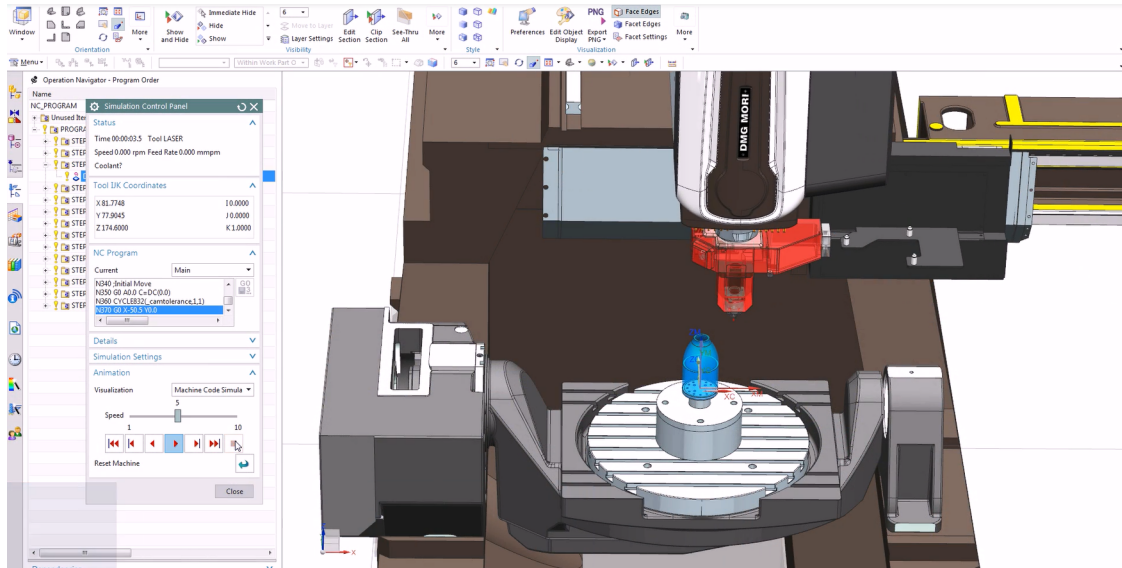


Figure 2.16: Interface of Siemens NX [0]

2.2.2 Path Planning

Path planning and generation are crucial features of CAM. It involves establishing the most effective toolpaths for machining operations, guaranteeing efficient and precise production [0].

Path planning involves determining the optimal sequence of movements for the machining tool to follow while producing a component. It considers factors such as part geometry, tool capabilities, machining constraints, and desired parameters. Its goal is to minimize machining time, reduce waste, and improve the finished product [0]. CAM software employs algorithms and mathematical models to determine the tool's position and orientation on the toolpath. Additionally, factors such as cutting direction, feed rate, and tool engagement need to be taken into account [0].

Adaptive machining is a critical part of path planning and generation. It enables the CAM software to adjust the toolpath and cutting parameters in real-time based on material properties, tool wear, and other factors. This constant monitoring and adaptation ensure precise and dependable outcomes, even in difficult manufacturing conditions [0].

Multi-axis machining is an advanced function of CAM software, ideal for intricate cuts and shapes on complex geometries. By allowing the tool to move simultaneously along multiple

axes, it delivers greater precision and accuracy during the machining of curved surfaces, free-form shapes, or parts with undercuts [0].

CAM software typically includes simulation tools that enable users to visualize and verify the toolpath prior to production. These simulations can detect and resolve potential collisions, interference, or errors that may occur during machining, leading to cost savings and increased safety [0].

Figure 2.17 shows three different path trajectories for planar milling operations. Depending on the area of application, different paths can be optimal. In generic 3D-printing as well as in WAAM multiple different infill methods, similar to the planar milling operations, can be used to build up the desired geometry.



Figure 2.17: Three exemplary tool paths for iso-planar milling [0]

2.3 Optimization Algorithms

Optimization algorithms are computational methods used to find the best possible solution to a problem within a given set of constraints. These algorithms aim to minimize or maximize an objective function by iteratively adjusting the values of decision variables [0]. They are widely used in various fields, including engineering, operations research, finance, and machine learning, to optimize resource allocation, scheduling, parameter tuning, and other complex tasks. For the problem described in 1.2 optimization algorithms can be used for determining optimal parameters for the redundant degrees of freedom while considering the defined objective, like reduction of direction changes or energy optimization.

Optimization algorithms are computational techniques employed to identify the optimal solution or set of solutions for a given problem. There are several types of optimization algorithms, each exhibiting a unique methodology and characteristics. Gradient-based optimization algorithms, like gradient descent, update the solution iteratively by following the direction of the steepest ascent or descent of the objective function [0]. These algorithms are efficient for convex optimization problems where the objective function is smooth and has a unique global minimum or maximum.

Another type of optimization algorithm is the evolutionary algorithm, which is inspired by

biological evolution. Evolutionary algorithms employ mutation, crossover, and selection to progressively shape a population of solutions over time. These techniques are especially applicable to resolving intricate optimization problems characterized by non-linear and non-convex objective functions. By reading a wider range of the search space, evolutionary algorithms can uncover tier-one solutions that draw near to the global optimum, although they may necessitate enhanced computational resources [0].

Genetic algorithms are evolutionary algorithms that use genetic operators, like crossover and mutation, to evolve solutions in a population. They can handle various types of optimization problems. Genetic algorithms are particularly effective for multi-objective optimization problems. They generate a set of solutions called the Pareto front, which represents the trade-off between conflicting objectives [0].

Particle swarm optimization (PSO) is a metaheuristic optimization algorithm based on the collective behavior of a particle swarm. In PSO, each particle represents a potential solution, and it moves through the search space to discover the optimal solution by exchanging information with nearby particles. This cooperative behavior enables the algorithm to efficiently converge to better solutions. PSO is especially beneficial for continuous optimization problems that have numerous local optima [0].

In recent years, there has been an increasing interest in metaheuristic optimization algorithms. Examples of such algorithms are ant colony optimization, differential evolution, and harmony search, which draw inspiration from natural phenomena or human behavior. These general-purpose algorithms can be applied to various optimization problems and provide efficient and flexible approaches to finding optimal solutions [0].

Optimization algorithms prove to be significant resources for uncovering optimal solutions to intricate issues. Be it via gradient-based means, evolutionary algorithms, metaheuristics, or other customized mechanisms. Optimization algorithms effectively fine-tune objectives, meet requirements, and refine decision-making processes across a broad spectrum of industries. The algorithm choice relies on the problem's characteristics, the available computational resources, and the desired balance between solution quality and computational efficiency.

2.4 Comparison of the State of the Art

In the following, a literature analysis is performed regarding the optimization of various process parameters. The focus lies on manufacturing systems with redundant DoF, specifically for tasks such as milling and WAAM. In cases where no literature is available that incorporates redundant DoF, non-redundant systems are analyzed. Table 2.1 summarizes the analyzed parameters.

| | |
|---------------------------|-------------------------|
| Singularity avoidance [0] | Joint accelerations [0] |
| Joint jerks [0] | Stiffness [0] |
| Energy use [0] | |

Table 2.1: Areas of influence of boundary conditions and process parameters

Additional parameters like transfer time, precision, and maximum load capacity can also be analyzed but are omitted from the detailed analysis due to the limitations of scope [0]. Direction changes in the joint are briefly mentioned in [0] but not discussed in detail in any other publication.

2.4.1 Singularity avoidance

As mentioned in Chapter 1.2, singularities occur when the robot manipulator loses control or achieves limited mobility due to certain configurations [0]. This results in the loss of a DoF or makes the system highly sensitive to small changes [0]. Figure 2.18 shows how the 5th joint needs to rotate significantly when moving along a straight line in Cartesian space. When an additional velocity boundary condition is set that defines the feed rate of that path, the rotation is very difficult to perform as the motor joints cannot keep up with the required angular acceleration. This is unnecessary movement that increases energy consumption and adds unnecessary wear to the joints.



Figure 2.18: Passing through a wrist singularity [0]

Due to the numerous possible solutions for the inverse kinematics of redundant manipulators, it is exceptionally challenging to predict and prevent the occurrence of singularity configurations during motion planning [0].

In tasks that involve functional redundancy, as where the manipulator has more DoF than required for the task, the general projection method cannot be applied [0]. Robotic industrial welding processes often have functional redundancy due to the presence of symmetry axes when using generic 6-DoF industrial robots. Different approaches have been proposed to solve functional redundancy, including adding a virtual joint to the manipulator or using the twist decomposition approach (TWA).

Most of the research is limited to the mathematical analysis of singularities and does not consider the industrial implementation of the proposed algorithms in an industrial setting. The manipulability measure and maximization of Jacobian minors are commonly used methods to avoid singularities. Other methods, such as condition number and singular value decomposition, can also be used [0]. Another mathematical analysis performs a differentiation between non-recoverable singularities and configurations where through self-motion recovery into a nonsingular configuration is possible [0]

Another approach proposes a kinetostatic performance index for evaluating the quality of robotic postures, which includes singularity avoidance and joint limit consideration [0]. This method is also transferable to applications like milling. A parameter called "condition number" and "manipulability" are introduced, which are used to calculate the "kinetostatic performance index". The presented method can increase the distance from singularities and lower the maximum rotation velocity of the fourth joint. One disadvantage of the proposed method is the manual selection of a parameter. This parameter is responsible for avoiding joint limits and minimizing joint velocities. Manual fine-tuning of that parameter is required for optimal performance.

Further approaches are proposing roll motion around the tool's symmetry axis to counter the loss of a degree of freedom at the singularity. Paths with varying tool roll or fixed roll angles can be chosen, with considerations for tool elevation changes. Selecting paths with a fixed roll angle simplifies implementation for existing robot controllers [0].

Another approach uses the non-square Jacobi matrix and, after analysis, derives a simplified version through the selection of coordinate systems and primary transformation. By using block matrix analysis, the singularity conditions of the articulated robot are determined. A singular configuration avoidance algorithm is used to avoid singular patterns through constraining redundant DoF [0].

Neural networks and other machine learning approaches are commonly used to solve the issue of inverse kinematics. In this case, the optimization variable is not only limited to singularity avoidance but can also be focused on precision or optimization of feed rate [0].

2.4.2 Optimization of Joint Accelerations and Jerk

Jerk and acceleration control are critical because high values can wear out the robot structure and significantly stimulate its resonance frequencies. Vibrations caused by non-smooth trajectories can harm the robot's actuators and produce substantial deviations when completing tasks like trajectory tracking. Furthermore, low-jerk trajectories can be accomplished more quickly and precisely [0].

One recently published approach uses an adaptive greedy algorithm to generate the jerk-optimized trajectory with discrete time constraints. The proposed algorithm improves the trajectory in an iterative routine after obtaining an initial trajectory by a graph-search method [0]. A further method proposes a sequential quadratic programming method. The results show that optimal time-jerk trajectories with traveling time constraints can be obtained [0].

Another method is proposing a method of reconstructing the path by a sequence of via-points that define the positions and orientations of the robot's end-effector. Unlike most minimum-jerk trajectory planning techniques, this algorithm does not force an execution time beforehand and takes into account constraints such as upper bounds on velocity, acceleration, and jerk. The algorithm uses a hybrid objective function that balances execution time and smoothness of the trajectory. The output of the algorithm is a vector of time intervals between consecutive via-points that minimizes the objective function [0].

A further method is using an algorithm for adjusting the increments of the generalized coordinate vector. By using a pseudo-inverse of the Jacobi matrix and a Taylor's expansion, the robot's acceleration and jerk can be calculated. Results show that when the end effector is closer to the center of the robot, joint jerk increases. It is also shown that if trajectories are designed on the OXZ plane and directed away from the robot's center, the jerk decreases [0].

2.4.3 Optimization of Stiffens

Stiffness plays a crucial role in machining with industrial robots. It refers to the ability of a machine or structure to resist deformation under an applied load. In the context of machining, stiffness directly affects the accuracy, precision, and overall performance of the robot. A high level of stiffness ensures that the robot remains stable and rigid during machining operations, minimizing unwanted vibrations, deflections, and inaccuracies [0]. This is particularly important when dealing with high-speed or heavy-duty machining tasks, as any lack of stiffness can result in poor surface finish, dimensional inaccuracies, and reduced tool life.

A recent publication is evaluating the stiffness of a robot using a newly defined performance index, which is maximized to optimize the robot's posture. The problem is solved using a discretization search algorithm, taking into account joint limits, singularity avoidance, and trajectory smoothness. Each joint of the robot is modeled as a linear torsion spring, which is transferred into a stiffness matrix. This method is applied to a 6-DoF robot that is used

for a milling operation. The goal of this method is to set the redundant angle in such a way that stiffness is maximized. Simulations and experiments on an industrial robot validate the performance index and optimization algorithm, demonstrating improved machining accuracy using this method [0].

Another approach is working with a dynamic model to reduce the chatter in a milling operation with a 6-DoF robot. By considering the frequency response function, the maximum possible cutting depth, without the occurrence of chatter can be determined. The cutting depth is a function of the redundant degree of freedom. In this case, the redundant degree of freedom is the rotation around the axis of the spindle. An experimental analysis of a full-slot cut is performed. The results show that a significant reduction in chatter can be achieved by setting the redundant degree of freedom to the optimal value [0].

A further publication performs a comparative study of robot pose optimization using static and dynamic stiffness models. The results suggest that the static stiffness model can achieve close to optimal results for pose selection for tasks where the process forces do not approach the resonant frequencies of the robot. It is also discussed that static and dynamic stiffness-based optimizations cannot reduce the deflections of the cutting tool to a range smaller than the robot's repeatability [0].

There are many more methods, like finite element analysis, matrix structure analysis, and virtual joint modeling. To enhance stiffness models, further investigation needs to be conducted. The current state of the art shows a need for standardization in stiffness modeling, as there is currently no universally accepted procedure for establishing such models. Developing a modeling process with standard principles, evaluation indicators, and measuring techniques can simplify the selection and application of modeling methods. Additionally, the application of machine learning techniques, such as artificial neural networks, can be explored for stiffness modeling. Processing experimental data using machine learning algorithms can yield high-precision stiffness models [0].

2.4.4 Optimization of Energy use

Energy-efficient usage of industrial robots is essential for achieving cost savings and sustainable manufacturing processes. Manufacturers can achieve this by implementing strategies such as optimizing robot movement paths, reducing idle time, and using energy-efficient components, resulting in significant reductions in energy consumption of their robotic systems. Incorporating advanced algorithms enables robots to adapt to changing conditions and operate at their most efficient levels, optimizing energy usage [0].

One paper analyzed the different methods at different development stages of a production environment in regards to energy optimization. The results show that operating speed and payload strongly influence power consumption, and reducing it can be achieved through optimizing speed, reducing weight, and smoothing motion [0].

Further analysis in a different publication shows that in a setting where a 6-DoF is used to perform a 5-DoF task, energy savings of up to 20.8% can be expected. The proposed method uses the yaw angle as an optimization variable that can be set to a value in a certain range [0].

Another publication analyzes the general energy consumption of an industrial robot. The results show that cooling and movement speed have the most significant impact on energy consumption. The axis drives are responsible for 23% of the energy consumption. Based on this result, it is shown that optimizing the robot's movement in regards to optimal movement will significantly reduce its energy usage [0].

2.4.5 Summary

Setting the appropriate process parameters directly impacts the performance and efficiency of a production system. By carefully fine-tuning parameters such as singularity avoidance, joint accelerations, and jerks, the system can operate smoothly, minimizing wear on the structure while achieving precise trajectory tracking. Moreover, optimizing energy usage through the adjustment of parameters related to movement speed not only contributes to environmental sustainability but also leads to economic benefits by reducing long-term operational costs. Additionally, the consideration of parameters like stiffness and joint limits ensures the safety of both the manufacturing system and its operators. The optimization of stiffness, for instance, enables the maximization of the system's performance and the attainment of improved machining accuracy. In conclusion, the careful selection and optimization of process parameters play a significant role in achieving optimal performance, efficiency, safety, and utilization of manufacturing systems, thereby contributing to overall operational success.

Chapter 3

Methodology

3.1 Introduction

The proposed method aims to provide a framework for optimizing various parameters of an industrial robot in order to achieve a specific objective. This method effectively utilizes the redundant degrees of freedom mentioned in Chapter 1.3, making it suitable for robotic milling operations and WAAM processes. Implementing this methodology can improve the overall performance and efficiency of the robot, ultimately leading to increased productivity in industrial operations. The methodology can be divided into two parts. Firstly, an evaluation of process parameters is conducted for a specific toolpath with user-defined boundary conditions. Secondly, the optimization of these boundary conditions is carried out in order to optimize the specific process parameters towards a defined global goal.

3.2 General Methodology for Process Analysis and Evaluation

3.2.1 General Methodology

The flowchart displayed in Figure 3.1 illustrates the interdependence of various factors, including the toolpath, manufacturing machine, material, and set boundary conditions. The manufacturing machine plays a crucial role as it determines important parameters such as the total working volume, degrees of freedom, maximum feed rates, and whether the manufacturing process is additive or subtractive. This machine can be a 6-axis CNC machine or an 8-DoF industrial robot.

The part refers to the finished geometry as designed in CAM, while the material is the user-defined element from which the part will be manufactured. These elements, along with the machine, directly influence the toolpath required for manufacturing. For instance, the machine's specifications determine whether the spindle or the work piece itself needs to be tilted during machining to achieve the desired geometric features.

In addition to the machine, part, and material, there are other factors that impact the toolpath. These include the availability of end-mills, the desired depth of cut, the machining strategy, and the operation sequence. These factors are considered as adjacent parameters within the overall manufacturing process.

Since the toolpath is a movement relative to the work piece, the user must specify additional parameters before initiating the manufacturing process. One example is the positioning of the raw stock material within the machine and establishing the coordinate system that serves as a reference for the TCP. These boundary conditions need to align with the capabilities of the machine and may necessitate a comprehensive understanding of both the machine and the specific manufacturing process being performed.

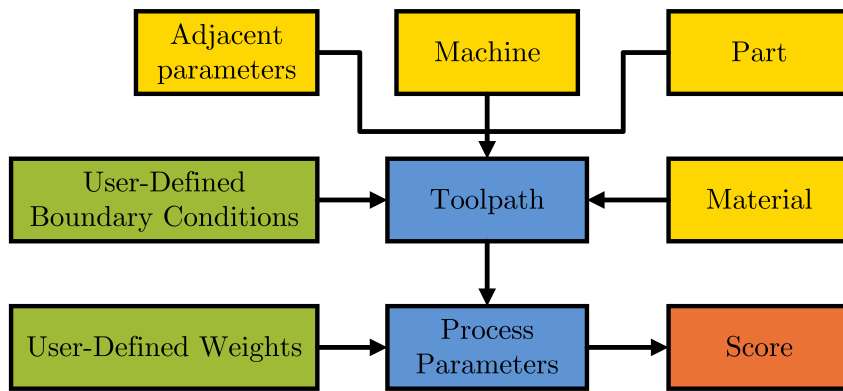


Figure 3.1: Interdependence of various parameters

Another parameter that must be defined in the "User-Defined Boundary Conditions" is the positioning or constraining of redundant DoF. A straightforward example to illustrate this constraining is when a 6-DoF robot is used for milling operations. In milling, the TCP position is determined by three coordinates: X, Y, and Z, as well as the rotation around the X and Y axes. However, the rotation around the Z-axis must be manually defined since the spindle is rotationally symmetric around this axis and thus does not affect the toolpath. This constraint ensures that the robot maintains a specific pose while carrying out milling operations.

The rotation around the Z-axis can theoretically be set to any value, but it can significantly affect the overall process parameters. In practical applications, this rotation value is often limited due to factors such as cable routing or joint limits. These same limitations apply in WAAM, where the wire feed system combined with the torch position restricts the possible orientations that can be achieved.

Once the constraints are established and the toolpath is generated, various process parameters can be analyzed. Some notable parameters include the total angular travel of a specific joint and the total angular acceleration. Alongside these numerical values, the user has the option to assign specific importance or weight to the analyzed process parameters. By weighting all available process parameters, an overall score for the determined toolpath with the set boundary condition can be calculated.

In the following, the elements "Adjacent parameters" and "Material" are excluded in this discussion, as they do not directly impact the optimization of the manufacturing process as explained in Chapter 1.3. These elements serve as hard constraints that define the feasible toolpath and are not directly linked to the redundant degrees of freedom. However, it is important to acknowledge that these adjacent parameters can still greatly enhance areas such as cycle time or surface finish of the manufactured part.

3.2.2 Process Parameters

Table 3.1 presents a comprehensive overview of the various process parameters and their numerical form, that can be derived from a toolpath with defined boundary conditions that is executed by an industrial robot.

| Process Parameter | Numerical Form |
|------------------------------------|----------------------------|
| Angular position of each joint | Time-series |
| Angular velocity of each joint | Time-series |
| Angular acceleration of each joint | Time-series |
| Angular jerk of each joint | Time-series |
| Direction changes of each joint | Scalar value |
| Total travel of each joint | Scalar value |
| TCP coordinates (X,Y,Z) | Time-series |
| TCP velocity (X,Y,Z) | Time-series |
| TCP acceleration (X,Y,Z) | Time-series |
| Continuous energy usage | Time-series |
| Total energy usage | Scalar value |
| Reachability index | Binary value / Time-series |
| Singularity Analysis | Scalar value / Time-series |
| Torch orientation | Time-series |

Table 3.1: Process parameter and their numerical form

Position, Velocity, Acceleration and Jerk

One of the primary parameters is the joint position, which is recorded as a one-dimensional array comprising the rotational position or extension values of each rotary or linear joint at each time step. This data serves as the foundation for calculating subsequent parameters like velocity, acceleration, and jerk. Analyzing these parameters is crucial to ensure that the joints are not excessively strained during the manufacturing process, thus prolonging their service life as much as possible.

To extend the lifespan of an industrial robot, it is essential to take into account the load on individual joints. An important factor in assessing joint load is the number of direction changes that occur during operation. High-frequency rotation changes can lead to degradation and reduced precision in manufacturing processes.

This process parameter, referred to as the number of direction changes, is a scalar value that can be derived from the angular position of each joint. By analyzing the joint position data further, the total travel of a joint can be determined by integrating the joint velocity over time.

Furthermore, it is important to analyze if velocity changes consistently occur at the same position, leading to wear on the same tooth flank. This can cause significant localized wear and shorten the lifespan of the joints.

Programs or toolpaths that require less overall joint travel are generally preferred. By minimizing the number of direction changes and optimizing joint travel, stress and wear on the robot joints can be reduced, ultimately extending the overall lifespan of the robot system.

TCP Position, Velocity and Acceleration

By utilizing a forward kinematics approach or extracting it from the G-code directly, it is possible to attain the position (X Y Z position) and orientation (rotation) of the TCP. Furthermore, the acceleration and jerk of the TCP can be calculated by deriving their respective values with respect to time. These derived parameters, along with the joint positions, are stored in arrays that track the temporal changes in their values. These parameters enable the determination of the number of deviations from the intended toolpath and the extent of deviation that can be expected in continuous path mode as explained in Chapter 2.1.3.

Energy Usage

Estimating energy usage in industrial robot applications is increasingly important in the current manufacturing environment. One accurate method to estimate energy consumption is through multi-body simulation, which requires a correct 3D model incorporating information about the weight and distribution of the robot joints. Another approach is to utilize machine learning (ML) techniques or other intermediate analyses.

Moreover, in cases where the industrial robot is used for WAAM, the power required for welding can be determined by analyzing the duration during which the welding torch remains active, which can be extracted from the G-code. Similar to the other parameters mentioned earlier, the continuous energy usage is also stored in the form of an array to capture variations over time.

Total energy usage, measured in kilowatt-hours (kWh), is a crucial parameter that can be directly measured during the manufacturing process. It offers valuable insights into the overall energy consumption of the industrial robot system. This parameter can be obtained by

monitoring and recording the real-time energy usage or by integrating the time-series data of continuous energy consumption.

By analyzing energy usage, manufacturers can identify energy-intensive processes or operations, optimize energy consumption, and implement strategies to reduce overall energy consumption. This not only leads to cost savings but also provides environmental benefits.

Reachability

The reachability index is a binary parameter used to assess the feasibility of executing a program in an industrial robot system. It determines whether all the necessary points defined in the toolpath are within the robot's working volume and can be reached by its TCP. This parameter ensures that the robot can physically access all required positions in the work area. If any point is found to be outside the reachable workspace, adjustments are necessary.

Reachability can also be influenced by additional factors such as cable routing. Even if the endpoints are within the robot's working volume, factors like wire-feed systems or optical fibers used for laser transmission may have limitations on bending degrees. When analyzing cable routing in relation to orientation, the reachability index can be represented as a time-series that records the deviation of the cable's bending angle from the optimal angle.

Singularity Analysis

The singularity analysis parameter can be represented either as a time-series or as a single numerical value. It is derived from the smallest eigenvalue of the Jacobian matrix, which is calculated using the current configuration of the robot. This parameter can be stored in an array format, capturing the variations in singularity analysis over time. Alternatively, only the smallest eigenvalue encountered throughout the entire toolpath can be recorded.

Analyzing the singularity time-series enables the optimization of non-optimal poses, ensuring that the robot avoids singular configurations that may result in reduced performance or unexpected behavior.

Torch Orientation

Torch orientation is a crucial parameter in WAAM, as it tracks the tilt angle of the welding torch during the process. Achieving optimal performance requires that the material deposition always occurs in the direction of gravity. When the welding head is positioned upside down, it represents a worst-case scenario where the welding process takes place against the force of gravity.

Significant deviation of the tilt angle from the gravity vector makes it challenging to maintain the stability of the molten metal pool, potentially leading to defects such as sagging.

To ensure proper monitoring of torch orientation, a time-series is used to record the deviation of the torch angle from the gravity vector. Analyzing this information helps identify any deviations or that may impact the quality of the deposited material.

Figure 3.2 illustrates the interconnectedness of the different parameters. It is evident that all parameters can be derived from the angular position of the joints. This highlights the significance of this information. The angular position data is vital for analyzing and optimizing the robot system's performance. By monitoring and analyzing the joint positions, users can gain insights into various aspects of the robot's operation and make informed decisions to enhance productivity.

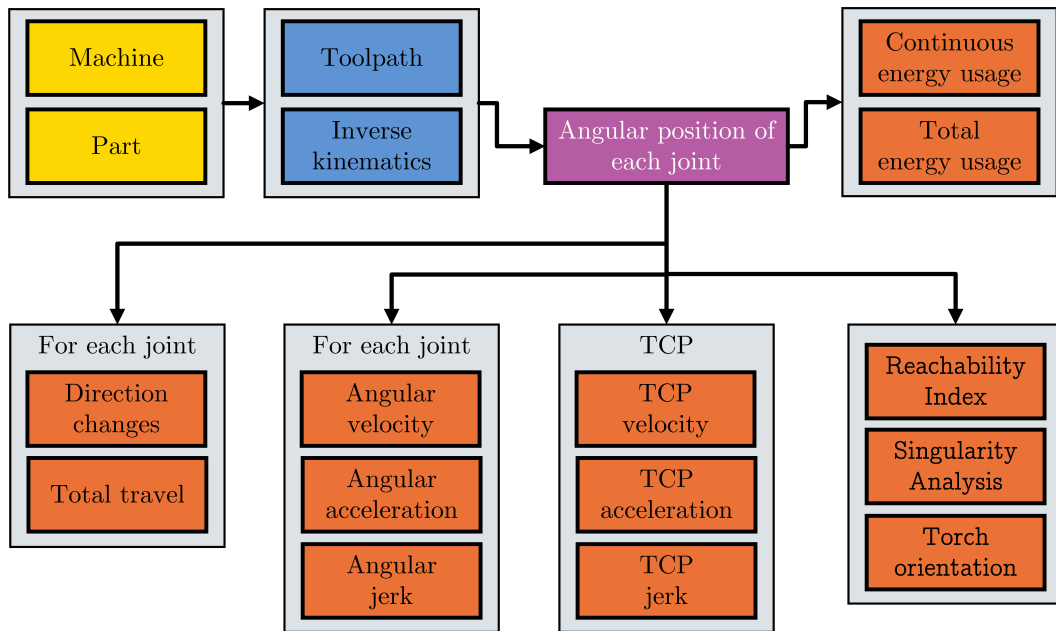


Figure 3.2: Parameter Flowchart

3.3 User-Defined Weights and Score Calculation

3.3.1 Local Rating and Global Score

In order to evaluate whether a toolpath, along with its boundary conditions, is optimal or can be improved, it is necessary to have a score or rating value that considers the process parameters and their importance.

Assigning relative importance to different parameters can involve subjective judgments, expert knowledge, and consideration of specific manufacturing constraints. For instance, in some cases, minimizing joint jerk may be the main objective, while in others, energy usage may be more important.

To quantify the performance of a toolpath, the user can assign weights or importance factors to each parameter based on their specific requirements. These weights can reflect the relative significance of each parameter in achieving the desired optimum. A weighted sum or scoring method can then be used to evaluate and compare different toolpaths with varying constraints, based on the aggregated scores of the individual parameters.

It's important to note that the subjective weighing of parameters can vary between different manufacturing scenarios and requires continuous evaluation and adjustment based on changing priorities or goals.

The score of a toolpath with its boundary conditions is calculated as shown in table 3.2. Each process parameter is assigned a local rating ranging from 0 to 100, where 0 represents the least optimal and 100 represents the best-case solution. This local rating is multiplied by the corresponding importance factor, resulting in a local score.

The local scores for all parameters are then summed to obtain the overall global score for that specific toolpath, taking into account the assigned importance values for each parameter. It is crucial to ensure that the sum of all defined importance values equals 1, so that the toolpath with the most optimal boundary conditions yields a global score of 100.

| Process Parameters | Local rating | Importance | Local score |
|---------------------|--------------|------------|-------------|
| Process Parameter 1 | 74 | 0.5 | 37 |
| Process Parameter 2 | 34 | 0.1 | 3.4 |
| Process Parameter 3 | 65 | 0.1 | 6.5 |
| Process Parameter 4 | 22 | 0.3 | 6.6 |
| Global Score | | | 53,5 |

Table 3.2: Calculation of a toolpath score

3.3.2 Local Rating Calculation

Calculating a local rating is not a straight-forward approach. The first problem is that based on a singular value like "direction changes," it is not possible to determine a local rating as it is not clear if that value is close to optimal or far from it. To address this issue, one possible solution is to generate multiple toolpaths with different boundary conditions or constraints, such as rotation around the C-axis, and compare the results.

Figure 3.3 shows how a local score can be calculated by means of variation. Each variation of the boundary condition results in a different number of direction changes in joint 1. The local score can be determined by essentially applying a Min-Max scaler, which normalizes the values between a minimum and maximum range. In this case the range is set from 0 to 100.

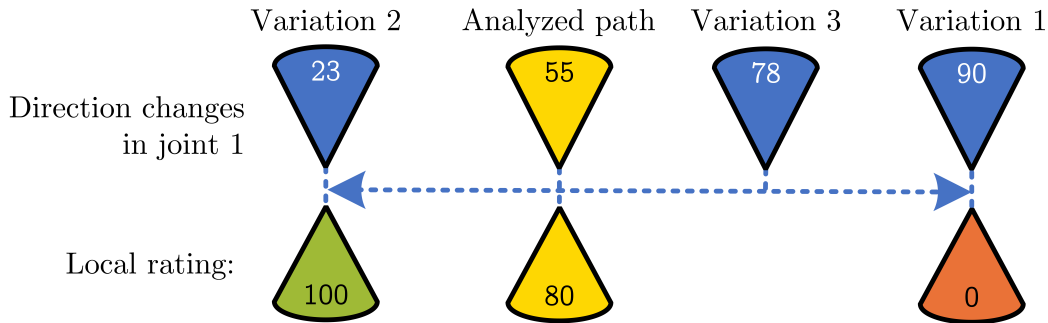
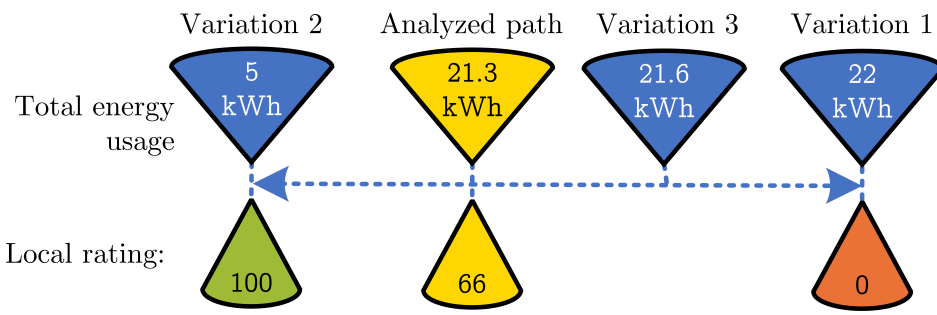
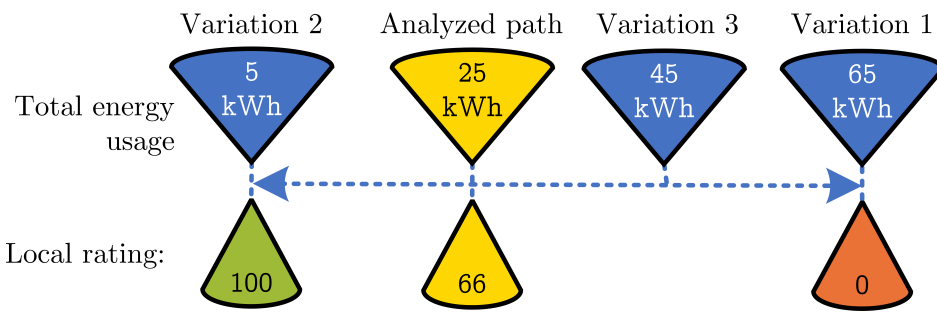


Figure 3.3: Calculation of the local score through variation

It is important to note that increasing the number of variations performed before calculating the local score will enhance the accuracy of this approach. If only a few variations are executed, there is a possibility that only similar outcomes will be identified, which can significantly affect the result. Furthermore, the user needs to specify whether a high or low scalar value of a process parameter is desired. The Min-Max scaler should return the local score accordingly.

Another factor that needs to be analyzed is whether the variations in the boundary conditions lead to different process parameter values that exceed a certain standard deviation. Figure 3.4 illustrates how a local score of 66 is calculated, despite the presence of very small absolute differences. In this case, the standard deviation is only 0.37. On the other hand, Figure 3.5 demonstrates how the same local score of 66 is calculated, even though the absolute differences are significantly higher. Here, the standard deviation is 22.36. The local score should only be used as input for the global score if the standard deviation exceeds a predetermined threshold. If the standard deviation criteria are not met, the corresponding process parameter should be excluded from the calculation of the global score.

**Figure 3.4:** Variation with low standard deviation**Figure 3.5:** Variation with high standard deviation

3.3.3 Information Extraction from Time-Series Data

It is important to note that, as discussed in Chapter 3.3.2, the computation of a local score requires transforming a time-series into a single scalar value. This transformation can be accomplished by directly manipulating the time-series data, such as summing up all values, or by conducting subsequent analyses. Since each time-series captures distinct physical phenomena, each one necessitates a unique process for converting it into a scalar value.

3.4 Information from Angular Position

In its isolated form, the angular position of a joint does not provide much information to enable extensive qualitative analysis. However, when supplemented with temporal information, it becomes a valuable source of information. By considering the angular position in conjunction with the temporal dimension, a more comprehensive understanding of joint behavior can be obtained, allowing for more in depth analysis.

Figure 3.6 visualizes what information needs to be added to enrich the analysis of these process parameters that are directly related to the angular position of joints.

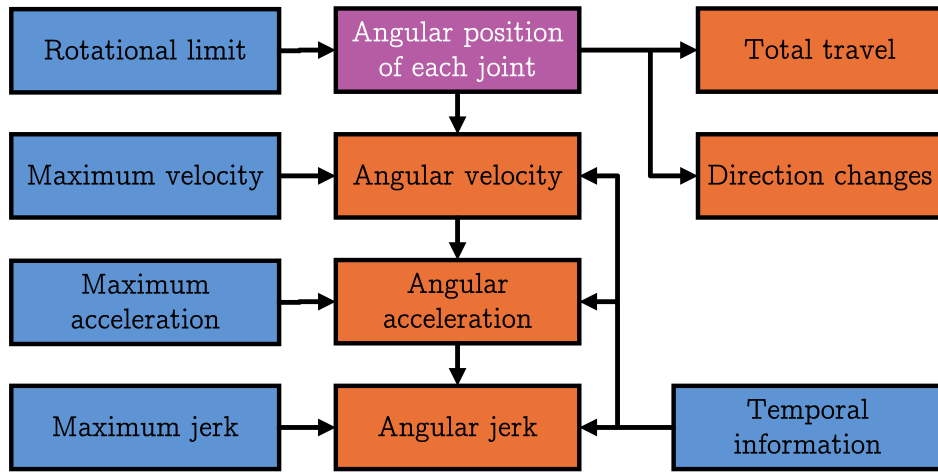


Figure 3.6: Additional Information for angular position of each joint

The first additional required piece of information is the temporal element, which specifies the exact time when a joint should be in a specific rotational position. This information can be recorded in equidistant time intervals, as depicted in Figure 3.7 on the left, or it can be adjusted to only record the positional changes, as shown on the right side. However, recording only the change in position is not ideal because it does not accurately represent the physical system. In reality, the position cannot change significantly from one time interval to the next. Additionally, this method does not provide information about the rotational velocity at which the joint should change position. On the other hand, continuous recording in small equidistant time intervals can result in a higher number of recorded values and, consequently, a longer time-series.

Figure 3.7 illustrates the rotational position of a rotary joint in radians. The left side of the figure illustrates the position recorded with equidistant fine grained time intervals, while the right side displays a time-series where only the destination positions and their corresponding times are recorded.

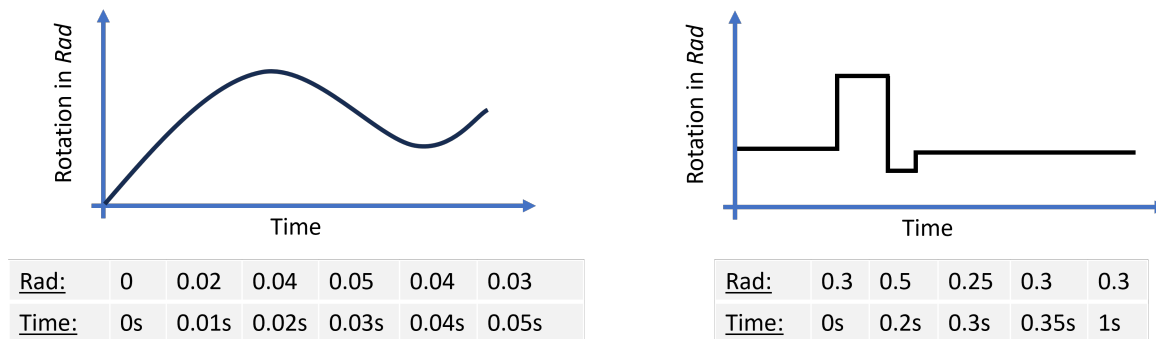


Figure 3.7: Two option for recording the joint position in a time-series

3.4.1 Total Joint Travel and Direction Changes

Parameters that can be analyzed without the need for any additional information include the number of direction changes and the total travel of a joint. The total travel can be determined by subtracting the position of two consecutive recorded points and summing up the absolute values. Furthermore, additional information can be derived by separately summing up the clockwise and counterclockwise rotations. By combining the absolute values of these rotations, the overall travel of the joint can be calculated.

Figure 3.8 provides a visual representation of the calculation of total travel. The total forward rotation can be determined by summing up the lengths of the green arrows, while the total backward rotation is obtained by summing up the lengths of the orange arrows.

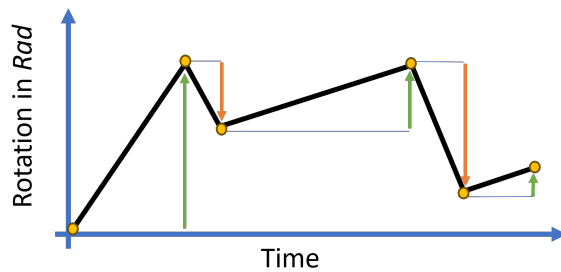


Figure 3.8: Summing up the rotation in the clockwise and anti-clockwise direction

The number of direction changes is a parameter that can be determined by analyzing the joint position alone, without the need for temporal information. This can be accomplished by identifying points where the position before and after either decreases or increases. However, it is important to note that this method may not be applicable to points where multiple positions are recorded at the same value consecutively.

To address the issue of multiple positions recorded at the same value, a potential solution is to introduce a tracking value that indicates whether the previous change in direction of two consecutive positions was either upward or downward. If the direction of two positions is

different from the tracking value, the direction change counter is incremented by 1. However, if the direction is the same as the previous points or if the positions are identical (neutral), the direction change counter and tracking values remain unchanged.

Figure 3.9 provides a visual representation of the points where the direction change counter is incremented.

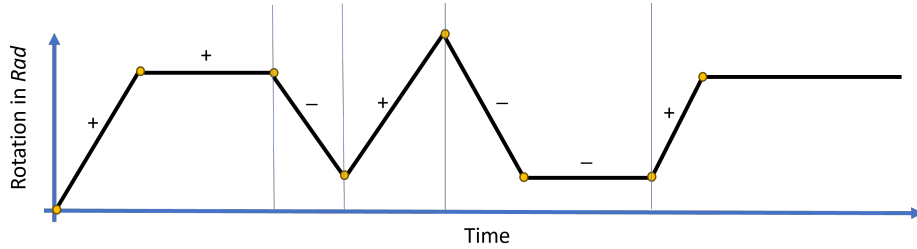


Figure 3.9: Calculating direction changes from a time-series

The counters for direction changes and total travel of each joint can be easily transformed into a local score, as explained in Chapter 3.3.2. This local score can then be multiplied by an importance factor to calculate the overall local score. The direction changes can be summed up over all joints, or they can be specifically grouped based on certain criteria or categories.

Table 3.3 provides an example of how a global score can be calculated based solely on the number of direction changes and total travel. The table illustrates how different joints and parameters can be weighted and grouped together to calculate the global score. By assigning different importance factors to each parameter, the overall global score can reflect the desired outcome. It is important to note that only the local scores are multiplied by the importance factor, not the actual counted direction changes or total travel values. This allows the local score to range from 0 to 100. In this example, due to the high local score and importance factor for the direction changes in joint 1, the overall global score is also very high. This clearly shows the significance of the importance factors in the calculation of the scores.

| Process Parameters | Local rating | Importance | Local score |
|-----------------------------------|--------------|------------|-------------|
| Direction changes in joint 1 | 95 | 0.7 | 66.5 |
| Direction changes in joint 2-6 | 45 | 0.1 | 4.5 |
| Total travel in joint 4 | 34 | 0.1 | 3.4 |
| Total travel in joint 1-3 and 5-6 | 46 | 0.1 | 4.6 |
| Global Score | | | 79 |

Table 3.3: Calculation of a score regarding only direction changes and total travel

In certain cases, adjusting the boundary conditions may not be sufficient to reduce the number of direction changes. It is important to note that having the same number of direction changes does not necessarily mean that two time-series are identical. Figure 3.10 visually demonstrates two time-series with the same number of direction changes but distinct characteristics.

To distinguish between these cases, the standard deviation can be utilized. By incorporating the standard deviation, toolpaths that result in frequent and closely spaced direction changes can be identified and are generally considered less desirable.

To combine the factor of standard deviation with the number of direction changes, they can be integrated into a single parameter. This can be achieved by dividing the number of direction changes by the standard deviation. By incorporating this calculation and the variation-approach, a local score can be determined. This approach provides an evaluation method that takes into account both the quantity of direction changes and the variability within the time-series data.

When there are only a few direction changes but with a high variance, the resulting parameter value will be low. Conversely, when there are numerous direction changes but with a low variance, the parameter value will be high.

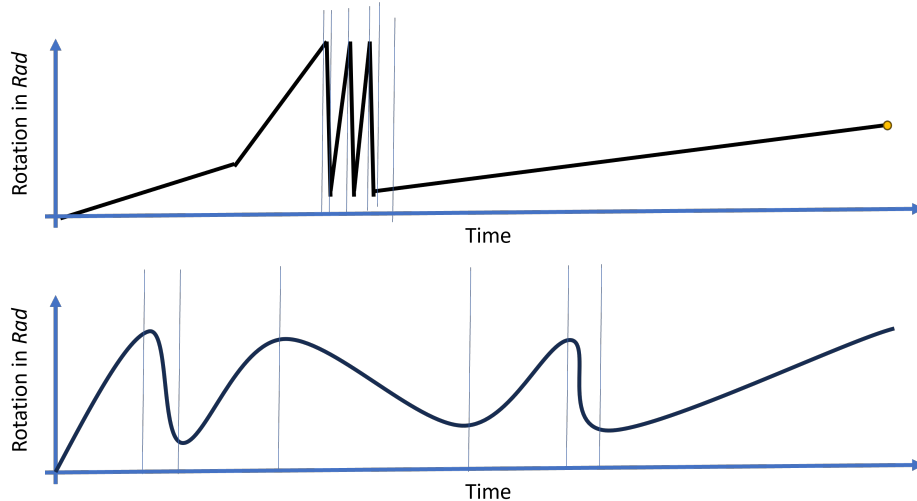


Figure 3.10: Two Time-Series with equal number of direction changes but different characteristics

3.4.2 Rotation Limits

Additionally, a straightforward analysis of rotational limits can be conducted, requiring knowledge of two distinct values. The first value is the physical limit that a joint cannot exceed, as surpassing this limit can cause significant damage to the robot. The second value relates to potential soft limits put in place to prevent over-rotation of the joint beyond its physical limits. To validate whether any rotational positions approach or exceed these limits, a simple comparison of all values can be performed. In cases where it is known that a joint is most

stable within a specific range, additional limits can be defined accordingly.

Once a toolpath with defined boundary conditions is established, the joint angles can be analyzed through a simple comparison process. If the joint positions exceed the soft limits or deviate excessively from the desired orientation, a "No-Go" exception is triggered. It is important to note that the analysis of rotation limits does not contribute to the calculation of the global score but serves as a validity assessment to determine if the required movement for the toolpath is physically feasible.

Figure 3.11 visually illustrates an example of how the analysis includes the hard and soft limits, as well as the desired position range, of a specific joint. If the limits are not exceeded, the toolpath with the set boundary conditions is deemed safe to be executed. At each time step, the amount by which the joint exceeds the desired area can be summed up to form a scalar value, which can then be used to calculate the local score. By doing so, the toolpath with the most optimal boundary conditions will ensure that the joint positions remain within the desired area.

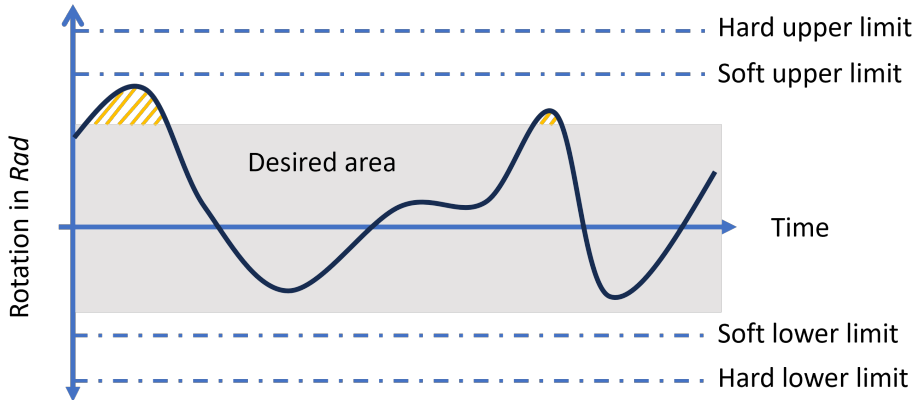


Figure 3.11

3.4.3 Velocity, Acceleration and Jerk of the Joints

To conduct a specific analysis of the rotational velocity, acceleration, and jerk of the joints, a time derivative needs to be applied. By performing simple comparisons of the time-series values, it becomes possible to determine whether the maximum capabilities of the motor driving the joint are being exceeded.

Figure 3.12 demonstrates how the velocity aspect can be transformed into a scalar value, which can then be utilized in the calculation of a local score. Firstly, the joint velocity is obtained by taking the time derivative of the joint position. Subsequently, an analysis is conducted to determine the duration for which the absolute velocity exceeds a certain threshold value. In the given example, the threshold is set at 80%.

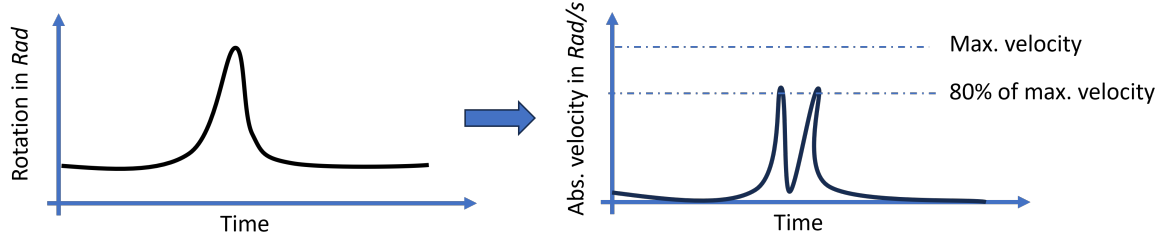


Figure 3.12: Calculating velocity from the joint position over time

Additionally, it is feasible to incorporate multiple thresholds and assign linear or exponential weights to them relative to each other. The combined outcome is then utilized to calculate the local score.

For example, if the 80%-threshold is exceeded for 15 seconds and the 90% threshold is exceeded for 5 seconds, the a scalar value is calculated by multiplying the corresponding time and threshold and summing them up. In this case the result is $80 * 15 + 90 * 5 = 1650$.

It is also possible to determine whether a short but significant peak over the threshold values is more desirable than a constant but small overstep. Figure 3.13 provides a visualization of these two cases. In the former case, where peaks are more desirable, it is sufficient to sum up the area between the velocity and the set threshold. If avoiding peaks is the top priority, all elements in the velocity time series can be cubed and summed up. By cubing the values, peaks will be exponentially weighted, making them easier to optimize for.

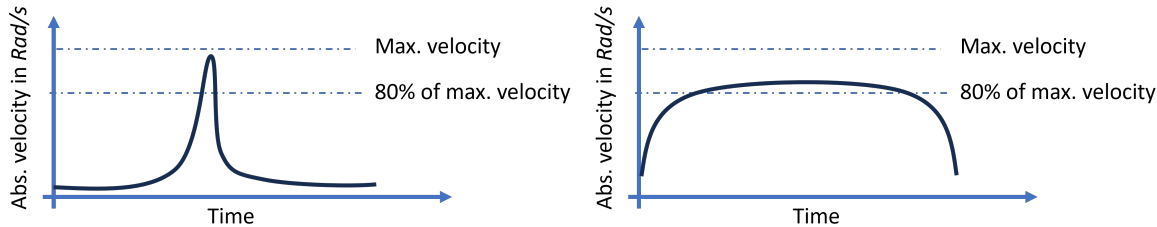


Figure 3.13: Overstepping the threshold value

The simplest approach, however, is to square all values and take the sum. This method eliminates the need to define threshold boundaries. Additionally, high peaks will have a greater impact on the resulting value compared to small, constant values, without overshadowing the final result.

If the velocity exceeds the maximum velocity, a "No-Go" exception must be triggered, indicating that the movement is not possible. The same rating principle can be applied to acceleration and jerk. Acceleration is obtained by taking the derivative of velocity, while jerk is obtained by taking the second derivative. Individual limits and thresholds can be set to determine the optimality of the robot's movement. If the maximum acceleration or jerk is exceeded, a "No-Go" error is also triggered.

Table 3.4 presents the calculation of a global score, which incorporates a weighting that prioritizes low acceleration in joint 2 and allows for high velocity in all joints. The acceleration in joint 1 and joints 3 to 6 are considered to be of lesser significance. The jerk is completely omitted from the rating in this example.

Due to the close-to-optimal acceleration in joint 2 and its high importance value, the overall score of the toolpath with the defined boundary condition is also very good.

| Process Parameters | Local rating | Importance | Local score |
|----------------------------------|--------------|------------|-------------|
| Velocity in Joints 1-6 | 45 | 0.1 | 4.5 |
| Accelerations in Joint 2 | 90 | 0.8 | 72 |
| Accelerations in Joint 1 and 3-6 | 15 | 0.1 | 1.5 |
| Jerk in joints 1-6 | 4 | 0 | 0 |
| Global Score | | | 78 |

Table 3.4: Calculation of a score regarding only velocity, acceleration and jerk

3.5 TCP Coordinates, Velocity and Acceleration

As discussed in Chapter 3.2.2, the forward kinematics approach allows for the calculation of the TCP's X-Y-Z coordinates and orientation. Alternatively, this information can be directly extracted from the G-code.

By calculating the time derivative of the positions, it is possible to determine both the velocity and acceleration of the TCP. These parameters play a significant role in milling applications, particularly when precise corners need to be fabricated. It is important to note that both robotic systems and CNC machines have limitations on their acceleration capabilities. As highlighted in Chapter 2.1.3, these limitations result in slight deviations occurring in the path, especially at corners. These deviations arise from the systems' inability to instantaneously change velocity or direction. Consequently, the TCP's path will not be perfectly followed as demanded by the G-Code and will exhibit minor variations in the corners.

To quantitatively analyze the magnitude and frequency of these deviations, it is crucial to examine the start and endpoints of the linear toolpath as defined in the G-code. When the endpoints are aligned along a vector in space, it indicates that no deviation from the desired toolpath is expected. However, a misalignment between the endpoints suggests an anticipated deviation.

Figure 3.14 gives a visual example of the position in the X-Y plane that the robot needs to traverse. The expected deviation is shown in red.

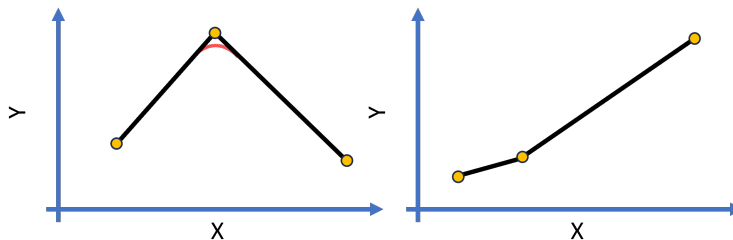


Figure 3.14: Deviation of the TCP from the actual toolpath

In order to obtain a qualitative estimate of the total deviation, it is necessary to additionally analyze the individual velocity vectors that characterize the toolpath. Perfect alignment of the velocity vectors indicates no expected deviation. However, as the angle between consecutive velocity vectors increases, the deviation also increases.

To quantitatively represent this information, the sine of each angle can be calculated and summed. An angle of 0 or 180 degrees will result in a value of 0, while an angle of 90 degrees will yield a value of 1. This scalar value provides an indication of the overall magnitude of the expected deviation.

Additionally, it is crucial to consider the magnitude or speed of the velocity vectors. In cases involving sharp corners with high velocities, the deviation is anticipated to be more significant compared to corners with lower velocities. To account for this, the result obtained from the sine calculation can be multiplied by the smaller of the two velocities.

This analysis is useful for operators in defining more optimal machining strategies (see Chapter 2.2.2). However, it is important to note that this analysis is separate from the optimization involving the redundant DoF.

In the context of WAAM, the acceleration of the welding torch plays a crucial role in the process. This is particularly evident when utilizing CMT technology, which involves wire retraction, as discussed in Chapter 2.1.2. A rapid acceleration of the welding torch can lead to unintended drop detachment and imprecise drop placement. Consequently, the quality and accuracy of the additive manufacturing process may be compromised, resulting in defects and deviations from the desired geometry.

However, it is worth noting that, similar to the deviation in the toolpath discussed earlier, this issue cannot be directly optimized by simply defining specific boundary conditions in the form of redundant DoF.

3.6 Energy Usage

Energy usage is a critical factor in modern manufacturing. To minimize unnecessary and energy-intensive movements, it is crucial to select appropriate boundary conditions for the additional constraint. The analysis of energy usage can be approached in two distinct ways.

Firstly, a continuous energy analysis allows for the attribution of specific energy consumption to each movement. This approach provides detailed insights into the energy usage of individual actions or operations. Secondly, considering the overall energy requirement throughout the entire manufacturing process provides a holistic perspective on energy utilization. This approach allows for optimizing energy usage and making informed decisions regarding energy efficiency in manufacturing.

3.6.1 Continuous Energy-Usage

Tracking energy consumption can be achieved through a straightforward method of monitoring the velocity and acceleration of individual joints. The energy demand is composed of two components: the rotational movement of a joint at a predetermined speed and the joint's acceleration.

To determine the energy consumed by each joint, the time-series data of joint velocity can be multiplied by the average energy consumption value associated with that particular joint. The same principle is applied to the time-series data of joint acceleration. By summing up these resultant time-series, an energy consumption profile for each joint can be obtained. The newly obtained time-series represent the energy consumption to move from one pose to another.

Aggregating the time-series data from all joints into one time-series provides an overall estimation of the robot's energy consumption. Table 3.5 gives exemplary values for the scaling factors.

| Joint Nr. | Velocity Scaling Factor in $\frac{\text{kWh}}{\text{m/sec}}$ | Acceleration Scaling Factor in $\frac{\text{kWh}}{\text{m/sec}^2}$ |
|-----------|--|--|
| Joint 1 | 0.1 | 0.5 |
| Joint 2 | 0.4 | 0.3 |
| Joint 3 | 0.3 | 0.2 |
| ... | ... | ... |

Table 3.5: Average scaling factors for energy calculations

This approach offers a notable advantage in its simplicity. Nevertheless, its primary limitation stems from the potential inaccuracies that may arise when working with an average scaling value. If this value is derived by averaging all possible positions, but only a limited number of positions are actually traversed by the robot, significant discrepancies can occur.

To address these limitations, more advanced approaches are necessary. For instance, the utilization of multi-body simulations (MBS) in CAM software enables a direct analysis of the exact energy requirements for a robot to move between different poses. This method requires precise modeling of weight distribution to achieve accurate outcomes. However, it is

important to consider that implementing this approach may require substantial computation and development time.

Another viable option to consider, is the utilization of a machine learning (ML) approach for estimating energy consumption during transitions between discrete poses. By employing a supervised learning technique, where the input data includes the current joint positions and velocities as well as the target pose, an ML model can be trained to predict the energy required for each transition. This approach offers the advantage of leveraging ML algorithms to provide accurate energy consumption estimates in a more efficient manner. However, it is important to acknowledge that generating high-quality training data and training the ML model can be time-intensive processes.

Figure 3.15 illustrates the three aforementioned options along with their key requirements. It is important to note that these examples only give an excerpt on how to get a energy estimation and do not cover all possible solutions to address this problem.

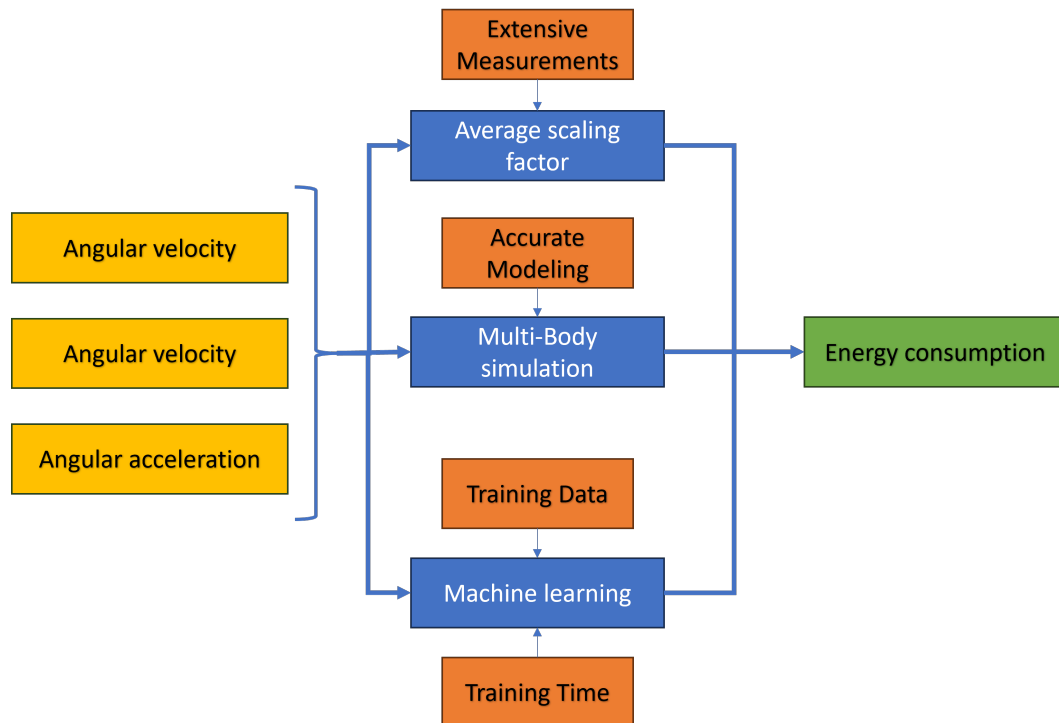


Figure 3.15: Exemplary methods for energy usage calculations

Once the time-series data for energy consumption is obtained, it becomes possible to identify peaks and associate them with specific movements. In line with the optimization objective, it is also feasible to establish threshold values, as discussed in Chapter 3.5, to optimize for a constant energy consumption.

3.6.2 Total Energy-Usage

When the aim is to obtain a single scalar value for energy consumption, the same procedures outlined in the preceding chapter can be applied, and the values from the time-series can be aggregated through summation.

In situations where the temporal information in energy consumption is considered irrelevant, alternative ML approaches can be employed. For example, Recurrent Neural Networks (RNNs) can be utilized, as they have the ability to take an entire time-series as input and generate a scalar value representing the total energy consumption. RNNs excel at capturing dependencies and patterns in sequential data. By training an RNN model using a time-series dataset, it can learn to predict the total energy consumption based on the provided input. However, it is important to note that, like most ML approaches, this method requires substantial effort and time for generating training data and conducting the training process.

In WAAM, it is important to consider the energy consumption associated with the welding process itself. The determination of energy use in welding involves various factors. The G-code, which comprises instructions for the welding process, can provide information on the wire-feed, voltage and the desired power input. By analyzing this code, it becomes possible to estimate the energy consumption during each welding operation. Alternatively, these parameters are often pre-defined as constants on the welding appliance, with the G-code solely specifying the turn-on and turn-off points. Figure 3.16 gives an example on how the turn-on and turn-off points can look in the G-code.

```
N10 WAAMSTART; - starts welding process
N20 G1 X=-19.988 Y=49.221 Z=56. A=0.0 B=0.0 C=10.0
N30 G1 X=-19.988 Y=46.19 Z=56. A=0.0 B=0.0 C=10.0
N40 G1 X=-19.988 Y=44.371 Z=56. A=0.0 B=0.0 C=10.0
N50 G1 X=-19.988 Y=41.34 Z=56. A=0.0 B=0.0 C=10.0
N60 G1 X=-19.988 Y=39.521 Z=56. A=0.0 B=0.0 C=10.0
N70 WAAMEND; - ends welding process
```

Figure 3.16: Turn-on and turn-off points in the G-code used in WAAM

In addition to the factors mentioned earlier, the duration of the welding process and the parameters of the welding equipment play crucial roles in determining energy consumption. By considering these factors, it is possible to accurately assess the energy usage during welding operations.

However, this specific part of the total energy consumption cannot be optimized by defining the boundary conditions of redundant DoFs. The energy required for the welding process is solely defined by the welding parameters and the final part geometry.

3.7 Reach, Singularities and Torch Orientation

The following discusses the robot poses with respect to reach and positioning, singularity avoidance, and torch orientation. These factors are essential in ensuring successful and efficient robotic operations.

3.7.1 Reach and Orientation

As mentioned in Chapter 3.2.2, the analysis of the reachability index can be conducted in various formats. The first format involves a simple analysis to determine if all the points that the robot needs to traverse lie within its work volume, without any self-collisions or exceeding the soft and hard joint limits. This aspect is closely related to the joint limits, as discussed in Chapter 3.4.2.

Additionally, it is necessary to analyze that there are no collisions between the robot and the workpiece. If all these parameters are met, a binary index can be used to indicate the feasibility and safety of executing the program. However, this index cannot be used for optimizing the robot's movement, as the parameters influencing this index are mostly defined by the G-Code.

When utilizing a robotic system with a specific tool, such as a milling spindle or a welding torch for WAAM, it is crucial to consider the boundary conditions associated with that tool.

Figure 3.17 illustrates a case where the rotation around the Z-axis of the welding torch can be manually defined. Each position leads to different strains on the wire-feed system and power-cables.

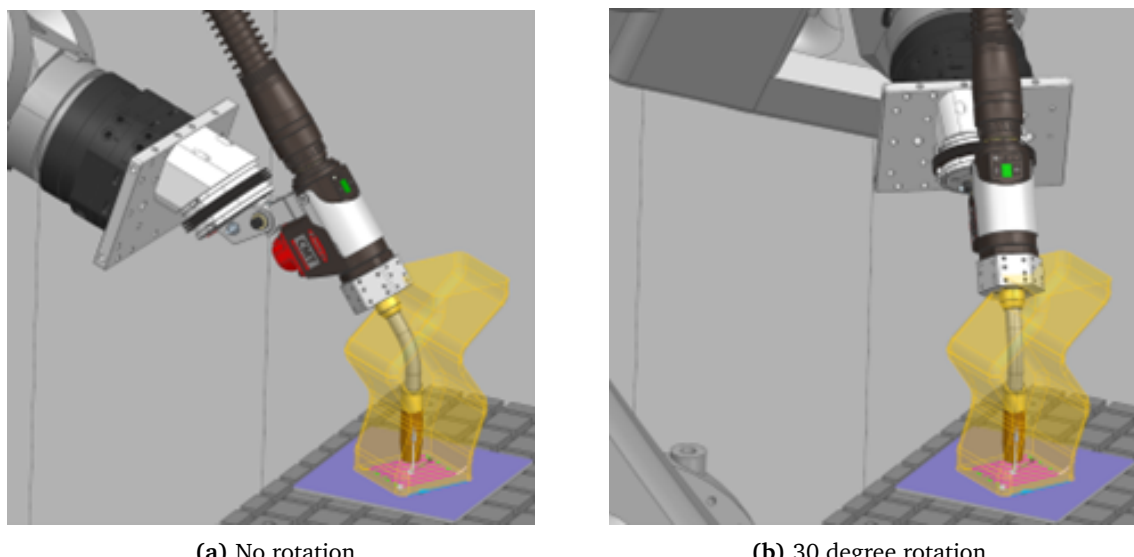


Figure 3.17: Rotation around the C-axis of a welding torch

In many cases, the spindle and welding torch come with cables that provide power from an external power supply. These cables have an optimal orientation where bending and wear are minimized. By positioning the cables in an optimal orientation, the robotic system can operate efficiently and effectively without any interference or limitations due to cable movement, potential damage, or excessive bending or twisting.

To assess the optimality of the robot's cable pose, it is important to consider additional parameters. In certain cases, it is preferable to route the cables in a specific orientation along a spatial vector, allowing for parallel translation or movement in the direction of that vector. In this case, the angle between the planes of the robot's base coordinate system and the optimal translation vector remains constant.

Figure 3.18a provides a visual representation of this example. The wire, shown in red, has an optimal orientation where the least amount of strain is present. Any position along that vector where the cable transitions to the welding torch tangentially is considered optimal. It is worth noting that this vector can be translated parallel in space while still maintaining its optimal status.

In other scenarios, it is more optimal to route the cables towards a specific point in space, such as a mounting point on a wall or ceiling. Figure 3.18b illustrates an example where the optimal orientation of a milling spindle is directed towards a designated point where the cables originate. In this case, any position is considered optimal as long as the extended spindle vector aligns with the vanishing point.

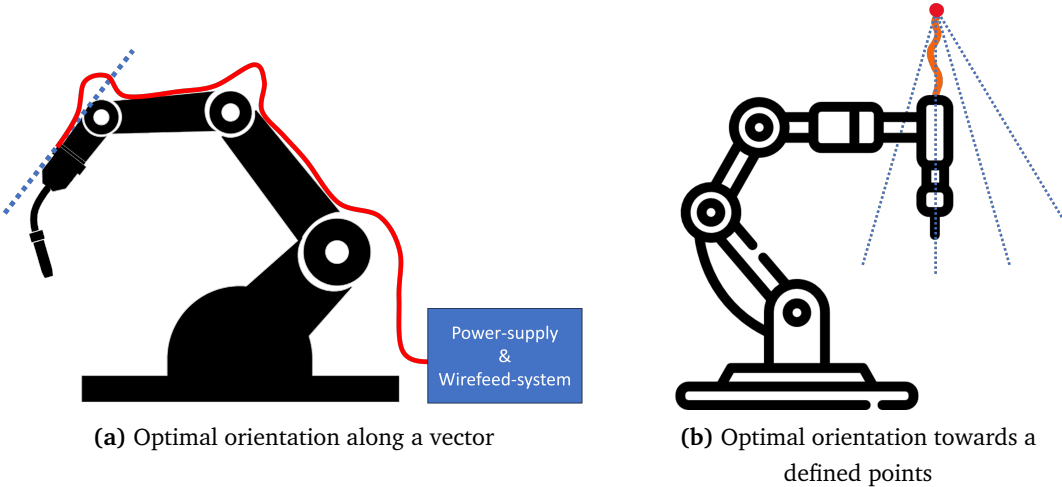


Figure 3.18: Two examples for optimal orientation along a vector in 2D

To minimize the deviation from the optimal vector or vanishing point, the redundant degrees of freedom can be utilized. One approach is to analyze the deviation and track it over time, creating a time-series. Each element in this time-series can be squared or cubed, depending on the weight assigned to small and constant deviations versus large but short offsets. The time-series is then summed up to form a scalar value, which can be used to calculate the local score through the variation method.

Figure 3.19 illustrates an example of how the scalar value is calculated. It is evident that when cubing the time series, more importance is placed on the larger deviations rather than small deviations.

| <u>Deviation in degrees:</u> | 1° | 2° | 2° | 2° | 3° | 10° | 0° | 2° | |
|------------------------------|----|----|----|----|----|------|----|----|------------------|
| Squared: | 1 | 4 | 4 | 4 | 9 | 100 | 0 | 4 | <u>Sum:</u> 126 |
| Cubed: | 1 | 8 | 8 | 8 | 27 | 1000 | 0 | 8 | <u>Sum:</u> 1060 |

Figure 3.19: From time-series of the deviation vector to scalar value

3.7.2 Singularities

In Chapter 2.4.1, the concept of singularities in robotic systems is discussed. Singularities occur when the robot's joints align in a way that limits its motion by reducing one or more DoF. To avoid singularities, it is important to optimize the boundary conditions in the redundant DoF. The singularity analysis, as described in Table 3.1, can be represented either as a scalar value or as a time series that classifies each position based on its proximity to a singularity.

The scalar value can represent the overall smallest eigenvalue of every Jacobi matrix. For this, every pose needs to be analyzed. After calculating the Jacobi matrix, all eigenvalues encountered are examined, and only the smallest one is recorded and used to calculate the local score. This approach allows for an analysis of the overall toolpath rather than specific poses.

Alternatively, a time-series can be used where the determinant, not the eigenvalues, is recorded and stored. By analyzing this time series, it becomes possible to directly associate the robot's movements with its proximity to a singularity. This enables a more precise understanding of where the robot's motions are close to a singularity, allowing for subsequent optimizations. To transform the time series into a scalar value, the same threshold method described in Chapter 3.4.3 can be applied.

3.7.3 Torch Orientation in WAAM

The torch orientation parameter in WAAM, similar to the cable routing orientation parameter, analyzes the angle at which the welding torch is positioned during the process. This parameter is specific to WAAM and ensures that the torch is at the optimal angle for welding. Achieving material deposition in the direction of gravity is crucial for obtaining the best results. The orientation of the TCP, which represents the welding torch tip, can be determined either through the forward kinematics approach or by extracting it directly from the G-code.

In both the forward kinematics approach and the G-code, the rotation is described as the rotation A, B, and C around the axes. However, the necessary information for torch orientation

is simply the angle between the tilted Z-axis of the tool and the vector of gravity. To obtain this information, a dot product is performed between the rotation matrix and the Z-axis of the base coordinate system. This yields a vector corresponding to the tilted Z-axis of the tool. The enclosed angle can then be calculated using the scalar product. This step assumes that the defined base coordinate system is oriented in a way that aligns the Z-axis parallel to the gravity vector.

Figure 3.20 gives a visual example in 2D on how the Z-axis of the tool is deviating from the vector of gravity.

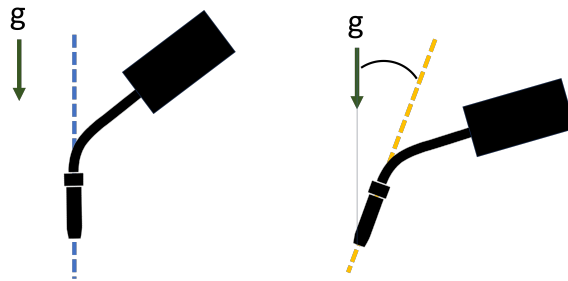


Figure 3.20: Example of non-optimal tilt in the welding torch

To quantify the torch orientation parameter, it is recorded in a time-series format. To obtain a scalar value for this parameter, all the values can be squared, cubed, or subjected to other mathematical operations, and then summed up. This process is similar to the one described in Chapter 3.7.1 for the cable routing orientation parameter.

3.8 Summery for Boundary Condition Evaluation

Image 3.21 gives a summary and visual representation in form of a flowchart on how a toolpath with defined boundary conditions is evaluated by calculating the individual local scores for the process parameters that can be optimized by the redundant DoF.

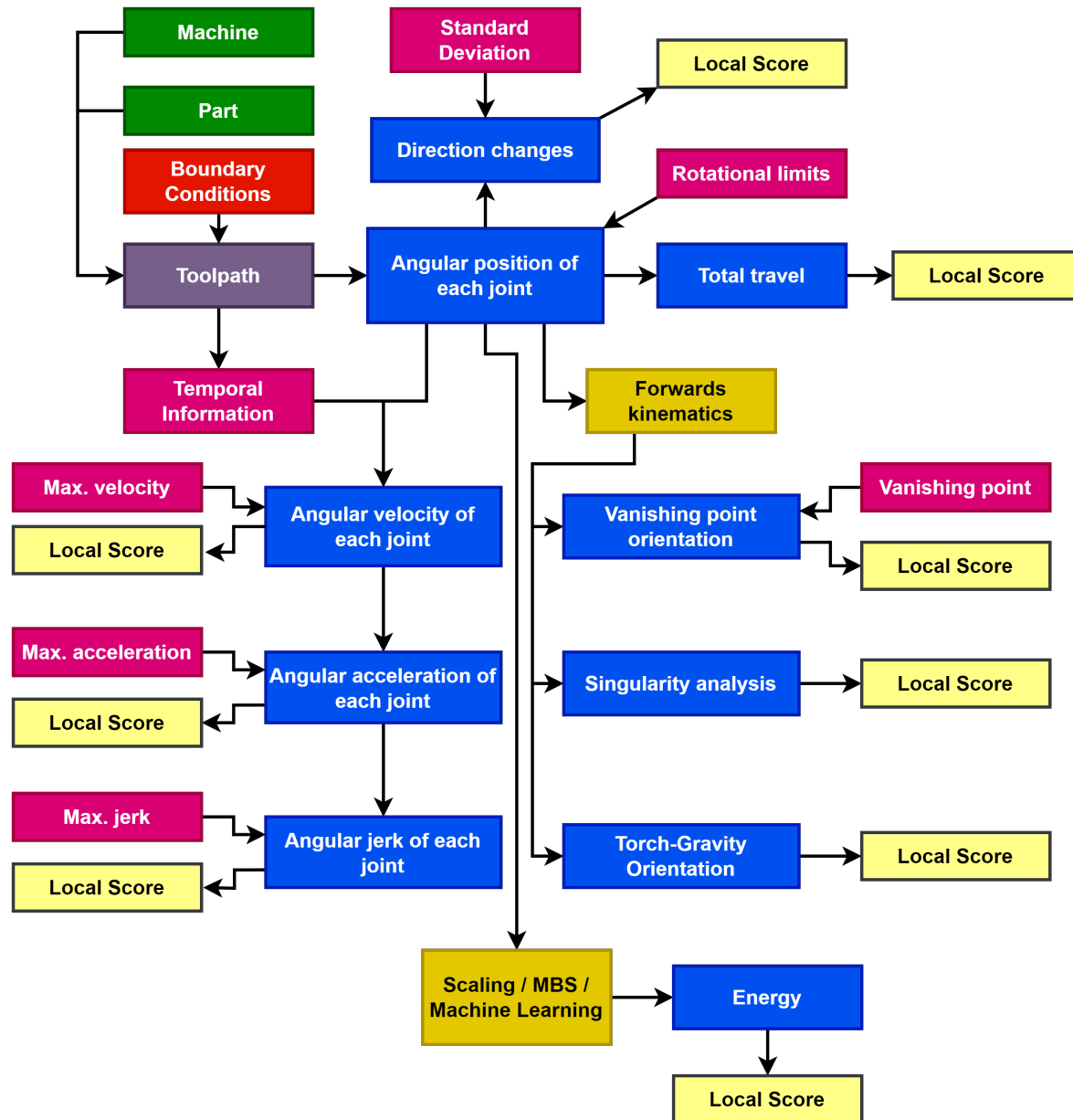


Figure 3.21: x

The local scores are then summed up to create the global score. It is important to note that multiple boundary conditions must be analyzed when calculating local scores.

Figure 3.22 illustrates how a boundary condition for a toolpath can be evaluated. In this case, the toolpath is defined using only 5 DoF, including X-Y-Z coordinates and rotation around the X- and Y-Axis. However, the rotation C around the Z-Axis, which is the axis of symmetry for

the tool, is not defined and must be specified manually.

Once this boundary condition is established, the joint positions are analyzed and individual parameters, such as direction changes, can be extracted. In this example, the objective is to assess the optimality of a rotation angle of zero degrees. To calculate a local score, additional variations of the rotation around the C-Axis are analyzed. With the help of user-defined weights, the local scores are weighted and summed up to form the global score for the boundary condition.

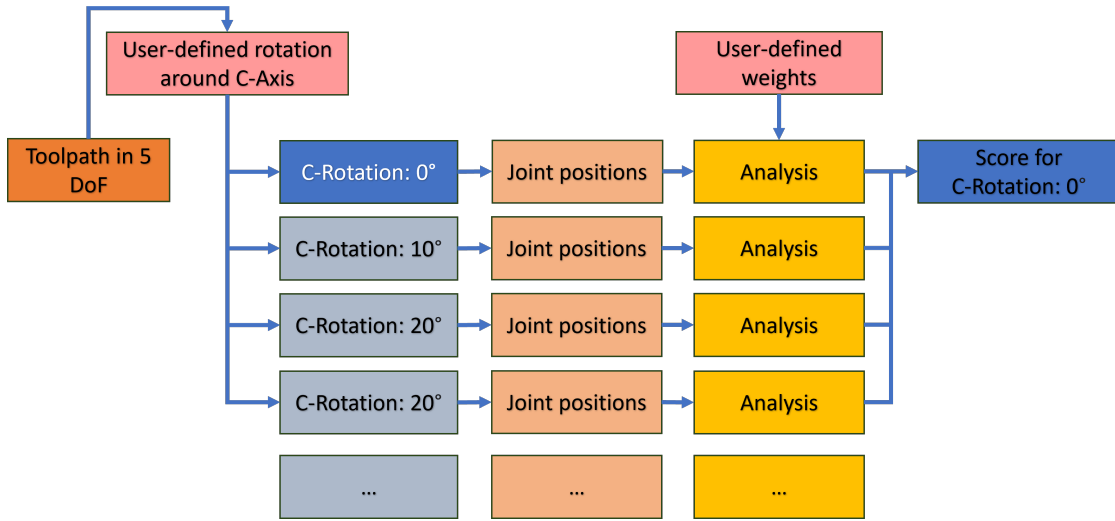


Figure 3.22: Process of evaluating a defined boundary condition

3.9 General Methodology for Process Optimization

So far only the analysis of a toolpath with set boundary conditions is discussed. In the following sections, two methods for optimizing boundary conditions towards a specific goal is presented. The main difference between these two methods lies in the different incorporation of a CAM software.

It is important to note that optimizing certain process parameters may have a direct negative impact on others. For example, optimizing the tools orientation towards a specific vanishing point can significantly increase the total number of direction changes in the joints. Therefore, the user must be aware of these cross-influences and adjust the weights accordingly.

3.9.1 Optimization Loop without CAM-software

Figure 3.23 illustrates the process of optimizing the redundant DoF based on a predefined goal determined by weighing the process parameters. In this method, the part and the robot are fixed components that are loaded into the CAM software. Before generating a toolpath, the redundant DoF must be set manually. These constraints can be set flexibly, as long as they do not lead to any "No-Go" exceptions caused by collisions or exceeding the joint limits.

When the toolpath is generated, it is defined in all available DoF. To evaluate the set boundary conditions, the redundant DoF is varied, resulting in multiple toolpaths. In some cases, this variation simply involves varying the rotation around the Z-Axis, while keeping all the coordinates (X-Y-Z) defined in the G-code unchanged.

In other cases, the redundant DoFs involve the rotation and tilt of a rotary-tilt table. In such situations, every single point in the G-code needs to be rotated around the origin or the rotary-tilt table.

After obtaining the multiple toolpaths, each one is subjected to an inverse kinematics algorithm. This algorithm utilizes the robot's parameters, such as arm length and joint sequence, to calculate the joint positions for every point. From these values, the score of the originally set boundary condition can be determined.

Following the score calculation, an optimization algorithm is employed to generate a new boundary condition for the redundant DoF. This cycle of optimization continues either for a predetermined number of iterations or a specified duration. Alternatively, a desired minimal score can be defined as the target that the toolpath needs to achieve.

Once the most optimal or close-to-optimal boundary condition is found, it is used as input for the CAM software to validate that no collisions or other exceptions are triggered. After this validation process, the G-code can be utilized in production.

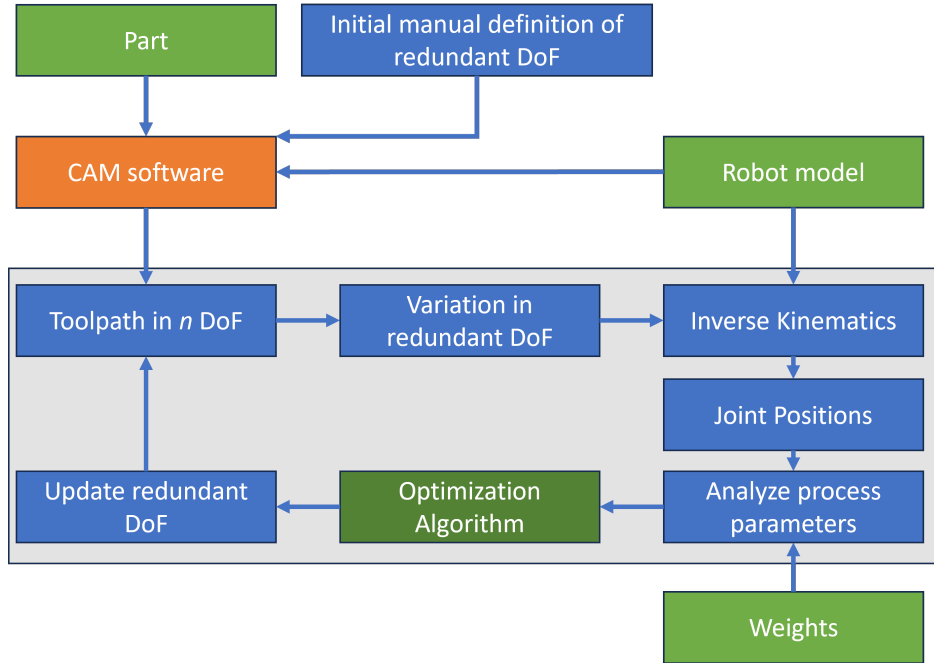


Figure 3.23: Schematic process of optimization without CAM software

In this method, the optimization of boundary conditions occurs externally to the CAM software. The CAM software is solely utilized for generating the initial toolpath and validating the most optimal boundary condition. The inverse kinematics process is performed outside of the CAM software and can be implemented in various programming languages such as Python or C++. The same is applicable to the optimization algorithm.

The advantage of this approach is that the external algorithms are independent and can be easily exchanged or modified. It does not necessitate in-depth knowledge or access to the source code of the CAM software. Therefore, any CAM software can be utilized with this approach, providing flexibility and compatibility.

However, it is important to note that one drawback of this approach is that the complete closure of the loop can only be achieved if the most optimal boundary condition can be automatically fed back to the CAM software for the final validation. If there is no Application Programming Interface (API) available or accessible for the CAM software, this step may need to be performed manually. This manual intervention can introduce additional time and effort into the optimization process.

Depending on the chosen optimization algorithm, it may be necessary to calculate multiple scores for multiple boundary conditions before generating a new suggestion. In this scenario, the variations in the redundant DoF can be utilized to calculate multiple scores relative to each other. These scores can then be used as input for the optimization algorithm, allowing for a more comprehensive evaluation and selection of the most optimal boundary condition. By considering multiple scores, the algorithm can effectively explore different possibilities and make informed suggestions for improving the boundary conditions.

Figure 3.24 illustrates the process of varying a simple toolpath. In this specific example, the toolpath is defined in six DoF, with the redundant DoF being the rotation around the Z-axis. Initially, the toolpath is set at its original configuration with C = 0.0.

To explore different possibilities, three variations of the toolpath are created by incrementing the rotation by 5 degrees for each variation. These variations allow for an examination of the impact of different orientations on the overall process. By systematically adjusting the rotation, the algorithm can evaluate the performance of each variation.

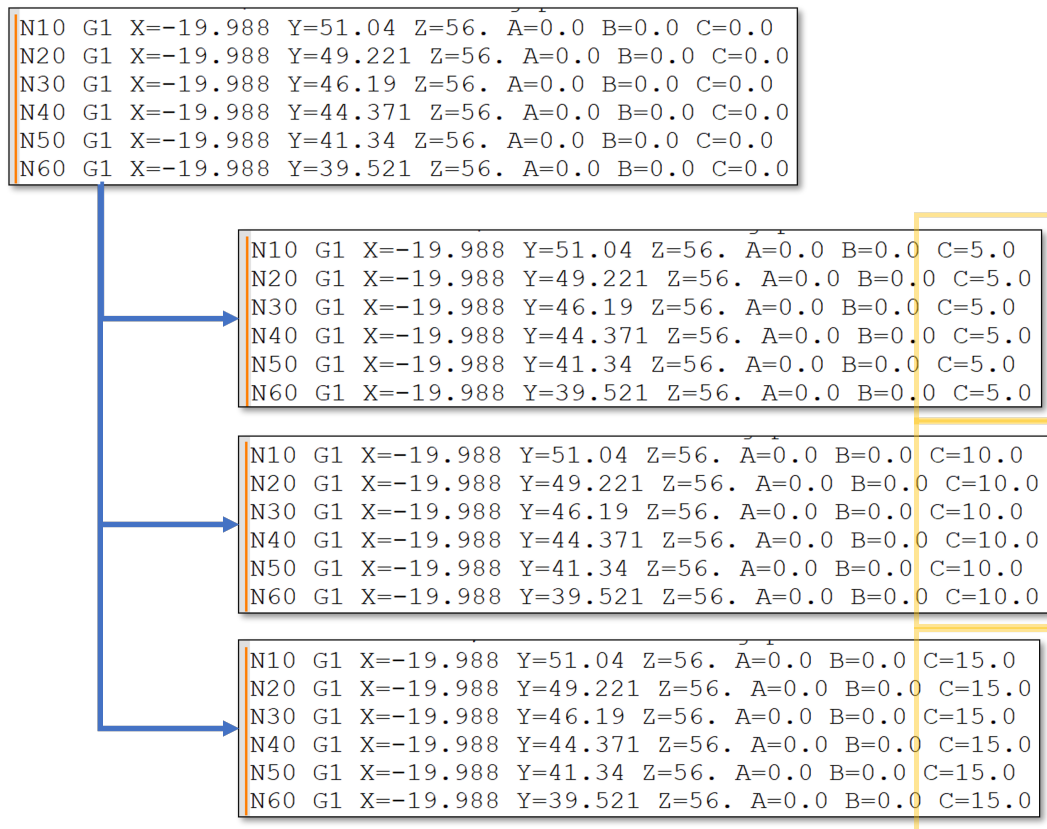


Figure 3.24: Variation of the redundant DoF in the G-code

3.9.2 Optimization Loop with CAM-software

The previously mentioned method in Chapter 3.9.1 described a process that does not involve a CAM software within the optimization loop. However, another method can be employed that directly incorporates a CAM software into the optimization process.

By directly including the CAM software, the optimization loop becomes more tightly integrated, enabling seamless feedback and iteration between the toolpath generation and the optimization of redundant DoF. This approach can significantly enhance the overall optimization process and improve the quality and efficiency of the final toolpath.

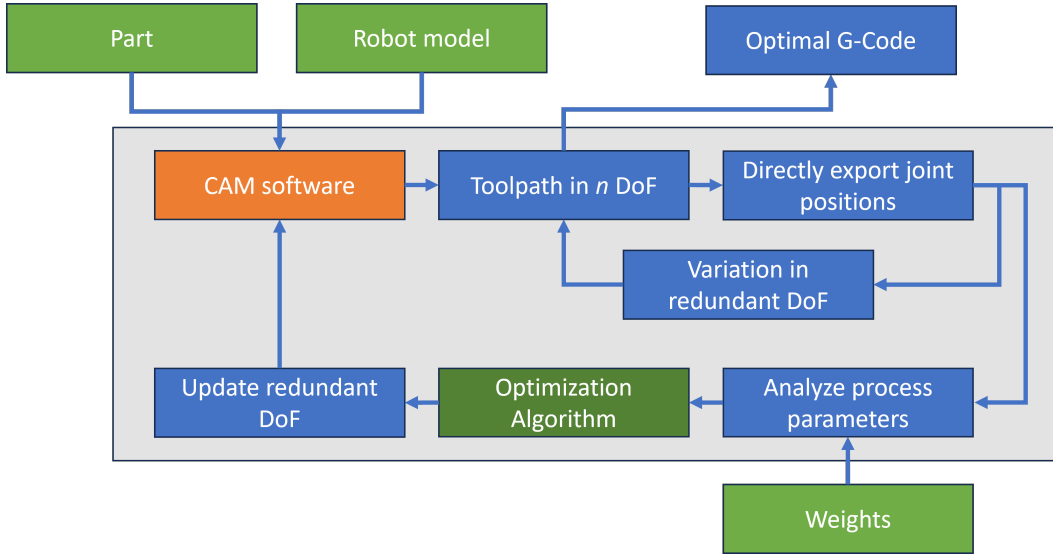


Figure 3.25: Schematic process of optimization with CAM software in the loop

In this method, the CAM software plays a crucial role in the optimization process. It first generates the initial toolpath by automatically setting the redundant DoF based on the given part geometry and robot configuration. Unlike traditional approaches, the CAM software does not export G-code but utilizes its internal resources and algorithms to calculate the joint positions via inverse kinematics.

The optimization process is performed iteratively, involving multiple variations in the redundant DoF. Each variation generates a different toolpath, which in turn results in different joint positions of the robot. The process parameters are then analyzed to calculate a score that represents the quality of the toolpath.

The optimization algorithm, seamlessly integrated within the CAM software, utilizes the obtained scores to propose a new setting for the redundant DoF. This new setting aims to improve the toolpath and optimize the process parameters further. The iteration continues until a defined score or a predetermined number of iterations is reached, indicating that the optimization loop has converged. Once the optimization loop is terminated, the CAM software exports the G-code with the best-found boundary conditions, representing the optimized toolpath.

The advantage of this approach lies in leveraging the CAM software's specialized capabilities and features for toolpath generation and optimization. By directly integrating with the software, the optimization process becomes more efficient and streamlined, eliminating the need for external scripts or algorithms.

However, a significant disadvantage of this method is the requirement for access to the source code of the CAM software to add the optimization algorithm and the specific post-processor that calculates the joint positions. Adding the necessary features and functionalities necessitates modifying the software, which may not be feasible or practical in all situations. In this case the method has to be implemented by the provider of the CAM software.

Chapter 4

Implementation and Validation

The first step of the validation process involves constructing a basic model that captures the kinematics and dynamics of an industrial robot. To test the method in a simple case, initial tests are performed on a 6-DoF model with a 5-DoF toolpath. The sixth DoF, which represents rotation around the Z-axis, is freely defined and used for optimization purposes. After successfully validating this simple model, an additional redundant DoF is introduced in the form of a rotary-tilt table.

Once the basic mathematical model is established, an optimization algorithm is implemented to determine the optimal values for each parameter associated with the redundant DoF. These methods and optimization algorithms take into account the specific objectives and constraints of the industrial robot, such as minimizing direction changes or joint accelerations.

4.1 Simple Implementation

4.1.1 Modeling a 6-DoF robot

To test the proposed method, a simplified articulated 6-DoF industrial robot is utilized as a model. A visual representation of this robot can be seen in Figure 4.1. The Denavit-Hartenberg (DH) parameters for this robot are provided in Table 4.1.

| | Values |
|-------|----------------------------|
| a | [200, 900, 150, 0, 150, 0] |
| alpha | [90, 0, 90, -90, 90, -90] |
| d | [600 0, 0, 800, 0, 200] |

Table 4.1: DH-parameters for the modeled robot

These parameters are essential for describing the geometry and kinematics of a robotic arm. They establish the relationship between adjacent links in the robot's kinematic chain. The DH

parameters consist of various values, including link lengths, link twists, and link offsets. In this particular model, "a" represents the link lengths between adjacent joints, "alpha" represents the link twists or rotations around the Z-axis between adjacent joints, and "d" represents the link offsets or distances along the Z-axis between adjacent joints.

It is worth noting that the last rotation is defined in the negative direction. This convention is employed to ensure that the end of the final joint can be interpreted as the tip of a tool without requiring additional transformations.

Figure 4.1 portrays the robot modeled using Python. The joint positions, in degrees, are as follows: [2, 75, -45, -88, -91, 61], corresponding to joints 1 to 6, respectively.

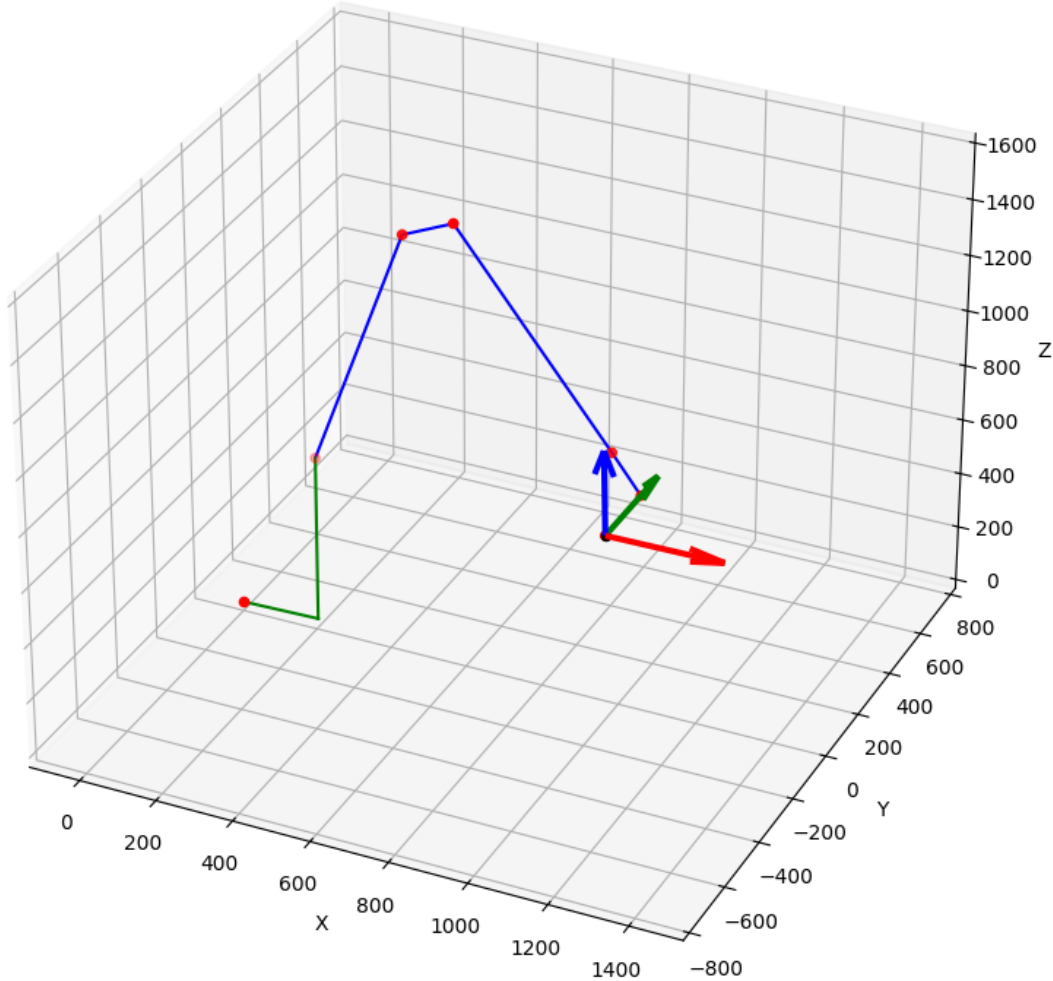


Figure 4.1: Visualization of the modeled robot

The arrows depicted in the figure represent the coordinate axes of the TCP. For simplicity, the TCP is considered to be the endpoint of the last joint. The X-axis is denoted in red, while the Y-axis and Z-axis are represented by the colors green and blue, respectively. The first link, originating from the point $X=0$, $Y=0$, $Z=0$, is displayed in green.

The schematic of the modeled robot can be observed in Figure 4.2. In this specific configura-

tion, all joints are in their initial position with no rotation applied.

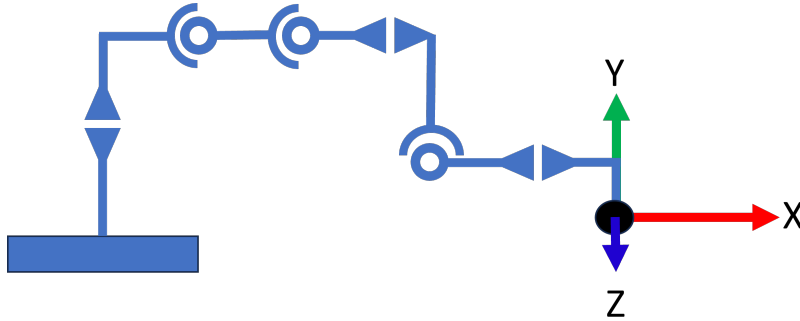


Figure 4.2: Schematics of the modeled robot

4.1.2 Modeling a basic Toolpath

Before analyzing the process parameters, it is necessary to define a toolpath for the TCP to follow. In this case, three options are presented, each consisting of 3000 coordinates. It should be noted that the redundant degree of freedom in these cases is the rotation around the Z-axis. This rotation will be adjusted to determine the optimal value for the desired outcome.

The first toolpath, depicted in Figure 4.3, represents a converging-diverging spiral. Figure 4.4 illustrates a converging infinity-loop, and Figure 4.5 displays a forward-moving sinusoidal curve.

The corresponding equations for these toolpaths are given by Equation 4.1, Equation 4.2, and Equation 4.3. The variable *iter* ranges from 0 to 3000 and is used to calculate the X, Y, and Z coordinates. Trigonometric functions are employed using the *Numpy* library. Currently, no rotation (A, B, or C) has been defined. Only the coordinates are specified. Each toolpath has specific dimensions and characteristics. Toolpaths 1 and 2 are continuous, while toolpath 3 exhibits abrupt changes in direction. Only toolpath 1 possesses rotational symmetry.

$$\begin{aligned} x &= \text{np.cos}(\text{np.deg2rad}(iter)) * (500 - iter/3) \\ y &= \text{np.sin}(\text{np.deg2rad}(iter)) * (500 - iter/3) \\ z &= iter/10 \end{aligned} \tag{4.1}$$

$$\begin{aligned} x &= \text{np.sin}(\text{np.deg2rad}(iter)) * (400 - iter/5) \\ y &= \text{np.sin}(\text{np.deg2rad}(iter)) * \text{np.cos}(\text{np.deg2rad}(iter)) * (500 - iter/6) \\ z &= iter/10 \end{aligned} \tag{4.2}$$

$$\begin{aligned}
 x &= np.sin(np.deg2rad(iter)) * 200 \\
 y &= iter / 3 - (2500 / 6) \\
 z &= np.sin(np.deg2rad(x)) * 100
 \end{aligned} \tag{4.3}$$

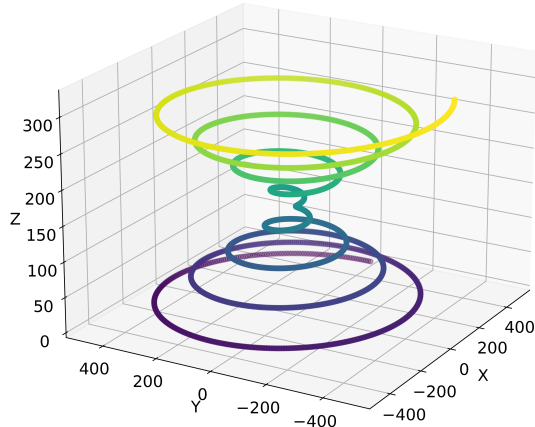


Figure 4.3: Toolpath 1: Converging-Diverging Spiral

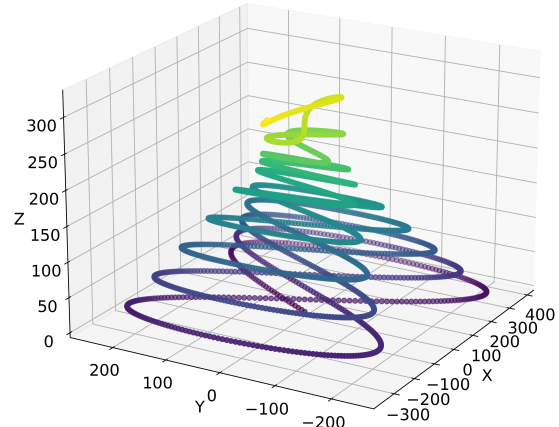


Figure 4.4: Toolpath 2: Converging Loop

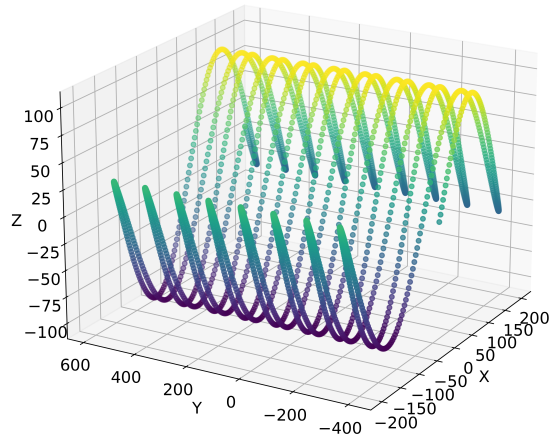


Figure 4.5: Toolpath 3: Pendulum Oscillation

Figure 4.6 illustrates the robot and Toolpath 1 (defined by Equation 4.1) at the toolpath's final position. The origin of the toolpath is shifted by X=1000 and Z=600 relative to the robot's coordinate system. No rotations are applied around the X, Y, and Z axes, resulting in A, B, and C being zero. Thus, the coordinate axes of the toolpath are parallel to the axes of the robot's coordinate system.

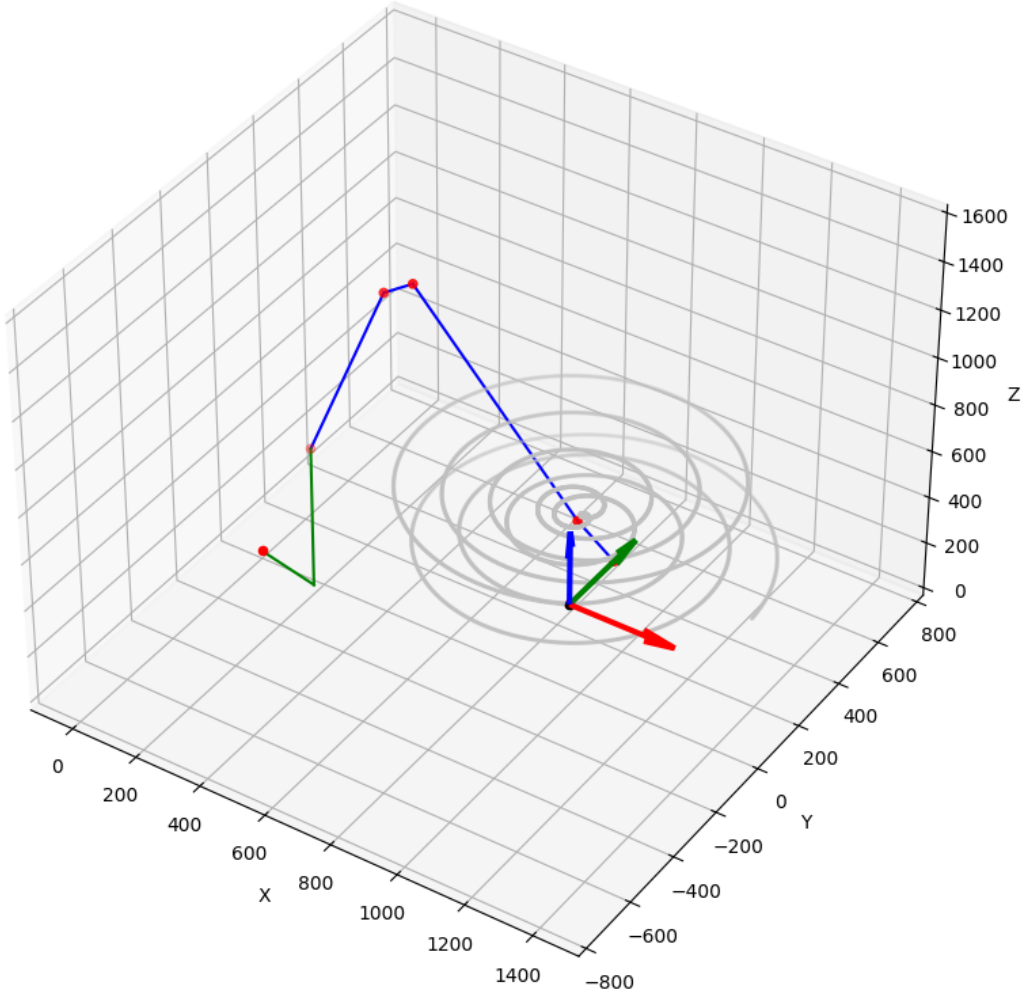


Figure 4.6: Toolpath 1 with robot model

4.1.3 Extracting process parameters

Using the inverse kinematics algorithm from the Python library *visual_kinematics*, the joint angles for each coordinate can be computed. To achieve this, the rotations A, B, and C need to be defined. The result is a time series that contains the corresponding joint positions. Currently, all coordinates must be traversed in equidistant time steps. With this information, it becomes possible to calculate the velocity and other related parameters. By transforming all the data from the time series into scalar values and calculating the local score, the global score can be determined.

4.2 Testing and Validation

4.2.1 Toolpath Evaluation with one Redundant DoF

As discussed in Chapter 4.1.2, the toolpath remains constant with respect to the X-Y-Z coordinates. The fixed boundary conditions for the robot are that there are no rotations around the X and Y axes, resulting in A and B both being equal to zero. The user has the ability to set the degree of freedom for the rotation around the Z-axis, which is the redundant degree of freedom. Figure 4.7 displays the variation of each joint over time for toolpath 1. In this specific case, the rotations A, B, and C are all set to 0. The entire toolpath is traversed in 300 seconds.

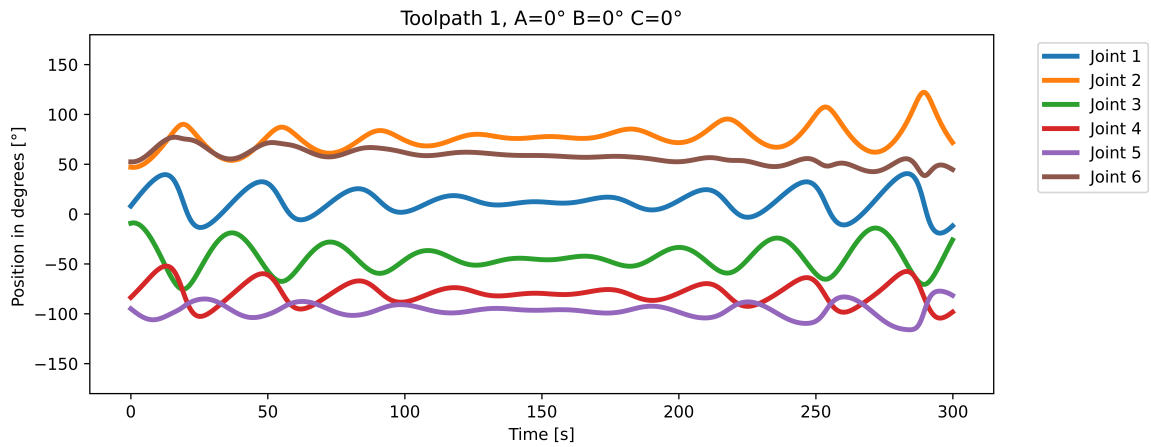


Figure 4.7: Visualization of the joint positions over time for toolpath 1 with C=0

Figure 4.8 depicts the joint positions over time for the toolpath with a 45° rotation around the Z-axis ($C = 45^\circ$). It is noticeable that joint 4 and joint 5 have undergone changes in their respective ranges. Furthermore, joint 6 exhibits a significantly larger amplitude towards the end of the toolpath, in comparison to the case with no rotation ($C=0$).

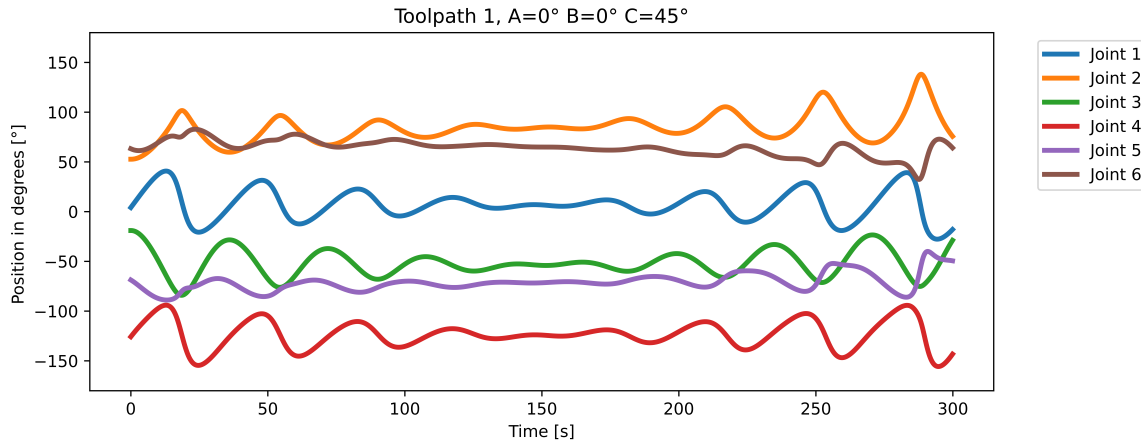


Figure 4.8: Visualization of the joint positions over time for toolpath 1 with $C=45^\circ$

Figure 4.7 illustrates the variations in each joint over time for toolpath 2 (Eq. 4.2) without any rotation. Unlike toolpath 1, the amplitudes notably decrease towards the end of the toolpath. This observation aligns with the unique characteristics of different toolpaths.

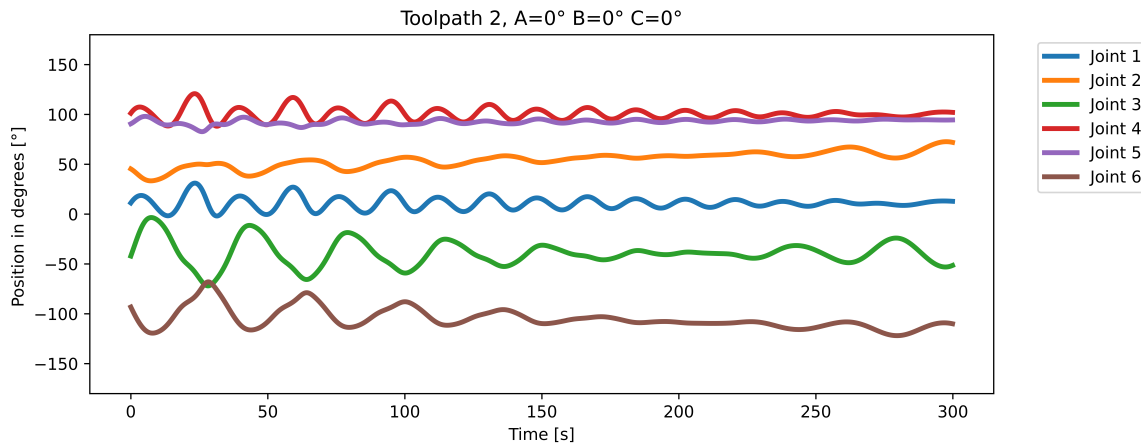


Figure 4.9: Visualization of the joint positions over time for toolpath 2

The next step involves selecting the process parameters of interest and assigning weights to each parameter. For that, a basic case is discussed. The selected process parameters are listed in table 4.2. The total number of direction changes in all joints and the total distance traveled are chosen due to their ease of implementation.

The number of direction changes is assigned an importance factor of 0.2. The total travel in all joints is combined and is given an importance factor of 0.4. Additionally, the acceleration of joint 1 is analyzed. To obtain a scalar value for the acceleration, the individual acceleration values are squared and then summed up. The importance factor for acceleration is 0.4. Velocity, acceleration, and jerk are disregarded for all other joints.

| Process parameters | Importance Factor |
|---------------------------------|-------------------|
| Direction changes in joints 1-6 | 0.2 |
| Total travel in joints 1-6 | 0.4 |
| Acceleration in joint 1 | 0.4 |

Table 4.2: Selected process parameters and their importance factors

Since only one degree of freedom is being analyzed, it is possible to represent the individual local scores and global score as a one-dimensional graph. Firstly, toolpath 1 is analyzed by incrementing the redundant degree of freedom by 5 degrees, starting from -135 degrees and ending at 135 degrees.

Figure 4.10 illustrates a case with a -45-degree rotation around the Z-axis for toolpath 1. Similarly, Figure 4.11 displays a case with a +45-degree rotation around the Z-axis for toolpath 1.

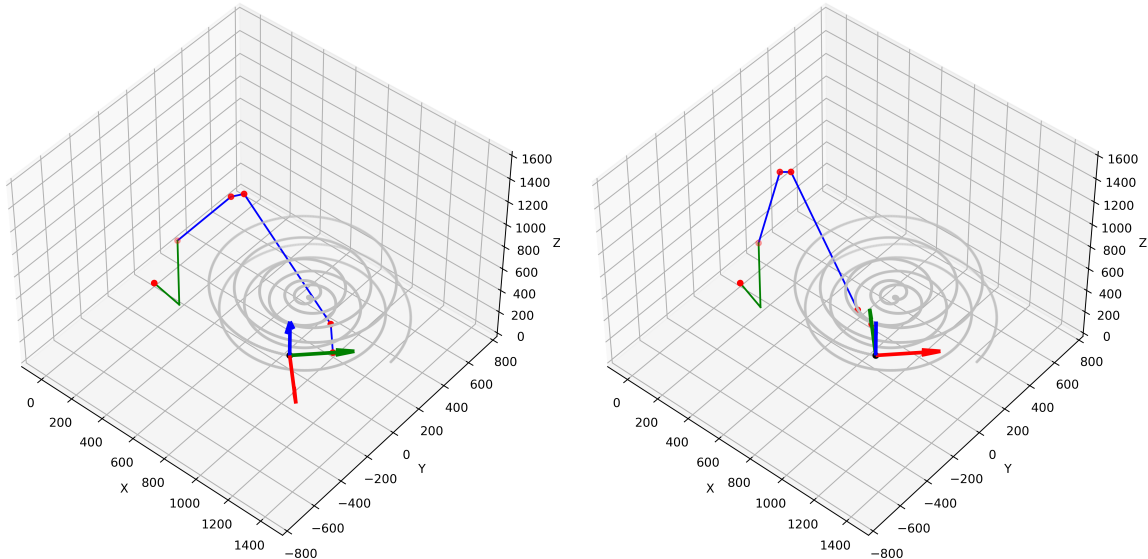


Figure 4.10: Toolpath 1 with $A=0$, $B=0$ and $C = -45^\circ$

Figure 4.11: Toolpath 1 with $A=0$, $B=0$ and $C = 45^\circ$

A total of 55 time series of joint positions are generated. On average, the inverse kinematics algorithm takes 35 seconds to calculate the joint values for all 3000 coordinates.

The process parameters are extracted and scaled in relation to each other, as described in Chapter 3.3.2. It is important to note that before scaling, the selected process parameters are pre-multiplied by -1, as each process parameter should be minimized.

The arrays of local ratings are then multiplied by the weights selected in table 4.2. Subsequently, the local scores of each process parameter can be plotted as a one-dimensional graph, as shown in figure 4.12.

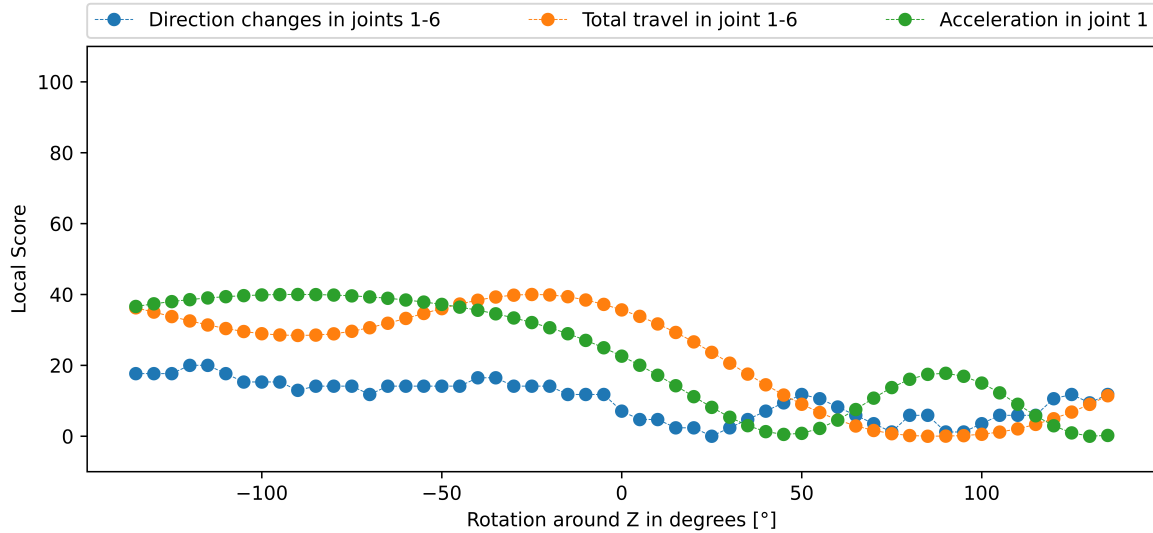


Figure 4.12: Local scores of each process parameter for toolpath 1

The acceleration in joint 1 and the combined total travel in the joints exhibit a smooth oscillating curve with a decreasing amplitude towards the positive end of the analyzed range. It is worth mentioning that the maximum value that the local score can reach is 40 for acceleration and total travel, while for direction changes, the maximum score is 20. This is due to the assigned importance factors. The direction changes display a less smooth trajectory.

Next, the local scores are summed up to calculate the global score. The resulting array, displayed in figure 4.13, represents the global score achieved by varying the rotation around the Z-axis in relation to all other analyzed values. The green cross on the graph indicates the maximum attainable score and its corresponding rotation, compared to all analyzed boundary conditions.

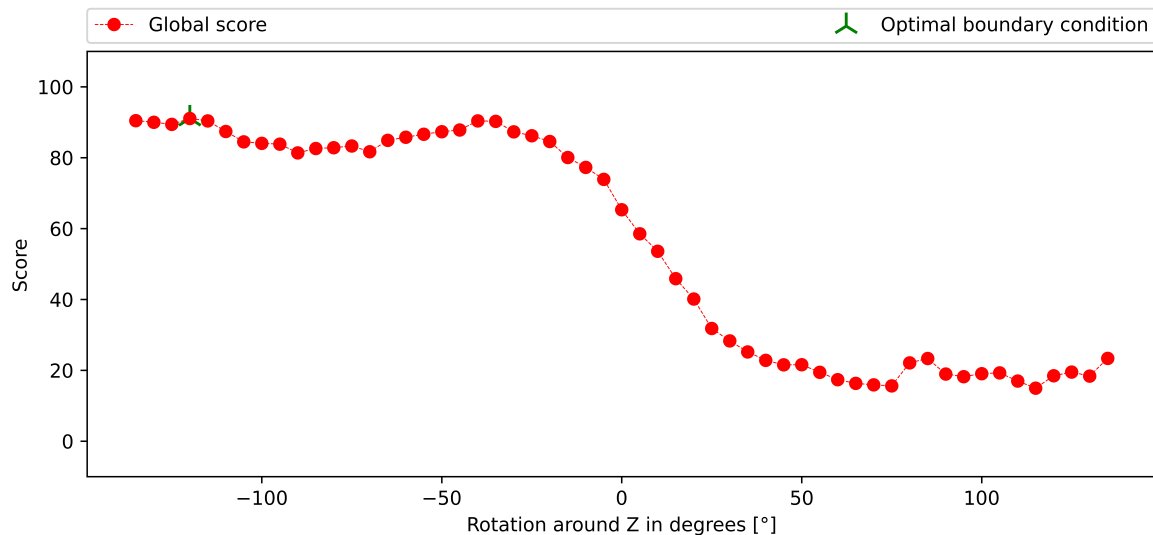


Figure 4.13: Global score for toolpath 1

In this particular case, the highest achievable score is 92.81 at -135 degrees. This nearly perfect score indicates that setting the rotation to -135 degrees results in minimal direction changes, minimal total travel, and close to minimal acceleration in joint 1. It is crucial to emphasize that this rating is only in comparison to the other analyzed boundary conditions.

The same analysis, using identical process parameters and weights, can be performed with toolpath 2 and toolpath 3. Figure 4.14 and figure 4.15 display the global and local scores for each analyzed value of the redundant degree of freedom. For toolpath 2, the best score is 93.4 at -115.0 degrees, while for toolpath 3, the best score is 88 at -80 degrees.

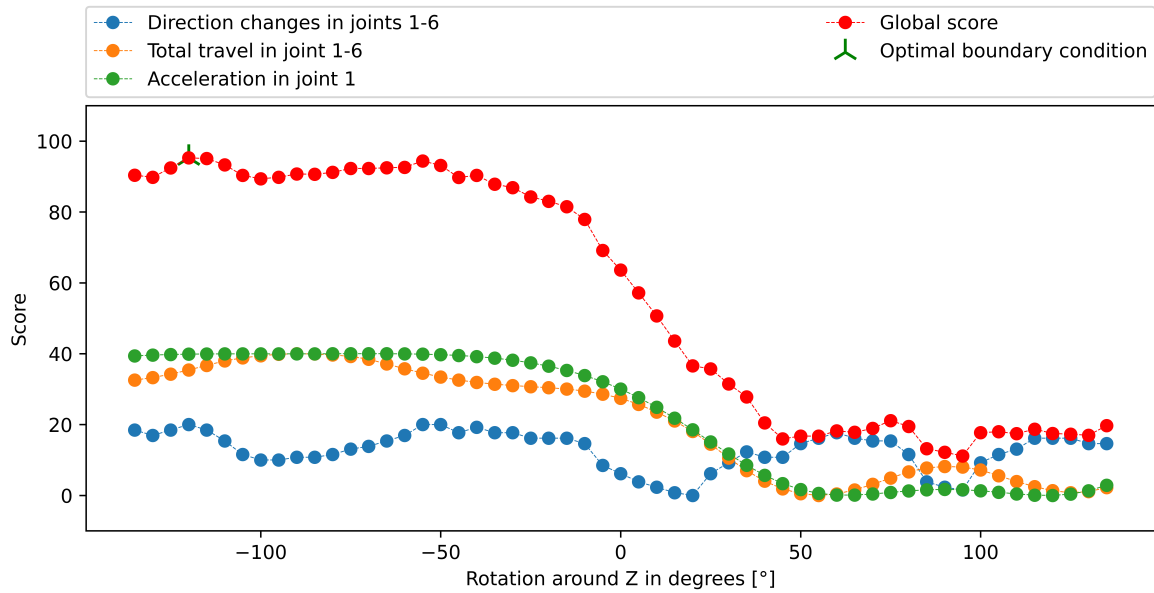


Figure 4.14: Global and local scores in toolpath 2 depending on the rotation around Z

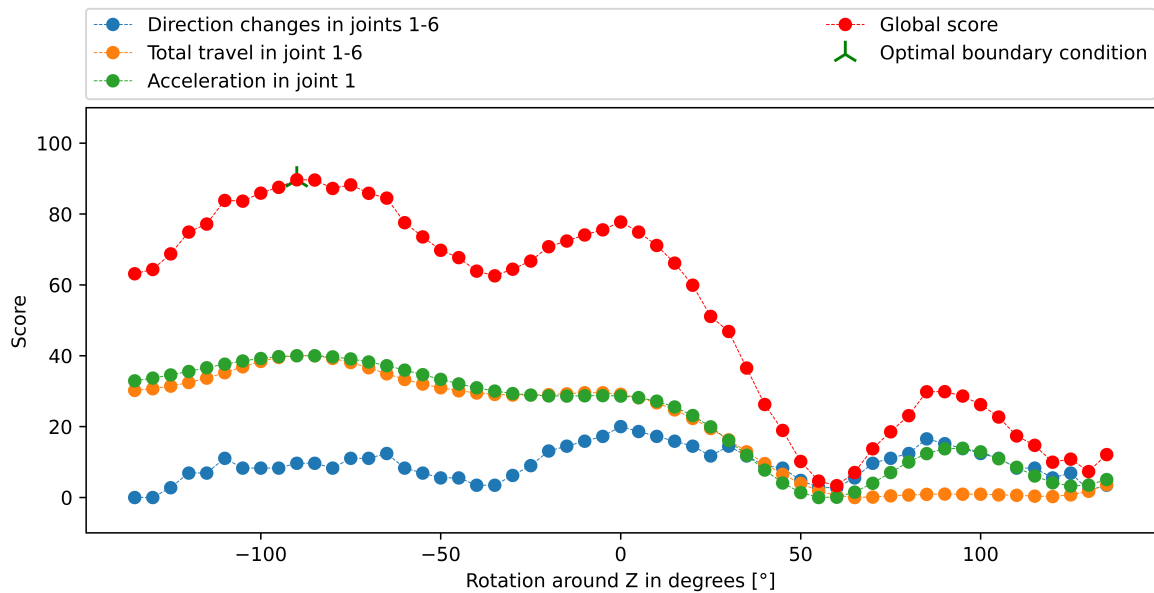


Figure 4.15: Global and local scores in toolpath 3 depending on the rotation around Z

Additionally, it is important to note that when a local score reaches its maximum value, it does not imply that the corresponding process parameter, such as the number of direction changes, becomes zero. Instead, it signifies that the number of direction changes is at its lowest compared to all other analyzed options.

4.2.2 Toolpath Evaluation with two Redundant DoF

To introduce an additional redundant degree of freedom, a rotary-tilt table is simulated. Currently, only the tilting aspect is being analyzed. All coordinates of the toolpath can be rotated by a specified degree around the X-axis. Figure 4.16 depicts toolpath 3 with no rotation around the X-axis of its coordinate system. Conversely, Figure 4.17 illustrates a rotation of +25 degrees.

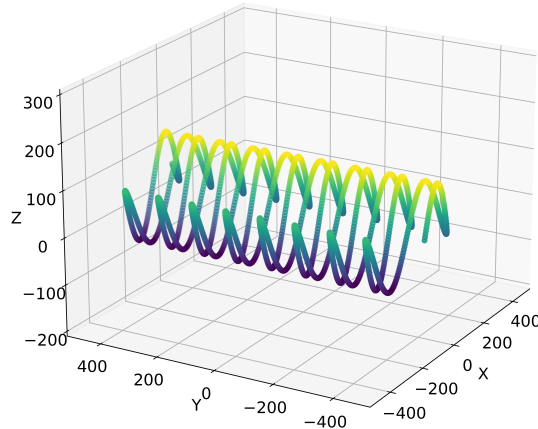


Figure 4.16: Toolpath 3 with no rotation around the X-axis

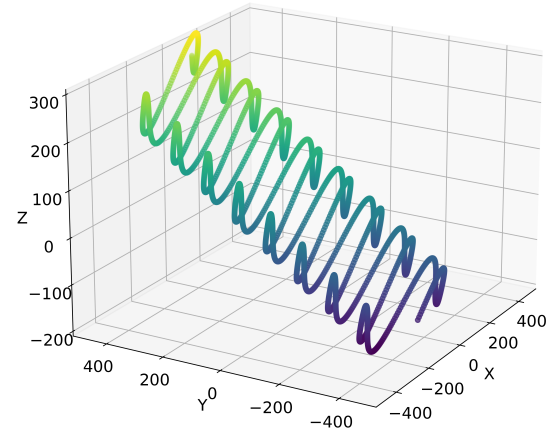


Figure 4.17: Toolpath 3 with a rotation of 25 degrees around the X-axis

Similar to the previous analysis, the same steps need to be followed. The newly selected process parameters are presented in table 4.3. The direction changes of the tilting joints (2+3+5) are combined and treated as one process parameter, weighted with a factor of 0.3. Direction changes in joint 1 and acceleration in joint 4 are considered as individual parameters, both individually weighted with 0.25. The final parameter is the velocity in joint 6, weighted with 0.2.

| Process parameters | Importance Factor |
|-----------------------------------|-------------------|
| Direction changes in joints 2+3+5 | 0.3 |
| Direction changes in joints 1 | 0.25 |
| Acceleration in joint 4 | 0.25 |
| Velocity in joint 6 | 0.2 |

Table 4.3: Selected process parameters and their importance factors for 2 redundant DoF

Figure 4.18 displays the robot and its orientation while following the tilted toolpath 3. It is crucial to note that since the toolpath is defined in 5 DoF in its own frame, the frame of the TCP must also tilt by the same degree as the table. The two redundant DoF in this case are the rotation around the Z-axis in the frame of the tilted toolpath and the tilting of the toolpath itself. This introduces an additional dimension, as now two parameters can be adapted for the optimization.

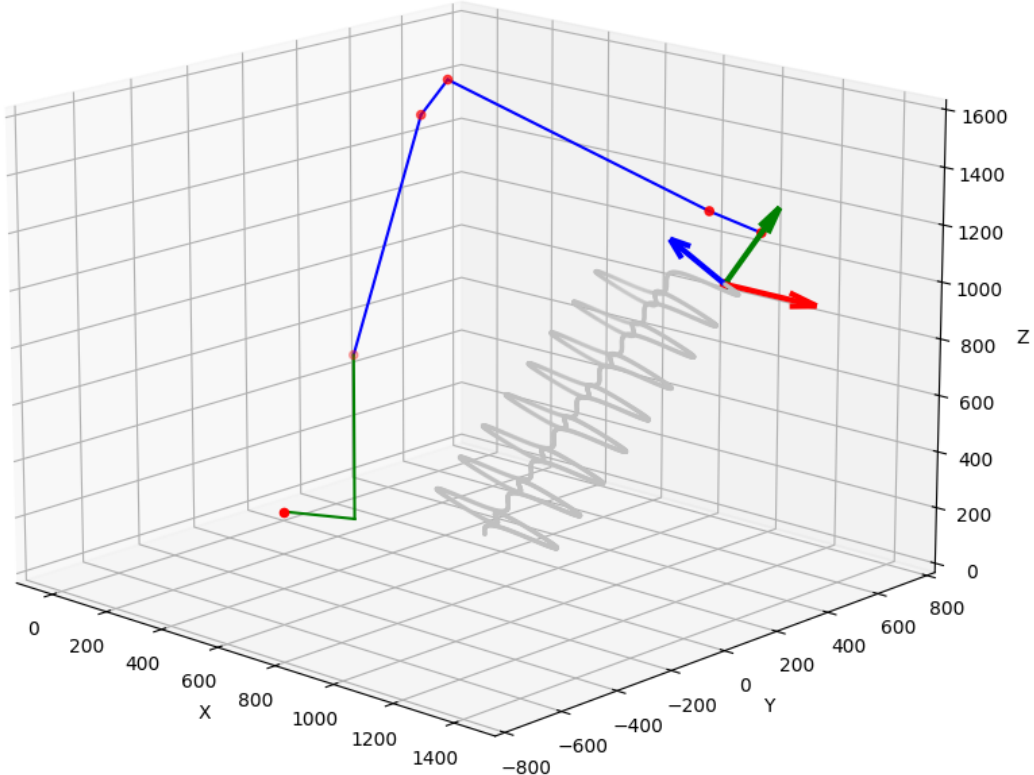


Figure 4.18: Robot following the tilted toolpath 3

The range of possible tilt positions ranges from -45° to 45° in 2-degree increments. For each tilt position and rotation, the joint angles are generated using inverse kinematics. To speed up the computation, only every third coordinate is utilized in the inverse kinematic algorithm. This reduces the toolpath by 2000 points and speeds up calculation time. On average, it now takes only 10 seconds to calculate the joint positions. A total of 2530 individual combinations are analyzed.

The extracted process parameters are again multiplied by -1, as the objective is to minimize them. Afterward, the Min-Max scaler is applied. The individual values are aggregated and presented in the form of a matrix. The values of this matrix are visualized in figure 4.19. The maximum achievable score from all possible combinations is 72.96, visualized by the red cross. This score was attained by setting the table tilt to -3 degrees and the rotation around the Z-axis of the tool to +35 degrees.

The resulting hyperplane exhibits two distinct local maxima. The entire surface displays a smooth curvature, although it appears less smooth in the range from -20 to 45 degrees.

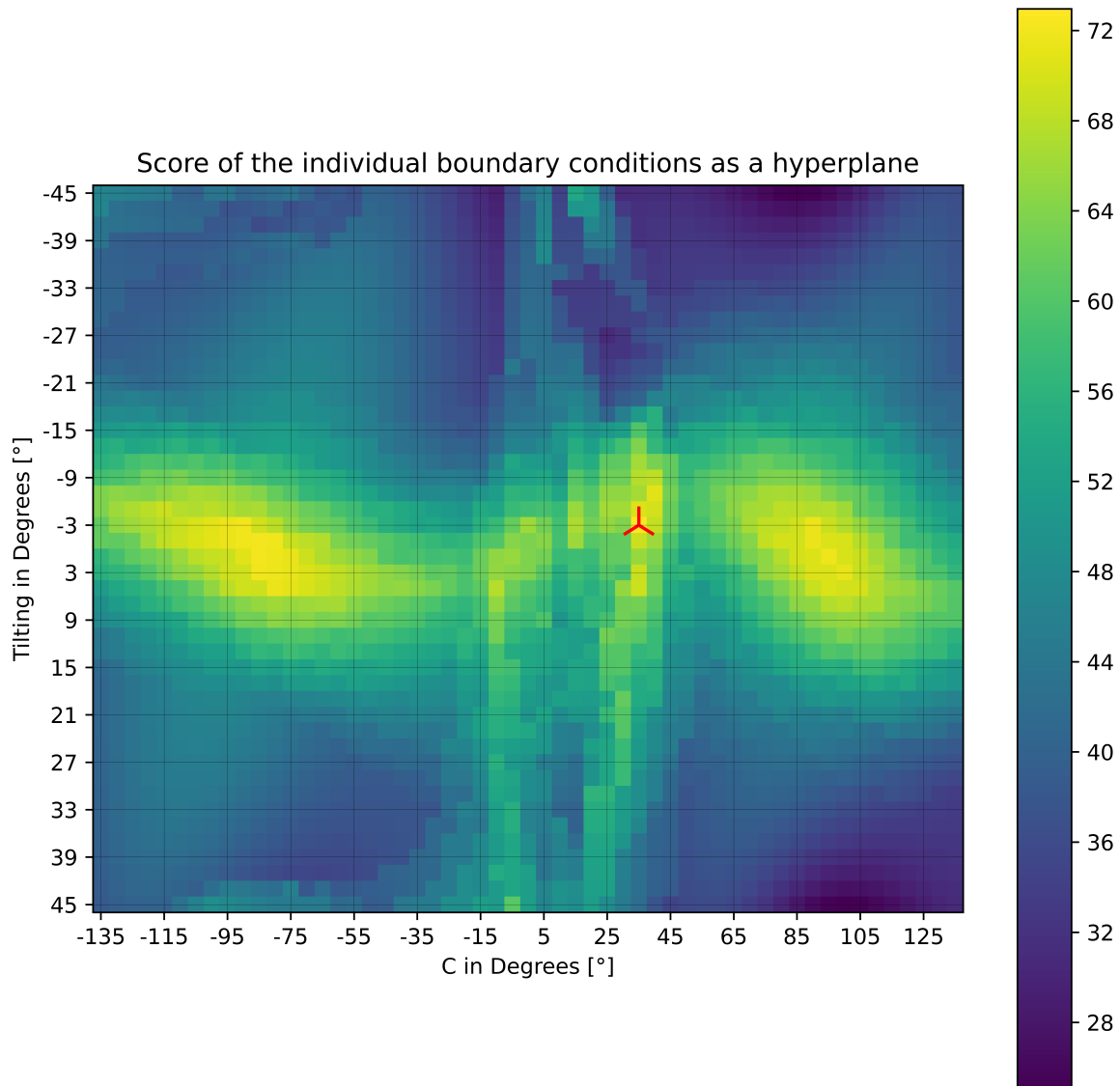


Figure 4.19: Hyperplane representing the global score of toolpath 3

Figure 4.20 and Figure 4.21 depict the visualization of the global score matrix for toolpath 2 and toolpath 1, respectively.

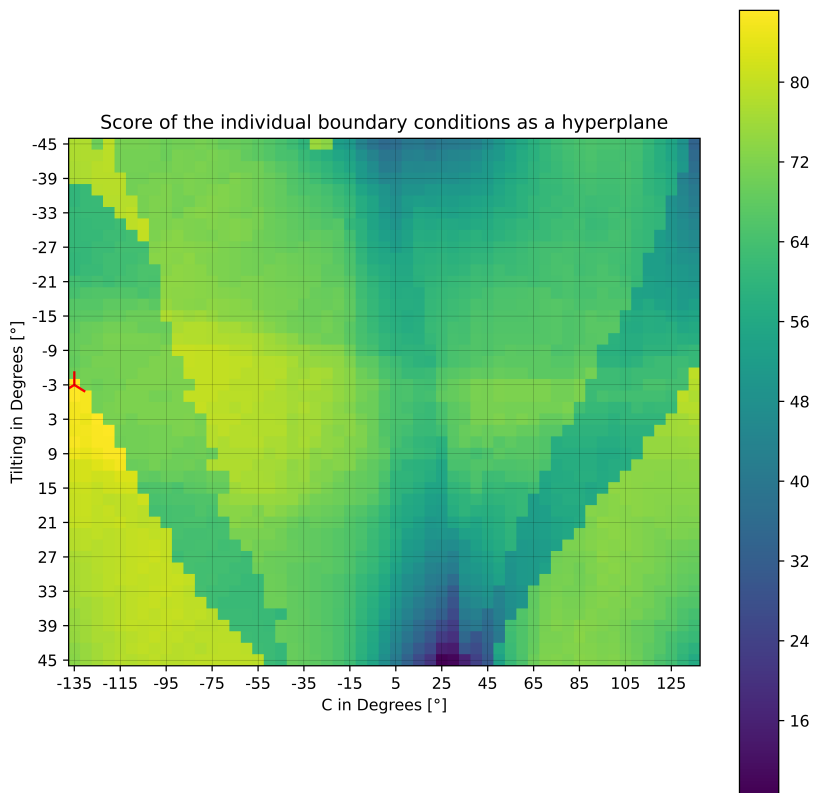


Figure 4.20: Hyperplane representing the global score of toolpath 2

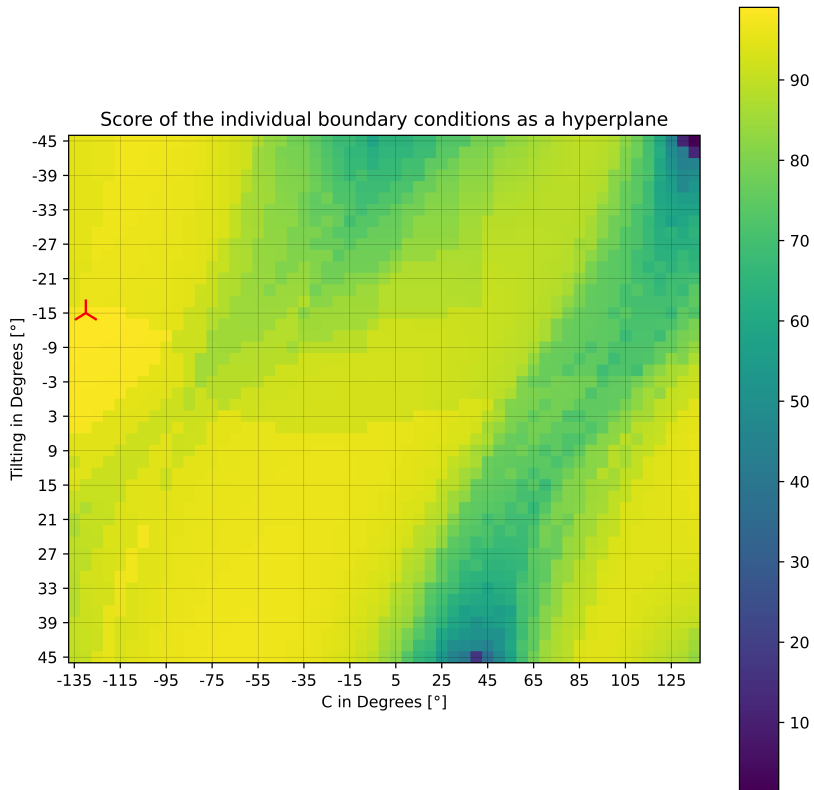


Figure 4.21: Hyperplane representing the global score of toolpath 1

4.2.3 Boundary Condition Optimization

So far, only the analysis of different boundary conditions has been performed by exploring the defined range of the redundant DoF. However, this approach is very time-consuming and scales exponentially with additional redundant degrees of freedom and a finer step size.

To efficiently search this vast space and propose optimal values for the redundant degrees of freedom, a PSO algorithm is proposed. In this algorithm, individual particles move through the search space by adjusting their positions based on their own best position and the best position found by the swarm. This cooperation allows the particles to explore the search space more effectively and converge towards the best solution.

The first test is conducted using the global score matrix of toolpath 3. Initially, 20 particles are randomly placed on the plane. Their individual scores are determined by the corresponding global score at their respective positions. By increasing the number of particles and iterations, the search space can be analyzed more densely.

Figure 4.22 shows the randomly placed particles on the pre-calculated global score matrix.

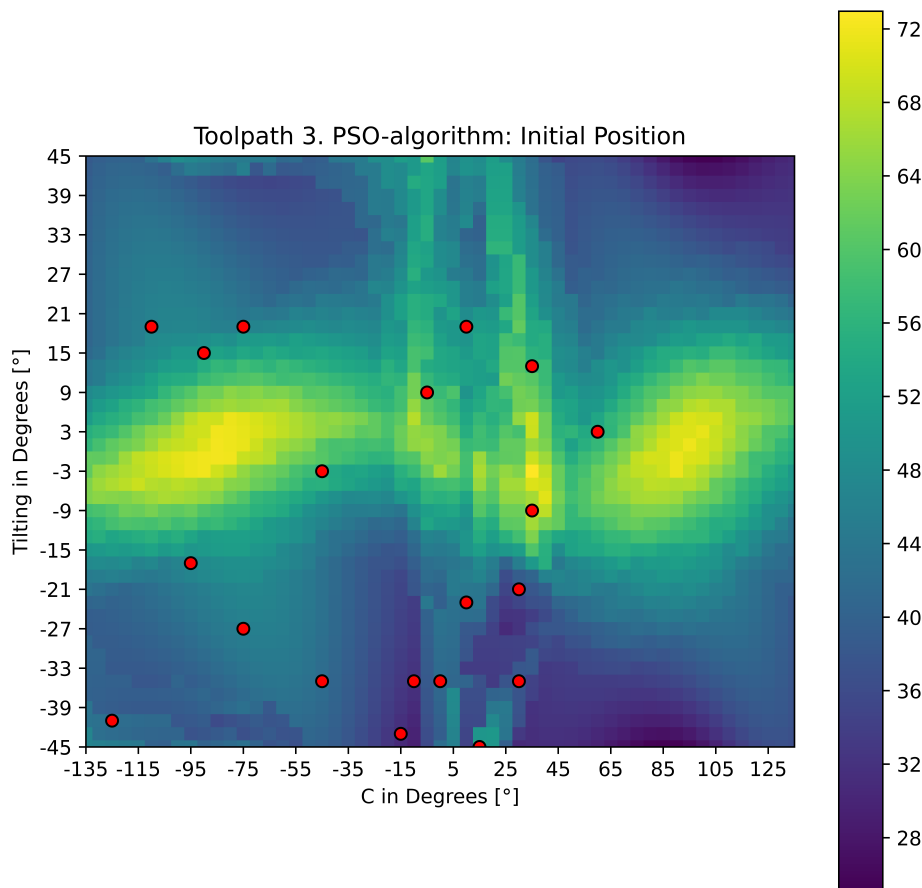


Figure 4.22: Distribution of particles after the first iteration

Figures 4.23 to 4.26 illustrate the convergence of the particles towards the identified maximum. This convergence is achieved within 5 iterations. It is noteworthy that the best position of all 5 particles matches the global maximum, as mentioned in Chapter 4.2.2. This example demonstrates that it is possible to explore a high-dimensional space without the need to compute all possible combinations.

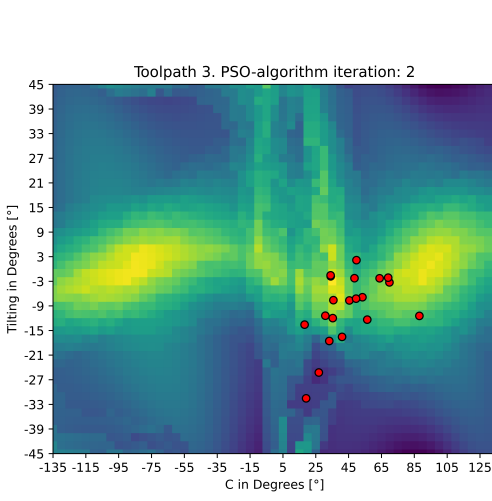


Figure 4.23: PSO Iteration 2 on toolpath 3

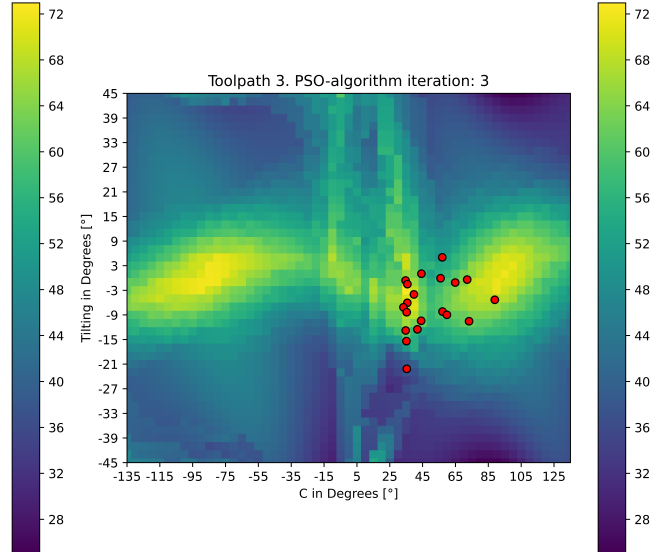


Figure 4.24: PSO Iteration 3 on toolpath 3

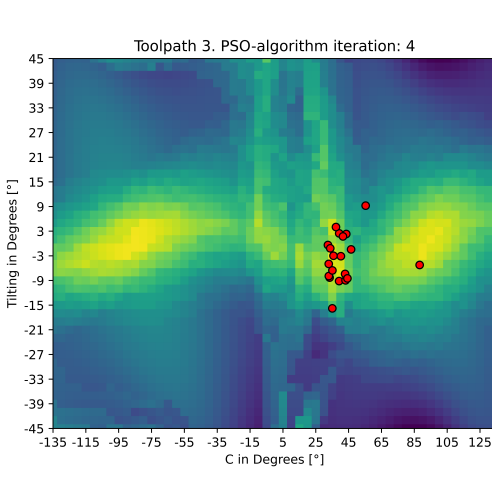


Figure 4.25: PSO Iteration 4 on toolpath 3

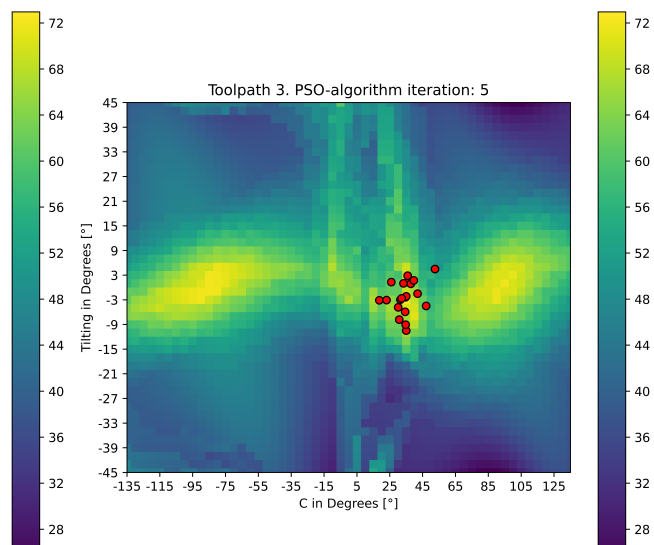


Figure 4.26: PSO Iteration 5 on toolpath 3

One crucial factor in this test is that the scores have already been calculated. The global score matrix is determined based on all possible combinations of different boundary conditions. However, in the intended scenario where this method is used to find the optimal boundary condition, such a matrix does not exist.

Therefore, the scores of individual positions need to be compared relative to each other at each iteration, taking into account the previous iterations. This method is depicted in Figure 4.27. Initially, a predetermined number of particles is randomly placed on the plane, with the X and Y values representing the selected boundary conditions. For each selected boundary condition, the joint angles are calculated using the inverse kinematic approach. Subsequently, the analyzed process parameters are extracted and the joint angles are stored. The score for each current position is calculated relative to all stored toolpaths.

It is possible that a particle had a position with a significantly higher score compared to the other available toolpaths in an early iteration. Therefore, after each iteration, it is necessary to update the score of the particle's most optimal position, as more boundary conditions are analyzed. This is done to ensure that an initially relative score, which may have been mistakenly chosen as the best, does not influence the subsequent search directions.

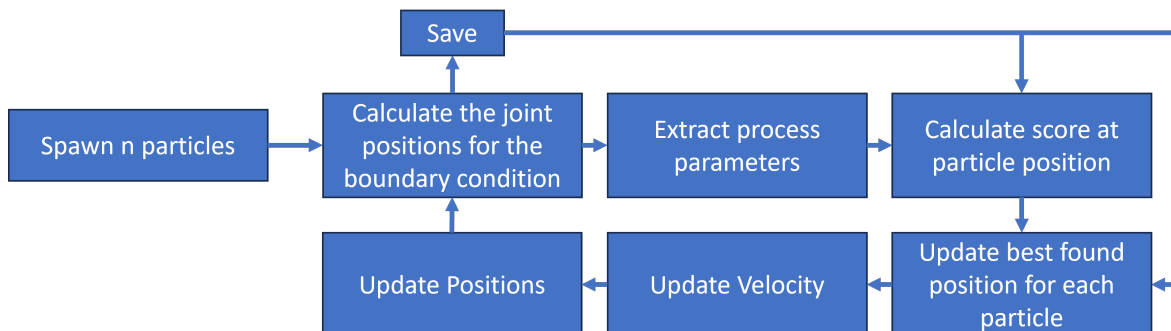


Figure 4.27: PSO-Loop

Utilizing this approach, the following results have been obtained. It is crucial to note that the colors from the global score matrix are not accessible to the PSO algorithm. They are solely used for evaluating the behavior of the particles and aiding in visualization.

Figures 4.28 to 4.31 demonstrate the progression of the individual particles. The green circle represents the overall best position discovered by the particles thus far.

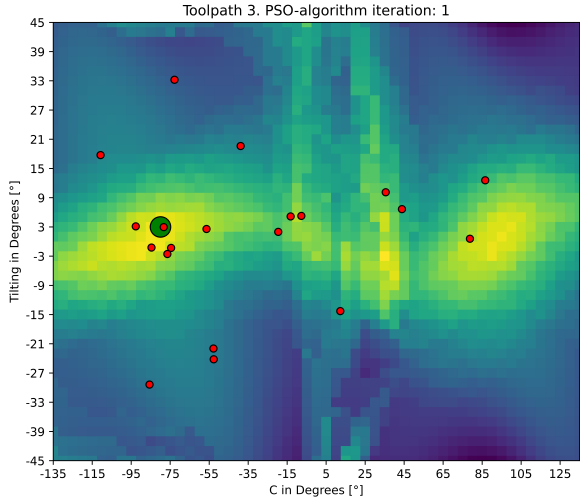


Figure 4.28: PSO Iteration 1 on toolpath 3

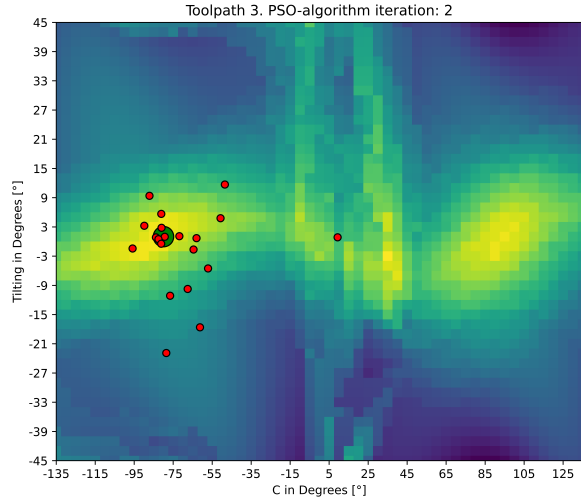


Figure 4.29: PSO Iteration 2 on toolpath 3

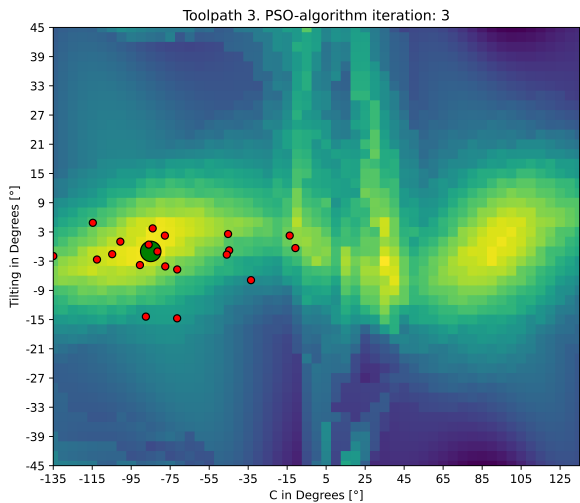


Figure 4.30: PSO Iteration 3 on toolpath 3

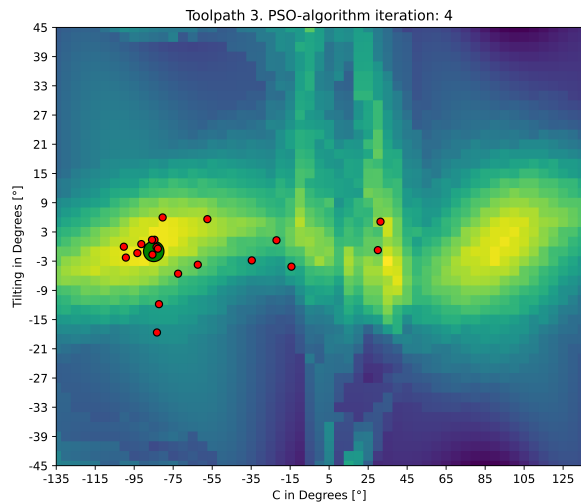


Figure 4.31: PSO Iteration 4 on toolpath 3

Figure 4.32 illustrates the positions of the particles after the fifth and final iteration.

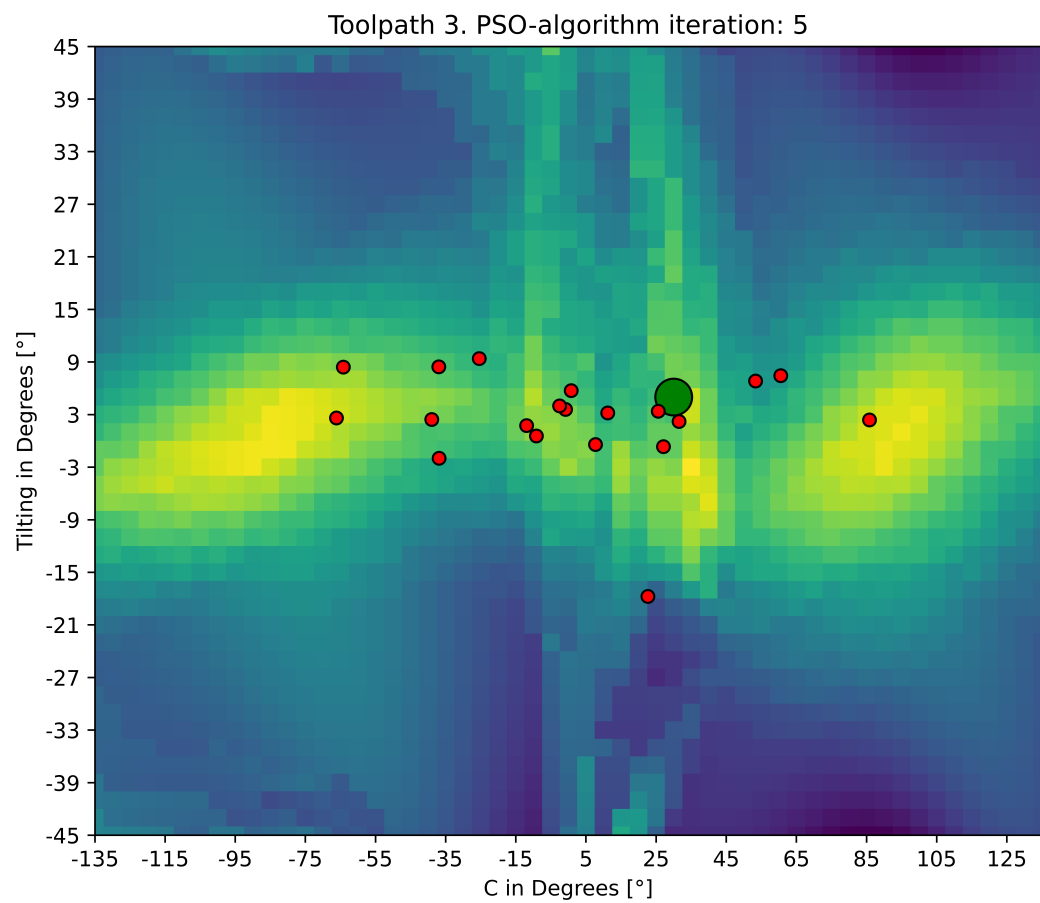


Figure 4.32: PSO iteration 5 on toolpath 3

Figures 4.33 through 4.34 and Figures 4.35 and 4.36 showcase the initial and final positions of the particles when analyzing the first and second toolpath, respectively. In both cases, the PSO algorithm successfully converged towards the optimal boundary condition.

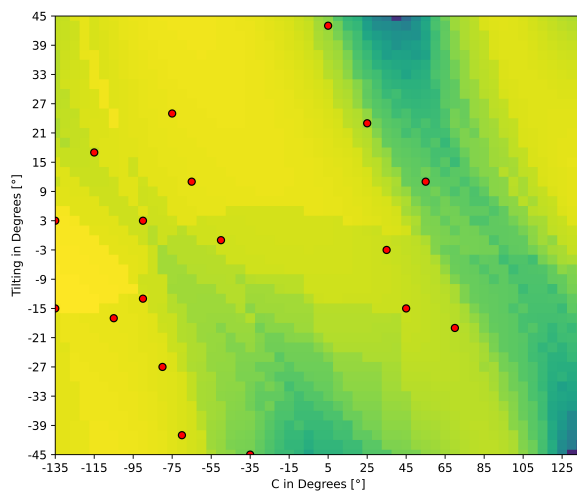


Figure 4.33: PSO Initial position toolpath 1

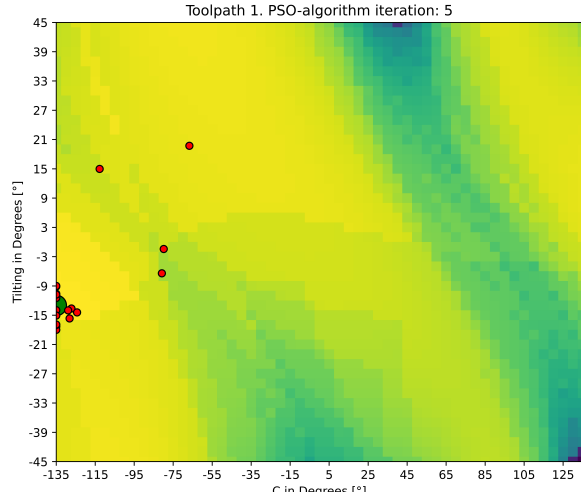


Figure 4.34: PSO Iteration 5 on toolpath 1

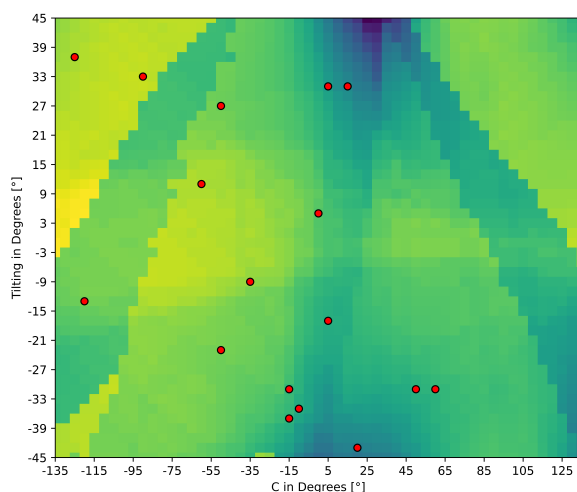


Figure 4.35: PSO Initial position toolpath 2

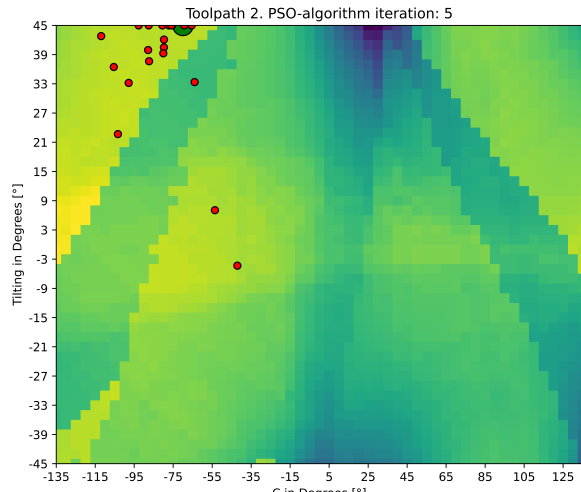


Figure 4.36: PSO Iteration 5 on toolpath 2

4.3 Analysis and Discussion of the Results

4.3.1 Analysis of the Results

When analyzing only one redundant degree of freedom, specifically the rotation around the Z-axis, it is clear that there is an improvement in the acceleration in joint 1 and the total combined travel with a increasing negative rotation. This improvement is observed in all three toolpaths. However, it is important to note that the local score of the direction changes is not as smooth as the other analyzed parameters. This is because this value, due to its physical nature, cannot be continuous.

When examining the global score, it becomes evident that finding the global optimum can be challenging. This is because multiple local minima are present. Additionally, the selected process parameters can further contribute to the irregularity of the global score curve. Depending on the selected process parameters and their importance factor, this process can either turn out a easy or very complicated.

In toolpath 1, the optimal boundary condition is determined as the maximum negative rotation around the Z-axis. This suggests that it may be possible to find an even better boundary condition. It is worth mentioning that the analysis of each toolpath takes approximately 30 minutes.

When considering the scenario where two degrees of freedom can be set, it is observed that toolpath 1 and toolpath 2 have very similar boundary conditions for the global optimum. This suggests that these two toolpaths do not differ significantly from each other when considering the process parameters alone.

In the case of toolpath 2 with two redundant degrees of freedom, distinct streaks can be observed originating from a positive rotation of 45 degrees of the tilt table. On the other hand, toolpath 1 exhibits a mostly flat area with a distinct trough. Such a scenario is optimal for a PSO algorithm. It is important to note that the calculation of each individual global score matrix takes approximately 50 minutes.

Based on the results obtained from the PSO algorithm, it can be concluded that achieving a close-to-optimal result is feasible when the global score matrix yields smooth surfaces. By implementing this approach, a significant reduction in computation time is possible. Instead of calculating the entire matrix, only 100 toolpaths need to be computed using the inverse kinematics algorithm, resulting in a computation time of just 15 minutes.

The number of particles is selected to be as high as possible while also considering the computational costs. Rather than increasing the number of particles, the number of iterations is set to 5 in order to facilitate convergence towards the global optima. The results clearly show that such a convergence is possible.

NO CAM EXPLAIN

WAS MUSS NOCH GEMACHR WERDEN DASSS ES Auf echtem Gcode und CAM läuft ???

4.3.2 Discussion of the Results

Even though the results show a very promising outcome, it is necessary to consider some additional factors. One of the most obvious elements is that only three very simple toolpaths are analyzed. To validate this method in detail, it is necessary to use real-life production G-code with correctly modeled robotic systems and analyze whether it can be optimized. One of the possible limiting factors is that the rotation values for A and B are always set to 0 in the toolpaths' coordinate system. It should be noted that this work only provides a limited excerpt and does not analyze complex multi-axis operations, which are a significant advantage and building block of the WAAM process.

The selected inverse kinematics algorithm is not designed for optimal high-performance calculations, making it infeasible to use when dealing with toolpaths that have millions of points. Additionally, the algorithm calculates the joint position numerically rather than analytically, which can result in unexpected robot poses. CAM software such as *Siemens NX* offers additional options for inverse kinematics that can be used to fine-tune the behavior of the robot.

When analyzing multiple process parameters, it is not guaranteed that the resulting surface will be smooth and optimal for the selected optimization algorithm. Additionally, when working with a PSO algorithm, the final result strongly depends on the initial distribution of the particles. If the optimum is a very tight and sharp spike, the probability of finding the optimal boundary condition is significantly lower. This is particularly true in systems with 3 or more redundant degrees of freedom, where simple optimization algorithms can lead to suboptimal results or require unfeasibly long computation times.

In general, the presented methodology does provide a solid basis as a proof of concept for the proposed method. However, additional implementations are necessary for it to be feasible in an industrial environment.

Chapter 5

Conclusion

5.1 Summary

This thesis proposes a method for optimizing the execution of a toolpath on robotic systems with redundant DoF.

Firstly, the problem formulation highlights the flexibility and various issues that arise with redundant DoF. It discusses how singularity avoidance can help industrial robots avoid sub-optimal poses that may lead to unexpected behavior. Redundant DoF can also affect joint accelerations and jerk, potentially causing excessive wear on parts and resulting in more downtime and sub-optimal part quality. Additionally, other factors such as extension control, precision, and energy use are mentioned, and their impact on the manufacturing process is discussed.

The aim of this thesis is to propose and validate a systematic approach to leveraging these redundant DoF in order to optimize towards a user-defined goal. Currently, there is no publication available that presents a general solution to this problem.

Chapter 2 provides a comprehensive discussion on the state of science and technology, aiming to provide a clear understanding of the individual components of manufacturing systems and optimization algorithms. Both subtractive and additive manufacturing are examined in detail, including a review of their respective strengths and weaknesses. An important focus is placed on one of the common processes in additive manufacturing, namely WAAM, which has a significant relationship with industrial robots. In Chapter 2.1.3, the functionality of these robots is described in detail, with special attention given to the issue of redundancy in such robotic systems.

Chapter 2.4 focuses on a comparative analysis of published research papers related to singularity avoidance, optimization of joint acceleration and jerk, optimization of energy use, and optimization of stiffness. Each section highlights the available options and approaches for leveraging redundant DoF to achieve improved performance in these specific areas. The examination of multiple methods serves as the foundation for understanding the current state of cutting-edge research and identifying any existing research gaps.

Thus far, no global optimization approach has been proposed that can consider a user-defined input with specified goals, based on multiple process parameters, and providing the optimal settings for the redundant DoF. This represents an important research opportunity in the field.

Chapter 3 presents a solution for the identified research gap. In order to address this problem, a carefully selected list of process parameters is introduced and thoroughly discussed. These parameters are derived from the movement of the robot arm and include variables such as the rotational position of joints over time, as well as their subsequent derivatives and direction changes.

After summarizing which process parameters can be extracted form a toolpath traversed by a industrial robot, the first main step of the methodology is presented. To calculate the global score it is necessary to calcualte the individual local shore

5.2 Outlook

This work focuses on a select number of process parameters, but this selection can be expanded to further optimize the real-world manufacturing process.

One potential additional parameter that can be optimized, is the stiffness value of the robotic system based on its current pose. Maintaining high stiffness in the orthogonal cutting direction is crucial for minimizing deviations, while low stiffness combined with high contact forces can result in significant dimensional errors. Finite-element analysis or multi-body simulation can be used to determine the stiffness value and optimize it for better performance by specifically defining the redundant DoF.

Another important parameter for future research is the collision index. The collision index is used to identify potential collisions between any part of the robot or the end-effector and the workpieces or other objects in the environment. This parameter is particularly significant in scenarios involving WAAM systems, where loose wires can change their position depending on the robots pose. Preventing collisions is essential to avoid damage to the workpiece, the robot, or other equipment. As of now the optimization algorithm does not consider this option.

One area where the PSO optimization process can lead to significant advantages is section-wise optimization. The toolpath can be divided into sections, and for each section, the optimal settings of the redundant DoF can be determined. To make this approach work effectively, it is important to consider the boundary conditions at the transition points between the individual sections.

Furthermore, implementing the proposed method in a CAM software can provide faster computation and enable the optimization of more complex toolpaths. Another option to speed up the computation is to program the algorithm in such a way that it is designed for multi-threading. Such implementation can result in significantly faster optimization.

Moving forward, it is necessary to conduct further validation processes, including real-world tests and simulations, to evaluate the performance of the optimized parameters and verify the effectiveness of the proposed methodology. Additionally, exploring the implementation of machine learning techniques for best-case calculations could be a valuable avenue for future research.

List of Figures

| | | |
|------|---|----|
| 2.1 | 3-Axis CNC Machine [0] | 7 |
| 2.2 | 5-Axis CNC Machine [0] | 8 |
| 2.3 | Schematic representation of WAAM [0] | 11 |
| 2.4 | Part produced by WAAM with post machining [0] | 11 |
| 2.5 | Current and Voltage wave forms of a CMT process [0] | 12 |
| 2.6 | Individual sections of a CMT cycle [0] | 13 |
| 2.7 | SCARA robot | 14 |
| 2.8 | Delta robot | 14 |
| 2.9 | 6-DoF industrial robot [0] | 15 |
| 2.10 | Industrial robots with an additional linear axis [0] | 17 |
| 2.11 | 7 DoF robot [0] | 17 |
| 2.12 | Desired path with constant velocity [0] | 18 |
| 2.13 | Influence of G-Code commands regarding feedrate compliance [0] | 19 |
| 2.14 | Predetermined deviation of the programmed and executed path [0] | 19 |
| 2.15 | Influence of commands G601 and G602 [0] | 20 |
| 2.16 | Interface of Siemens NX [0] | 22 |
| 2.17 | Three exemplary tool paths for iso-planar milling [0] | 23 |
| 2.18 | Passing through a wrist singularity [0] | 25 |
| 3.1 | Interdependence of various parameters | 32 |
| 3.2 | Parameter Flowchart | 36 |
| 3.3 | Calculation of the local score through variation | 38 |
| 3.4 | Variation with low standard deviation | 39 |
| 3.5 | Variation with high standard deviation | 39 |
| 3.6 | Additional Information for angular position of each joint | 40 |

| | |
|---|----|
| 3.7 Two option for recording the joint position in a time-series | 41 |
| 3.8 Summing up the rotation in the clockwise and anti-clockwise direction | 41 |
| 3.9 Calculating direction changes from a time-series | 42 |
| 3.10 Two Time-Series with equal number of direction changes but different characteristics | 43 |
| 3.11 | 44 |
| 3.12 Calculating velocity from the joint position over time | 45 |
| 3.13 Overstepping the threshold value | 45 |
| 3.14 Deviation of of the TCP from the actual toolpath | 47 |
| 3.15 Exemplary methods for energy usage calculations | 49 |
| 3.16 Turn-on and turn-off points in the G-code used in WAAM | 50 |
| 3.17 Rotation around the C-axis of a welding torch | 51 |
| 3.18 Two examples for optimal orientation along a vector in 2D | 52 |
| 3.19 From time-series of the deviation vector to scalar value | 53 |
| 3.20 Example of non-optimal tilt in the welding torch | 54 |
| 3.21 x | 55 |
| 3.22 Process of evaluating a defined boundary condition | 56 |
| 3.23 Schematic process of optimization without CAM software | 58 |
| 3.24 Variation of the redundant DoF in the G-code | 59 |
| 3.25 Schematic process of optimization with CAM software in the loop | 60 |
| 4.1 Visualization of the modeled robot | 62 |
| 4.2 Schematics of the modeled robot | 63 |
| 4.3 Toolpath 1: Converging-Diverging Spiral | 64 |
| 4.4 Toolpath 2: Converging Loop | 64 |
| 4.5 Toolpath 3: Pendulum Oscillation | 64 |
| 4.6 Toolpath 1 with robot model | 65 |
| 4.7 Visualization of the joint positions over time for toolpath 1 with C=0 | 66 |
| 4.8 Visualization of the joint positions over time for toolpath 1 with C=45° | 67 |
| 4.9 Visualization of the joint positions over time for toolpath 2 | 67 |
| 4.10 Toolpath 1 with A=0, B=0 and C = -45° | 68 |
| 4.11 Toolpath 1 with A=0, B=0 and C = 45 | 68 |

| | |
|---|----|
| 4.12 Local scores of each process parameter for toolpath 1 | 69 |
| 4.13 Global score for toolpath 1 | 69 |
| 4.14 Global and local scores in toolpath 2 depending on the rotation around Z | 70 |
| 4.15 Global and local scores in toolpath 3 depending on the rotation around Z | 70 |
| 4.16 Toolpath 3 with no rotation around the X-axis | 71 |
| 4.17 Toolpath 3 with a rotation of 25 degrees around the X-axis | 71 |
| 4.18 Robot following the tilted toolpath 3 | 72 |
| 4.19 Hyperplane representing the global score of toolpath 3 | 73 |
| 4.20 Hyperplane representing the global score of toolpath 2 | 74 |
| 4.21 Hyperplane representing the global score of toolpath 1 | 74 |
| 4.22 Distributed of particles after the first iteration | 75 |
| 4.23 PSO Iteration 2 on toolpath 3 | 76 |
| 4.24 PSO Iteration 3 on toolpath 3 | 76 |
| 4.25 PSO Iteration 4 on toolpath 3 | 76 |
| 4.26 PSO Iteration 5 on toolpath 3 | 76 |
| 4.27 PSO-Loop | 77 |
| 4.28 PSO Iteration 1 on toolpath 3 | 78 |
| 4.29 PSO Iteration 2 on toolpath 3 | 78 |
| 4.30 PSO Iteration 3 on toolpath 3 | 78 |
| 4.31 PSO Iteration 4 on toolpath 3 | 78 |
| 4.32 PSO iteration 5 on toolpath 3 | 79 |
| 4.33 PSO Initial position toolpath 1 | 80 |
| 4.34 PSO Iteration 5 on toolpath 1 | 80 |
| 4.35 PSO Initial position toolpath 2 | 80 |
| 4.36 PSO Iteration 5 on toolpath 2 | 80 |

List of Tables

| | | |
|-----|--|----|
| 2.1 | Areas of influence of boundary conditions and process parameters | 25 |
| 3.1 | Process parameter and their numerical form | 33 |
| 3.2 | Calculation of a toolpath score | 37 |
| 3.3 | Calculation of a score regarding only direction changes and total travel | 42 |
| 3.4 | Calculation of a score regarding only velocity, acceleration and jerk | 46 |
| 3.5 | Average scaling factors for energy calculations | 48 |
| 4.1 | DH-parameters for the modeled robot | 61 |
| 4.2 | Selected process parameters and their importance factors | 68 |
| 4.3 | Selected process parameters and their importance factors for 2 redundant DoF | 72 |

Bibliography

- [0] Singh, M., Fuenmayor, E., Hinchy, E., Qiao, Y., Murray, N., and Devine, D. “Digital Twin: Origin to Future”. In: *Applied System Innovation* 4.2 (2021), p. 36. ISSN: 2571-5577. DOI: 10.3390/asi4020036. URL: <https://www.mdpi.com/2571-5577/4/2/36>.
- [0] Ghobakhloo, M. “Industry 4.0, digitization, and opportunities for sustainability”. In: *Journal of Cleaner Production* 252 (2020), p. 119869. ISSN: 0959-6526. DOI: 10.1016/j.jclepro.2019.119869. URL: <https://www.sciencedirect.com/science/article/pii/s0959652619347390>.
- [0] Bibby, L. and Dehe, B. “Defining and assessing industry 4.0 maturity levels – case of the defence sector”. In: *Production Planning & Control* 29.12 (2018), pp. 1030–1043. DOI: 10.1080/09537287.2018.1503355.
- [0] Simonis, K., Gloy, Y.-S., and Gries, T. “INDUSTRIE 4.0 - Automation in weft knitting technology”. In: *IOP Conference Series: Materials Science and Engineering* 141.1 (2016), p. 012014. ISSN: 1757-899X. DOI: 10.1088/1757-899X/141/1/012014. URL: <https://iopscience.iop.org/article/10.1088/1757-899x/141/1/012014/meta>.
- [0] Feldhausen, T., Heinrich, L., Saleeby, K., Burl, A., Post, B., MacDonald, E., Saldana, C., and Love, L. “Review of Computer-Aided Manufacturing (CAM) strategies for hybrid directed energy deposition”. In: *Additive Manufacturing* 56 (2022), p. 102900. ISSN: 2214-8604. DOI: 10.1016/j.addma.2022.102900.
- [0] Lalit Narayan, K., Mallikarjuna Rao, K., and Sarcar, M. M. M. *Computer aided design and manufacturing*. Second printing. Delhi: PHI Learning Private Limited, 2013. ISBN: 9788120333420.
- [0] Dubovska, R., Jambor, J., and Majerik, J. “Implementation of CAD/CAM System CATIA V5 in Simulation of CNC Machining Process”. In: *1877-7058* 69 (2014), pp. 638–645. ISSN: 1877-7058. DOI: 10.1016/j.proeng.2014.03.037. URL: <https://www.sciencedirect.com/science/article/pii/s1877705814002835>.
- [0] Saxena, P., Stavropoulos, P., Kechagias, J., and Salonitis, K. “Sustainability Assessment for Manufacturing Operations”. In: *Energies* 13.11 (2020), p. 2730. ISSN: 1996-1073. DOI: 10.3390/en13112730. URL: <https://www.mdpi.com/1996-1073/13/11/2730>.

- [0] Pan, Z., Polden, J., Larkin, N., van Duin, S., and Norrish, J. “Recent progress on programming methods for industrial robots”. In: *Robotics and Computer-Integrated Manufacturing* 28.2 (2012), pp. 87–94. ISSN: 0736-5845. DOI: 10.1016/j.rcim.2011.08.004. URL: <https://www.sciencedirect.com/science/article/pii/s0736584511001001>.
- [0] Bi, Z. and Wang, X. *Computer aided design and manufacturing*. 1st edition. Wiley-ASME press series. Hoboken, New Jersey and West Sussex, England: Wiley and ASME Press, 2020. ISBN: 9781119534211.
- [0] Liberman, Y. L. and Gorbunova, L. N. “Selection of Positioning Devices for the Components of CNC Machines”. In: *Russian Engineering Research* 41.11 (2021), pp. 1067–1070. ISSN: 1934-8088. DOI: 10.3103/S1068798X21110204. URL: <https://link.springer.com/article/10.3103/s1068798x21110204>.
- [0] Jia, Z.-y., Ma, J.-w., Song, D.-n., Wang, F.-j., and Liu, W. “A review of contouring-error reduction method in multi-axis CNC machining”. In: *International Journal of Machine Tools and Manufacture* 125 (2018), pp. 34–54. ISSN: 0890-6955. DOI: 10.1016/j.ijmachtools.2017.10.008.
- [0] Sherwani, F., Asad, M. M., and Ibrahim, B. “Collaborative Robots and Industrial Revolution 4.0 (IR 4.0)”. In: *2020 International Conference on Emerging Trends in Smart Technologies (ICETST)*. IEEE, 2020. DOI: 10.1109/icetst49965.2020.9080724.
- [0] Iglesias, I., Sebastián, M. A., and Ares, J. E. “Overview of the State of Robotic Machining: Current Situation and Future Potential”. In: *1877-7058* 132 (2015), pp. 911–917. ISSN: 1877-7058. DOI: 10.1016/j.proeng.2015.12.577. URL: <https://www.sciencedirect.com/science/article/pii/s1877705815044896>.
- [0] Billard, A. and Kragic, D. “Trends and challenges in robot manipulation”. In: *Science* 364.6446 (2019). DOI: 10.1126/science.aat8414.
- [0] Goel, R. and Gupta, P. “Robotics and Industry 4.0”. In: *A Roadmap to Industry 4.0: Smart Production, Sharp Business and Sustainable Development*. Springer, Cham, 2020, pp. 157–169. DOI: 10.1007/978-3-030-14544-6{\textunderscore}9. URL: https://link.springer.com/chapter/10.1007/978-3-030-14544-6_9.
- [0] Gadaleta, M., Pellicciari, M., and Berselli, G. “Optimization of the energy consumption of industrial robots for automatic code generation”. In: *Robotics and Computer-Integrated Manufacturing* 57 (2019), pp. 452–464. ISSN: 0736-5845. DOI: 10.1016/j.rcim.2018.12.020. URL: <https://www.sciencedirect.com/science/article/pii/s0736584518301856>.
- [0] Kyrtatsis, P., Kakoulis, K., and Markopoulos, A. P. “Advances in CAD/CAM/CAE Technologies”. In: *Machines* 8.1 (2020), p. 13. ISSN: 2075-1702. DOI: 10.3390/machines8010013. URL: <https://www.mdpi.com/2075-1702/8/1/13/htm>.
- [0] Maiti, C. K. *Introducing technology computer-aided design (TCAD): Fundamentals, simulations and applications*. Temasek Boulevard, Singapore: Pan Stanford Publishing, 2017. ISBN: 9789814745529.

- [0] Uhlmann, E., Reinkober, S., and Hollerbach, T. "Energy Efficient Usage of Industrial Robots for Machining Processes". In: 2212-8271 48 (2016), pp. 206–211. ISSN: 2212-8271. DOI: 10.1016/j.procir.2016.03.241. URL: <https://www.sciencedirect.com/science/article/pii/s2212827116305303>.
- [0] Anjum, Z., Samo, S., Nighat, A., Nisa, A. U., Soomro, M. A., and Alayi, R. "Design and Modeling of 9 Degrees of Freedom Redundant Robotic Manipulator". In: *Journal of Robotics and Control (JRC)* 3.6 (2022), pp. 800–808. ISSN: 2715-5056. DOI: 10.18196/jrc.v3i6.15958. URL: <https://journal.umy.ac.id/index.php/jrc/article/view/15958>.
- [0] Boscariol, P., Caracciolo, R., Richiedei, D., and Trevisani, A. "Energy Optimization of Functionally Redundant Robots through Motion Design". In: *Applied Sciences* 10.9 (2020), p. 3022. DOI: 10.3390/app10093022.
- [0] Liu, Y., Wang, L., Yu, Y., Zhang, J., and Shu, B. "Optimization of redundant degree of freedom in robot milling considering chatter stability". In: (2022). DOI: 10.21203/rs.3.rs-1360661/v1. URL: <https://www.researchsquare.com/article/rs-1360661/latest>.
- [0] Malyshev, D. I., Rybak, L. A., Pisarenko, A. S., and Cherkasov, V. V. "Analysis of the Singularities Influence on the Forward Kinematics Solution and the Geometry of the Workspace of the Gough-Stewart Platform". In: *Advances in Service and Industrial Robotics*. Ed. by Müller, A. and Brandstötter, M. Vol. 120. Mechanisms and Machine Science. Cham: Springer International Publishing and Imprint: Springer, 2022, pp. 60–67. ISBN: 978-3-031-04869-2. DOI: 10.1007/978-3-031-04870-8{\textunderscore}8.
- [0] Zhao, H., Zhang, B., Yin, X., Zhang, Z., Xia, Q., and Zhang, F. "Singularity Analysis and Singularity Avoidance Trajectory Planning for Industrial Robots". In: *2021 China Automation Congress (CAC)*. IEEE, 2021. DOI: 10.1109/cac53003.2021.9727497.
- [0] Milenkovic, P. "Wrist singularity avoidance with a robot end-effector adding an oblique, redundant axis". In: *Mechanism and Machine Theory* 162 (2021), p. 104355. ISSN: 0094-114X. DOI: 10.1016/j.mechmachtheory.2021.104355. URL: <https://www.sciencedirect.com/science/article/pii/s0094114x21001130>.
- [0] Faria, C., Ferreira, F., Erlhagen, W., Monteiro, S., and Bicho, E. "Position-based kinematics for 7-DoF serial manipulators with global configuration control, joint limit and singularity avoidance". In: *Mechanism and Machine Theory* 121 (2018), pp. 317–334. ISSN: 0094-114X. DOI: 10.1016/j.mechmachtheory.2017.10.025. URL: <https://www.sciencedirect.com/science/article/pii/s0094114x17306559>.
- [0] Duong, X. B. "On the Effect of the End-effector Point Trajectory on the Joint Jerk of the Redundant Manipulators". In: *Journal of Applied and Computational Mechanics* 7.3 (2021), pp. 1575–1582. ISSN: 2383-4536. DOI: 10.22055/jacm.2021.35350.2635. URL: https://jacm.scu.ac.ir/article_16660.html.
- [0] R.V. Dubey, J.A. Euler, and S.M. Babcock. *Robotics and Automation, 5th IEEE International Conference on, 1988: Proceedings*. Los Alamitos: IEEE Computer Society Press, 1988. ISBN: 0818608528. URL: <http://ieeexplore.ieee.org/servlet/opac?punumber=202>.

- [0] Valente, A., Baraldo, S., and Carpanzano, E. “Smooth trajectory generation for industrial robots performing high precision assembly processes”. In: *CIRP Annals* 66.1 (2017), pp. 17–20. ISSN: 00078506. DOI: 10.1016/j.cirp.2017.04.105. URL: <https://www.sciencedirect.com/science/article/pii/s0007850617301051>.
- [0] Lin, J., Ye, C., Yang, J., Zhao, H., Ding, H., and Luo, M. “Contour error-based optimization of the end-effector pose of a 6 degree-of-freedom serial robot in milling operation”. In: *Robotics and Computer-Integrated Manufacturing* 73 (2022), p. 102257. ISSN: 0736-5845. DOI: 10.1016/j.rcim.2021.102257. URL: <https://www.sciencedirect.com/science/article/pii/s073658452100137x>.
- [0] Xiong, G., Ding, Y., and Zhu, L. “Stiffness-based pose optimization of an industrial robot for five-axis milling”. In: *Robotics and Computer-Integrated Manufacturing* 55 (2019), pp. 19–28. ISSN: 0736-5845. DOI: 10.1016/j.rcim.2018.07.001. URL: <https://www.sciencedirect.com/science/article/pii/s0736584517304556>.
- [0] Shi, X., Guo, Y., Chen, X., Chen, Z., and Yang, Z. “Kinematics and Singularity Analysis of a 7-DOF Redundant Manipulator”. In: *Sensors* 21.21 (2021), p. 7257. ISSN: 1424-8220. DOI: 10.3390/s21217257. URL: <https://www.mdpi.com/1424-8220/21/21/7257>.
- [0] Huynh, H. N., Assadi, H., Rivière-Lorphèvre, E., Verlinden, O., and Ahmadi, K. “Modelling the dynamics of industrial robots for milling operations”. In: *Robotics and Computer-Integrated Manufacturing* 61 (2020), p. 101852. ISSN: 0736-5845. DOI: 10.1016/j.rcim.2019.101852. URL: <https://www.sciencedirect.com/science/article/pii/s0736584519301784>.
- [0] Chen-Gang, Li-Tong, Chu-Ming, Xuan, J.-Q., and Xu, S.-H. “Review on kinematics calibration technology of serial robots”. In: *International Journal of Precision Engineering and Manufacturing* 15.8 (2014), pp. 1759–1774. ISSN: 2005-4602. DOI: 10.1007/s12541-014-0528-1. URL: <https://link.springer.com/article/10.1007/s12541-014-0528-1>.
- [0] Gasparetto, A. and Zanotto, V. “Optimal trajectory planning for industrial robots”. In: *Advances in Engineering Software* 41.4 (2010), pp. 548–556. ISSN: 0965-9978. DOI: 10.1016/j.advengsoft.2009.11.001. URL: <https://www.sciencedirect.com/science/article/pii/s0965997809002464>.
- [0] Vande Weghe, M., Ferguson, D., and Srinivasa, S. S. “Randomized path planning for redundant manipulators without inverse kinematics”. In: *2007 7th IEEE-RAS International Conference on Humanoid Robots*. IEEE, 2007. DOI: 10.1109/ichr.2007.4813913.
- [0] Reiter, A., Muller, A., and Gatringer, H. “Inverse kinematics in minimum-time trajectory planning for kinematically redundant manipulators”. In: *IECON 2016 - 42nd Annual Conference of the IEEE Industrial Electronics Society*. IEEE, 2016. DOI: 10.1109/iecon.2016.7793436.
- [0] Doan, N. C. N., Tao, P. Y., and Lin, W. “Optimal redundancy resolution for robotic arc welding using modified particle swarm optimization”. In: *2016 IEEE International Conference on Advanced Intelligent Mechatronics (AIM)*. IEEE, 2016. DOI: 10.1109/aim.2016.7576826.

- [0] Boscariol, P. and Richiedei, D. “Energy Saving in Redundant Robotic Cells: Optimal Trajectory Planning”. In: Springer, Cham, 2019, pp. 268–275. doi: 10.1007/978-3-030-00365-4_32. URL: https://link.springer.com/chapter/10.1007/978-3-030-00365-4_32.
- [0] Ayten, K. K., Sahinkaya, M. N., and Dumlu, A. “Optimum Trajectory Generation for Redundant/Hyper-Redundant Manipulators”. In: *IFAC-PapersOnLine* 49.21 (2016), pp. 493–500. ISSN: 2405-8963. doi: 10.1016/j.ifacol.2016.10.651. URL: <https://www.sciencedirect.com/science/article/pii/s2405896316322637>.
- [0] Iqbal, A., Zhao, G., Suhaimi, H., He, N., Hussain, G., and Zhao, W. “Readiness of subtractive and additive manufacturing and their sustainable amalgamation from the perspective of Industry 4.0: a comprehensive review”. In: *The International Journal of Advanced Manufacturing Technology* 111.9-10 (2020), pp. 2475–2498. ISSN: 1433-3015. doi: 10.1007/s00170-020-06287-6. URL: <https://link.springer.com/article/10.1007/s00170-020-06287-6>.
- [0] Watson, J. K. and Taminger, K. M. B. “A decision-support model for selecting additive manufacturing versus subtractive manufacturing based on energy consumption”. In: *Journal of Cleaner Production* 176 (2015), pp. 1316–1322. ISSN: 0959-6526. doi: 10.1016/j.jclepro.2015.12.009. URL: <https://www.sciencedirect.com/science/article/pii/s0959652615018247>.
- [0] Dilberoglu, U. M., Gharehpapagh, B., Yaman, U., and Dolen, M. “The Role of Additive Manufacturing in the Era of Industry 4.0”. In: *Procedia Manufacturing* 11 (2017), pp. 545–554. ISSN: 2351-9789. doi: 10.1016/j.promfg.2017.07.148. URL: <https://www.sciencedirect.com/science/article/pii/s2351978917303529>.
- [0] Bandyopadhyay, A. *Additive Manufacturing, Second Edition*. 2nd ed. Milton: Taylor & Francis Group, 2020. ISBN: 9780429881022.
- [0] van Le, T., Paris, H., and Mandil, G. “Environmental impact assessment of an innovative strategy based on an additive and subtractive manufacturing combination”. In: *Journal of Cleaner Production* 164 (2017), pp. 508–523. ISSN: 0959-6526. doi: 10.1016/j.jclepro.2017.06.204. URL: <https://www.sciencedirect.com/science/article/pii/s0959652617313732>.
- [0] Wang, W., Guo, Q., Yang, Z., Jiang, Y., and Xu, J. “A state-of-the-art review on robotic milling of complex parts with high efficiency and precision”. In: *Robotics and Computer-Integrated Manufacturing* 79 (2023), p. 102436. ISSN: 0736-5845. doi: 10.1016/j.rcim.2022.102436. URL: <https://www.sciencedirect.com/science/article/pii/s073658452200120x>.
- [0] Calleja, A., Bo, P., González, H., Bartoň, M., and López de Lacalle, Luis Norberto. “Highly accurate 5-axis flank CNC machining with conical tools”. In: *The International Journal of Advanced Manufacturing Technology* 97.5-8 (2018), pp. 1605–1615. ISSN: 1433-3015. doi: 10.1007/s00170-018-2033-7. URL: <https://link.springer.com/article/10.1007/s00170-018-2033-7>.

- [0] Abdulhameed, O., Al-Ahmari, A., Ameen, W., and Mian, S. H. “Additive manufacturing: Challenges, trends, and applications”. In: *Advances in Mechanical Engineering* 11.2 (2019). doi: 10.1177/1687814018822880.
- [0] Kumar, K., Ranjan, C., and Davim, J. P. *CNC Programming for Machining*. 1st ed. 2020. Materials Forming, Machining and Tribology. Cham: Springer International Publishing and Imprint: Springer, 2020. ISBN: 978-3-030-41278-4. doi: 10.1007/978-3-030-41279-1.
- [0] Amanullah, A., Murshiduzzaman, Saleh, T., and Khan, R. “Design and Development of a Hybrid Machine Combining Rapid Prototyping and CNC Milling Operation”. In: 1877-7058 184 (2017), pp. 163–170. ISSN: 1877-7058. doi: 10.1016/j.proeng.2017.04.081.
- [0] Tomaz, I., Gupta, M. K., and Pimenov, D. Y. “Subtractive Manufacturing of Different Composites”. In: *Additive and Subtractive Manufacturing of Composites*. Springer, Singapore, 2021, pp. 137–165. doi: 10.1007/978-981-16-3184-9{\textunderscore}6. URL: https://link.springer.com/chapter/10.1007/978-981-16-3184-9_6.
- [0] Yang, B., Zhang, G., Ran, Y., and Yu, H. “Kinematic modeling and machining precision analysis of multi-axis CNC machine tools based on screw theory”. In: *Mechanism and Machine Theory* 140 (2019), pp. 538–552. ISSN: 0094-114X. doi: 10.1016/j.mechmachtheory.2019.06.021. URL: <https://www.sciencedirect.com/science/article/pii/s0094114x19307992>.
- [0] Nee, A. Y. C. *Handbook of Manufacturing Engineering and Technology*. 1st ed. 2015. London: Springer London and Imprint: Springer, 2015. ISBN: 978-1-4471-4669-8. doi: 10.1007/978-1-4471-4670-4.
- [0] Tien, D. H., Duc, Q. T., Van, T. N., Nguyen, N.-T., Do Duc, T., and Duy, T. N. “Online monitoring and multi-objective optimisation of technological parameters in high-speed milling process”. In: *The International Journal of Advanced Manufacturing Technology* 112.9-10 (2021), pp. 2461–2483. ISSN: 1433-3015. doi: 10.1007/s00170-020-06444-x. URL: <https://link.springer.com/article/10.1007/s00170-020-06444-x>.
- [0] Jayawardane, H., Davies, I. J., Gamage, J. R., John, M., and Biswas, W. K. “Sustainability perspectives – a review of additive and subtractive manufacturing”. In: *Sustainable Manufacturing and Service Economics* 2 (2023), p. 100015. ISSN: 2667-3444. doi: 10.1016/j.smse.2023.100015.
- [0] Gu, X. and Koren, Y. “Manufacturing system architecture for cost-effective mass-individualization”. In: *Manufacturing Letters* 16 (2018), pp. 44–48. ISSN: 2213-8463. doi: 10.1016/j.mfglet.2018.04.002. URL: <https://www.sciencedirect.com/science/article/pii/s2213846317300974>.
- [0] Faludi, J., Bayley, C., Bhogal, S., and Iribarne, M. “Comparing environmental impacts of additive manufacturing vs traditional machining via life-cycle assessment”. In: *Rapid Prototyping Journal* 21.1 (2015), pp. 14–33. doi: 10.1108/RPJ-07-2013-0067. URL: <https://www.emerald.com/insight/content/doi/10.1108/rpj-07-2013-0067/full/pdf>.

- [0] Hesser, D. F. and Markert, B. "Tool wear monitoring of a retrofitted CNC milling machine using artificial neural networks". In: *Manufacturing Letters* 19 (2019), pp. 1–4. ISSN: 2213-8463. DOI: 10.1016/j.mfglet.2018.11.001. URL: <https://www.sciencedirect.com/science/article/pii/s2213846318301524>.
- [0] YUE, C., GAO, H., LIU, X., LIANG, S. Y., and Wang, L. "A review of chatter vibration research in milling". In: *1000-9361* 32.2 (2019), pp. 215–242. ISSN: 1000-9361. DOI: 10.1016/j.cja.2018.11.007. URL: <https://www.sciencedirect.com/science/article/pii/s1000936119300147>.
- [0] Aslan, D. and Altintas, Y. "On-line chatter detection in milling using drive motor current commands extracted from CNC". In: *International Journal of Machine Tools and Manufacture* 132 (2018), pp. 64–80. ISSN: 0890-6955. DOI: 10.1016/j.ijmachtools.2018.04.007. URL: <https://www.sciencedirect.com/science/article/pii/s0890695518300841>.
- [0] Giorgio Bort, C. M., Leonesio, M., and Bosetti, P. "A model-based adaptive controller for chatter mitigation and productivity enhancement in CNC milling machines". In: *Robotics and Computer-Integrated Manufacturing* 40 (2016), pp. 34–43. ISSN: 0736-5845. DOI: 10.1016/j.rcim.2016.01.006. URL: <https://www.sciencedirect.com/science/article/pii/s0736584516300242>.
- [0] Wan, S., Li, X., Su, W., Yuan, J., Hong, J., and Jin, X. "Active damping of milling chatter vibration via a novel spindle system with an integrated electromagnetic actuator". In: *Precision Engineering* 57 (2019), pp. 203–210. ISSN: 0141-6359. DOI: 10.1016/j.precisioneng.2019.04.007. URL: <https://www.sciencedirect.com/science/article/pii/s0141635918307931>.
- [0] CNC Masters - Just another WordPress site. *CNC Machine Buyer's Guide: Types, Uses, Price, & Definitions*: Last access: 30.10.2023. 2022. URL: <https://www.cncmasters.com/cnc-machine-buyers-guide/>.
- [0] *5-axis milling*: Last access: 30.10.2023. URL: <https://www.manufacturingguide.com/en/5-axis-milling>.
- [0] Prakash, K. S., Nancharaih, T., and Rao, V. S. "Additive Manufacturing Techniques in Manufacturing -An Overview". In: *Materials Today: Proceedings* 5.2 (2018), pp. 3873–3882. ISSN: 2214-7853. DOI: 10.1016/j.matpr.2017.11.642. URL: <https://www.sciencedirect.com/science/article/pii/s2214785317329152>.
- [0] Wickramasinghe, S., Do, T., and Tran, P. "FDM-Based 3D Printing of Polymer and Associated Composite: A Review on Mechanical Properties, Defects and Treatments". In: *Polymers* 12.7 (2020), p. 1529. ISSN: 2073-4360. DOI: 10.3390/polym12071529. URL: <https://www.mdpi.com/2073-4360/12/7/1529>.
- [0] Wang, J., Goyanes, A., Gaisford, S., and Basit, A. W. "Stereolithographic (SLA) 3D printing of oral modified-release dosage forms". In: *International Journal of Pharmaceutics* 503.1-2 (2016), pp. 207–212. ISSN: 0378-5173. DOI: 10.1016/j.ijpharm.2016.03.016. URL: <https://www.sciencedirect.com/science/article/pii/s0378517316302150>.

- [0] Meier, C., Penny, R. W., Zou, Y., Gibbs, J. S., and Hart, A. J. “THERMOPHYSICAL PHENOMENA IN METAL ADDITIVE MANUFACTURING BY SELECTIVE LASER MELTING: FUNDAMENTALS, MODELING, SIMULATION, AND EXPERIMENTATION”. In: *Annual Review of Heat Transfer* 20.1 (2017), pp. 241–316. ISSN: 1049-0787. DOI: 10.1615/AnnualRevHeatTransfer.2018019042. URL: <https://www.dl.begellhouse.com/references/5756967540dd1b03,562e7b3835dec96e,0860d4f32b9f248d.html>.
- [0] Bose, S., Ke, D., Sahasrabudhe, H., and Bandyopadhyay, A. “Additive manufacturing of biomaterials”. In: *Progress in materials science* 93 (2018), pp. 45–111. ISSN: 0079-6425. DOI: 10.1016/j.pmatsci.2017.08.003.
- [0] Attaran, M. “The rise of 3-D printing: The advantages of additive manufacturing over traditional manufacturing”. In: *Business Horizons* 60.5 (2017), pp. 677–688. ISSN: 0007-6813. DOI: 10.1016/j.bushor.2017.05.011. URL: <https://www.sciencedirect.com/science/article/pii/s0007681317300897>.
- [0] Plocher, J. and Panesar, A. “Review on design and structural optimisation in additive manufacturing: Towards next-generation lightweight structures”. In: *Materials & Design* 183 (2019), p. 108164. ISSN: 02641275. DOI: 10.1016/j.matdes.2019.108164.
- [0] Jandyal, A., Chaturvedi, I., Wazir, I., Raina, A., and Ul Haq, M. I. “3D printing – A review of processes, materials and applications in industry 4.0”. In: 2666-4127 3 (2022), pp. 33–42. ISSN: 2666-4127. DOI: 10.1016/j.susoc.2021.09.004. URL: <https://www.sciencedirect.com/science/article/pii/s2666412721000441>.
- [0] Haleem, A. and Javaid, M. “Additive Manufacturing Applications in Industry 4.0: A Review”. In: *Journal of Industrial Integration and Management* 04.04 (2019), p. 1930001. ISSN: 2424-8622. DOI: 10.1142/S2424862219300011.
- [0] Svetlizky, D., Das, M., Zheng, B., Vyatskikh, A. L., Bose, S., Bandyopadhyay, A., Schoenung, J. M., Lavernia, E. J., and Eliaz, N. “Directed energy deposition (DED) additive manufacturing: Physical characteristics, defects, challenges and applications”. In: *Materials Today* 49 (2021), pp. 271–295. ISSN: 1369-7021. DOI: 10.1016/j.mattod.2021.03.020. URL: <https://www.sciencedirect.com/science/article/pii/s1369702121001139>.
- [0] DIN EN ISO/ASTM 52900:2022-03, *Additive Fertigung - Grundlagen - Terminologie (ISO/ASTM 52900:2021); Deutsche Fassung EN ISO/ASTM 52900:2021*. Berlin. DOI: 10.31030/3290011.
- [0] Ou, W., Mukherjee, T., Knapp, G. L., Wei, Y., and DebRoy, T. “Fusion zone geometries, cooling rates and solidification parameters during wire arc additive manufacturing”. In: *International Journal of Heat and Mass Transfer* 127 (2018), pp. 1084–1094. ISSN: 0017-9310. DOI: 10.1016/j.ijheatmasstransfer.2018.08.111. URL: <https://www.sciencedirect.com/science/article/pii/s0017931018323974>.
- [0] Cunningham, C. R., Flynn, J. M., Shokrani, A., Dhokia, V., and Newman, S. T. “Invited review article: Strategies and processes for high quality wire arc additive manufacturing”. In: *Additive Manufacturing* 22 (2018), pp. 672–686. ISSN: 2214-8604. DOI:

- 10.1016/j.addma.2018.06.020. URL: <https://www.sciencedirect.com/science/article/pii/s2214860418303920>.
- [0] Ding, D., Pan, Z., Cuiuri, D., and Li, H. “Wire-feed additive manufacturing of metal components: technologies, developments and future interests”. In: *The International Journal of Advanced Manufacturing Technology* 81.1-4 (2015), pp. 465–481. ISSN: 1433-3015. DOI: 10.1007/s00170-015-7077-3. URL: <https://link.springer.com/article/10.1007/s00170-015-7077-3>.
- [0] Schmitz, M., Wiartalla, J., Gelfgren, M., Mann, S., Corves, B., and Hüsing, M. “A Robot-Centered Path-Planning Algorithm for Multidirectional Additive Manufacturing for WAAM Processes and Pure Object Manipulation”. In: *Applied Sciences* 11.13 (2021), p. 5759. DOI: 10.3390/app11135759. URL: <https://www.mdpi.com/2076-3417/11/13/5759>.
- [0] Nagasai, B. P., Malarvizhi, S., and Balasubramanian, V. “Effect of welding processes on mechanical and metallurgical characteristics of carbon steel cylindrical components made by wire arc additive manufacturing (WAAM) technique”. In: *CIRP Journal of Manufacturing Science and Technology* 36 (2022), pp. 100–116. ISSN: 1755-5817. DOI: 10.1016/j.cirpj.2021.11.005. URL: <https://www.sciencedirect.com/science/article/pii/s1755581721001887>.
- [0] Iván Tabernero, Paskual, A., Álvarez, P., and Suárez, A. “Study on Arc Welding Processes for High Deposition Rate Additive Manufacturing”. In: *2212-8271* 68 (2018), pp. 358–362. ISSN: 2212-8271. DOI: 10.1016/j.procir.2017.12.095. URL: <https://www.sciencedirect.com/science/article/pii/s2212827117310363>.
- [0] Li, J. Z., Alkahari, M. R., Rosli, N. A. B., Hasan, R., Sudin, M. N., and Ramli, F. R. “Review of Wire Arc Additive Manufacturing for 3D Metal Printing”. In: *International Journal of Automation Technology* 13.3 (2019), pp. 346–353. ISSN: 1883-8022. DOI: 10.20965/ijat.2019.p0346. URL: https://www.jstage.jst.go.jp/article/ijat/13/3/13_346/_article/-char/ja/.
- [0] Wu, B., Pan, Z., Ding, D., Cuiuri, D., Li, H., Xu, J., and Norrish, J. “A review of the wire arc additive manufacturing of metals: properties, defects and quality improvement”. In: *Journal of Manufacturing Processes* 35 (2018), pp. 127–139. ISSN: 1526-6125. DOI: 10.1016/j.jmapro.2018.08.001. URL: <https://www.sciencedirect.com/science/article/pii/s1526612518310739>.
- [0] Chaurasia, M. and Sinha, M. K., eds. *Investigations on Process Parameters of Wire Arc Additive Manufacturing (WAAM): A Review*. 2021. DOI: 10.1007/978-981-15-8542-5{\textunderscore}74.
- [0] *Fabricación aditiva en metales - WAAM | Lortek*: Last access: 30.10.2023. URL: <https://www.lortek.es/en/technological-areas/metal-additive-manufacturing/waam>.
- [0] Dutra, J. C., Gonçalves e Silva, R. H., and Marques, C. “Melting and welding power characteristics of MIG–CMT versus conventional MIG for aluminium 5183”. In: *Welding International* 29.3 (2015), pp. 181–186. DOI: 10.1080/09507116.2014.932974.

- [0] Selvi, S., Vishvaksenan, A., and Rajasekar, E. “Cold metal transfer (CMT) technology - An overview”. In: 2214-9147 14.1 (2018), pp. 28–44. ISSN: 2214-9147. DOI: 10.1016/j.dt.2017.08.002. URL: <https://www.sciencedirect.com/science/article/pii/s2214914717301022>.
- [0] Srinivasan, D., Sevvel, P., John Solomon, I., and Tanushkumaar, P. “A review on Cold Metal Transfer (CMT) technology of welding”. In: *Materials Today: Proceedings* 64 (2022), pp. 108–115. ISSN: 2214-7853. DOI: 10.1016/j.matpr.2022.04.016. URL: <https://www.sciencedirect.com/science/article/pii/s2214785322021289>.
- [0] Scotti, F. M., Teixeira, F. R., Da Silva, L. J., Araújo, D. B. de, Reis, R. P., and Scotti, A. “Thermal management in WAAM through the CMT Advanced process and an active cooling technique”. In: *Journal of Manufacturing Processes* 57 (2020), pp. 23–35. ISSN: 1526-6125. DOI: 10.1016/j.jmapro.2020.06.007. URL: <https://www.sciencedirect.com/science/article/pii/s1526612520303807>.
- [0] Cong, B., Ouyang, R., Qi, B., and Ding, J. “Influence of Cold Metal Transfer Process and Its Heat Input on Weld Bead Geometry and Porosity of Aluminum-Copper Alloy Welds”. In: *Rare Metal Materials and Engineering* 45.3 (2016), pp. 606–611. ISSN: 1875-5372. DOI: 10.1016/S1875-5372(16)30080-7. URL: <https://www.sciencedirect.com/science/article/pii/s1875537216300807>.
- [0] Pickin, C. G. and Young, K. “Evaluation of cold metal transfer (CMT) process for welding aluminium alloy”. In: *Science and Technology of Welding and Joining* 11.5 (2006), pp. 583–585. DOI: 10.1179/174329306X120886.
- [0] Dalton, R. *Imaging CMT Welding with a Weld Camera*: Last access: 30.10.2023. URL: <https://blog.xiris.com/blog/imaging-cmt-welding-with-a-weld-camera>.
- [0] Rahul, S. G., Dhivyasri, G., Kavitha, P., Arungalai Vendan, S., Kumar, K. R., Garg, A., and Gao, L. “Model reference adaptive controller for enhancing depth of penetration and bead width during Cold Metal Transfer joining process”. In: *Robotics and Computer-Integrated Manufacturing* 53 (2018), pp. 122–134. ISSN: 0736-5845. DOI: 10.1016/j.rcim.2018.03.013. URL: <https://www.sciencedirect.com/science/article/pii/s0736584517304519>.
- [0] Pickin, C. G., Williams, S. W., and Lunt, M. “Characterisation of the cold metal transfer (CMT) process and its application for low dilution cladding”. In: *Journal of Materials Processing Technology* 211.3 (2011), pp. 496–502. ISSN: 0924-0136. DOI: 10.1016/j.jmatprotec.2010.11.005. URL: <https://www.sciencedirect.com/science/article/pii/s0924013610003456>.
- [0] Ji, W. and Wang, L. “Industrial robotic machining: a review”. In: *The International Journal of Advanced Manufacturing Technology* 103.1-4 (2019), pp. 1239–1255. ISSN: 1433-3015. DOI: 10.1007/s00170-019-03403-z. URL: <https://link.springer.com/article/10.1007/s00170-019-03403-z>.

- [0] Siciliano, B. and Khatib, O. *Springer handbook of robotics: With 1375 figures and 109 tables*. 2nd edition. Berlin and Heidelberg: Springer, 2016. ISBN: 978-3-319-32550-7. DOI: 10.1007/978-3-319-32552-1.
- [0] Hanafusa, H., Yoshikawa, T., and Nakamura, Y. “Analysis and Control of Articulated Robot Arms with Redundancy”. In: *IFAC Proceedings Volumes* 14.2 (1981), pp. 1927–1932. ISSN: 1474-6670. DOI: 10.1016/S1474-6670(17)63754-6. URL: <https://www.sciencedirect.com/science/article/pii/s1474667017637546>.
- [0] Jain, R., Nayab Zafar, M., and Mohanta, J. C. “Modeling and Analysis of Articulated Robotic Arm for Material Handling Applications”. In: *IOP Conference Series: Materials Science and Engineering* 691.1 (2019), p. 012010. ISSN: 1757-899X. DOI: 10.1088/1757-899X/691/1/012010. URL: <https://iopscience.iop.org/article/10.1088/1757-899x/691/1/012010/meta>.
- [0] Kim, H. S. and Tsai, L.-W. “Design Optimization of a Cartesian Parallel Manipulator”. In: *Journal of Mechanical Design* 125.1 (2003), pp. 43–51. ISSN: 1050-0472. DOI: 10.1115/1.1543977.
- [0] Das, M. T. and Canan Dülger, L. “Mathematical modelling, simulation and experimental verification of a scara robot”. In: *Simulation Modelling Practice and Theory* 13.3 (2005), pp. 257–271. ISSN: 1569-190X. DOI: 10.1016/j.simpat.2004.11.004. URL: <https://www.sciencedirect.com/science/article/pii/s1569190x04001200>.
- [0] Bonev, I. *Delta parallel robot-the story of success*. Newsletter, available at <http://www.parallelmic.org>, 2001. URL: <http://www.robotics.caltech.edu/~jwb/courses/me115/handouts/deltarobothistory.pdf>.
- [0] Liu, L., Guo, F., Zou, Z., and Duffy, V. G. “Application, Development and Future Opportunities of Collaborative Robots (Cobots) in Manufacturing: A Literature Review”. In: *International Journal of Human–Computer Interaction* (2022), pp. 1–18. DOI: 10.1080/10447318.2022.2041907.
- [0] Hägele, M., Nilsson, K., Pires, J. N., and Bischoff, R. “Industrial Robotics”. In: *Springer Handbook of Robotics*. Springer, Cham, 2016, pp. 1385–1422. DOI: 10.1007/978-3-319-32552-1_54. URL: https://link.springer.com/chapter/10.1007/978-3-319-32552-1_54.
- [0] Kubela, T., Pochyly, A., and Singule, V. “Assessment of industrial robots accuracy in relation to accuracy improvement in machining processes”. In: *2016 IEEE International Power Electronics and Motion Control Conference (PEMC)*. IEEE, 2016. DOI: 10.1109/epepemc.2016.7752083.
- [0] Heyer, C. “Human-robot interaction and future industrial robotics applications”. In: *2010 IEEE/RSJ International Conference on Intelligent Robots and Systems*. IEEE, 2010. DOI: 10.1109/iros.2010.5651294.

- [0] Jung, J. H. and Lim, D.-G. “Industrial robots, employment growth, and labor cost: A simultaneous equation analysis”. In: *0040-1625* 159 (2020), p. 120202. ISSN: 0040-1625. DOI: 10.1016/j.techfore.2020.120202. URL: <https://www.sciencedirect.com/science/article/pii/s0040162520310283>.
- [0] Joshi, K., Melkote, S. N., Anderson, M., and Chaudhari, R. “Investigation of cycle time behavior in the robotic grinding process”. In: *CIRP Journal of Manufacturing Science and Technology* 35 (2021), pp. 315–322. ISSN: 1755-5817. DOI: 10.1016/j.cirpj.2021.06.021. URL: <https://www.sciencedirect.com/science/article/pii/s1755581721001139>.
- [0] Ye, W. “Exploring the Use of Industrial Robots in CNC Machine Tool Programming and Operation Courses”. In: *2022 7th International Conference on Mechatronics System and Robots (ICMSR)*. IEEE, 2022. DOI: 10.1109/icmsr2020.2022.00017.
- [0] Wu, K., Li, J., Zhao, H., and Zhong, Y. “Review of Industrial Robot Stiffness Identification and Modelling”. In: *Applied Sciences* 12.17 (2022), p. 8719. DOI: 10.3390/app12178719. URL: <https://www.mdpi.com/2076-3417/12/17/8719>.
- [0] Heimann, O. and Guhl, J. “Industrial Robot Programming Methods: A Scoping Review”. In: *2020 25th IEEE International Conference on Emerging Technologies and Factory Automation (ETFA)*. IEEE, 2020. DOI: 10.1109/etfa46521.2020.9211997.
- [0] Singh, R., Kukshal, V., and Yadav, V. S. “A Review on Forward and Inverse Kinematics of Classical Serial Manipulators”. In: *Advances in Engineering Design*. Ed. by Rakesh, P. K., Sharma, A. K., and Singh, I. Lecture Notes in Mechanical Engineering. Singapore: Springer Singapore and Imprint: Springer, 2021, pp. 417–428. ISBN: 978-981-33-4017-6. DOI: 10.1007/978-981-33-4018-3{\textunderscore}39.
- [0] Huynh Hoai Nam, Edouard Riviere, and Olivier Verlinden. “Multibody modelling of a flexible 6-axis robot dedicated to robotic machining”. In: 2018. URL: https://www.researchgate.net/profile/huynh-hoai-nam/publication/326106790_multibody_modelling_of_a_flexible_6-axis_robot_dedicated_to_robotic_machining.
- [0] Lin, Y., Zhao, H., and Ding, H. “Real-time path correction of industrial robots in machining of large-scale components based on model and data hybrid drive”. In: *Robotics and Computer-Integrated Manufacturing* 79 (2023), p. 102447. ISSN: 0736-5845. DOI: 10.1016/j.rcim.2022.102447. URL: <https://www.sciencedirect.com/science/article/pii/s0736584522001302>.
- [0] Bosscher, P. and Hedman, D. “Real-time collision avoidance algorithm for robotic manipulators”. In: *Industrial Robot: An International Journal* 38.2 (2011), pp. 186–197. DOI: 10.1108/01439911111106390. URL: <https://www.emerald.com/insight/content/doi/10.1108/01439911111106390/full/pdf>.
- [0] Domae, Y. “Recent Trends in the Research of Industrial Robots and Future Outlook”. In: *Journal of Robotics and Mechatronics* 31.1 (2019), pp. 57–62. ISSN: 1883-8049. DOI: 10.20965/jrm.2019.p0057. URL: https://www.jstage.jst.go.jp/article/jrobomech/31/1/31_57/_article/-char/ja/.

- [0] Yuan, L., Pan, Z., Ding, D., He, F., van Duin, S., Li, H., and Li, W. “Investigation of humping phenomenon for the multi-directional robotic wire and arc additive manufacturing”. In: *Robotics and Computer-Integrated Manufacturing* 63 (2020), p. 101916. ISSN: 0736-5845. DOI: 10.1016/j.rcim.2019.101916. URL: <https://www.sciencedirect.com/science/article/pii/s0736584519304260>.
- [0] “KUKA linear units: Last access: 30.10.2023”. In: (). URL: <https://www.kuka.com/en-de/products/robot-systems/robot-periphery/linear-units>.
- [0] Hagane, S. and Venture, G. “Robotic Manipulator’s Expressive Movements Control Using Kinematic Redundancy”. In: *Machines* 10.12 (2022), p. 1118. ISSN: 2075-1702. DOI: 10.3390/machines10121118.
- [0] Halevi, Y., Carpanzano, E., Montalbano, G., and Koren, Y. “Minimum energy control of redundant actuation machine tools”. In: *CIRP Annals* 60.1 (2011), pp. 433–436. ISSN: 00078506. DOI: 10.1016/j.cirp.2011.03.032.
- [0] Ahangar, S., Mehrabani, M. V., Pouransari Shorijeh, A., and Masouleh, M. T. “Design a 3-DOF Delta Parallel Robot by One Degree Redundancy along the Conveyor Axis, A Novel Automation Approach”. In: *2019 5th Conference on Knowledge Based Engineering and Innovation (KBEI)*. IEEE, 2019. DOI: 10.1109/kbei.2019.8734975.
- [0] Erdős, G., Kovács, A., and Váncza, J. “Optimized joint motion planning for redundant industrial robots”. In: *CIRP Annals* 65.1 (2016), pp. 451–454. ISSN: 00078506. DOI: 10.1016/j.cirp.2016.04.024. URL: <https://www.sciencedirect.com/science/article/pii/s0007850616300245>.
- [0] Zhang, Y., Wang, T., Dong, J., Peng, P., Liu, Y., and Ke, R. “An analytical G3 continuous corner smoothing method with adaptive constraints adjustments for five-axis machine tool”. In: *The International Journal of Advanced Manufacturing Technology* 109.3-4 (2020), pp. 1007–1026. ISSN: 1433-3015. DOI: 10.1007/s00170-020-05402-x.
- [0] Li, F., Chen, S., Wu, Z., and Yan, Z. “Adaptive process control of wire and arc additive manufacturing for fabricating complex-shaped components”. In: *The International Journal of Advanced Manufacturing Technology* 96.1-4 (2018), pp. 871–879. ISSN: 1433-3015. DOI: 10.1007/s00170-018-1590-0. URL: <https://link.springer.com/article/10.1007/s00170-018-1590-0>.
- [0] Sun, S. and Altintas, Y. “A G3 continuous tool path smoothing method for 5-axis CNC machining”. In: *CIRP Journal of Manufacturing Science and Technology* 32 (2021), pp. 529–549. ISSN: 1755-5817. DOI: 10.1016/j.cirpj.2020.11.002. URL: <https://www.sciencedirect.com/science/article/pii/s1755581720301280>.
- [0] Yang, J. and Yuen, A. “An analytical local corner smoothing algorithm for five-axis CNC machining”. In: *International Journal of Machine Tools and Manufacture* 123 (2017), pp. 22–35. ISSN: 0890-6955. DOI: 10.1016/j.ijmachtools.2017.07.007.

- [0] *Continuous-path mode (G64, G641, G642, G643, G644, G645, ADIS, ADISPOS) - SINUMERIK ... - ID: 28705635 - Industry Support Siemens: Last Access: 24/10/2023. URL: <https://support.industry.siemens.com/cs/mdm/28705635?c=19192781067&lc=en-AO>.*
- [0] Shahzadeh, A., Khosravi, A., Robinette, T., and Nahavandi, S. “Smooth path planning using biclothoid fillets for high speed CNC machines”. In: *International Journal of Machine Tools and Manufacture* 132 (2018), pp. 36–49. ISSN: 0890-6955. DOI: 10.1016/j.ijmachtools.2018.04.003. URL: <https://www.sciencedirect.com/science/article/pii/s0890695518300804>.
- [0] Li, B., Zhang, H., and Ye, P. “Error constraint optimization for corner smoothing algorithms in high-speed CNC machine tools”. In: *The International Journal of Advanced Manufacturing Technology* 99.1-4 (2018), pp. 635–646. ISSN: 1433-3015. DOI: 10.1007/s00170-018-2489-5.
- [0] Liu, Y., Wan, M., Qin, X.-B., Xiao, Q.-B., and Zhang, W.-H. “FIR filter-based continuous interpolation of G01 commands with bounded axial and tangential kinematics in industrial five-axis machine tools”. In: *International Journal of Mechanical Sciences* 169 (2020), p. 105325. ISSN: 00207403. DOI: 10.1016/j.ijmecsci.2019.105325.
- [0] Boujelbene, M., Moisan, A., Tounsi, N., and Brenier, B. “Productivity enhancement in dies and molds manufacturing by the use of C1 continuous tool path”. In: *International Journal of Machine Tools and Manufacture* 44.1 (2004), pp. 101–107. ISSN: 0890-6955. DOI: 10.1016/j.ijmachtools.2003.08.005.
- [0] Bi, Z. “Computer-Aided Manufacturing (CAM)”. In: *Practical Guide to Digital Manufacturing*. Springer, Cham, 2021, pp. 223–320. DOI: 10.1007/978-3-030-70304-2{\textunderscore}4. URL: https://link.springer.com/chapter/10.1007/978-3-030-70304-2_4.
- [0] Kumar, L. J., Pandey, P. M., and Wimpenny, D. I., eds. *3D Printing and Additive Manufacturing Technologies*. Springer eBook Collection. Singapore: Springer Singapore, 2019. ISBN: 9789811303050. DOI: 10.1007/978-981-13-0305-0.
- [0] Bui, H., Pierson, H. A., Nurre, S. G., and Sullivan, K. M. “Tool Path Planning Optimization for Multi-Tool Additive Manufacturing”. In: *2351-9789* 39 (2019), pp. 457–464. ISSN: 2351-9789. DOI: 10.1016/j.promfg.2020.01.389. URL: <https://www.sciencedirect.com/science/article/pii/s2351978920304601>.
- [0] Ramazanov, S., Babenko, V., Honcharenko, O., Moisieieva, N., and Dykan, V. “Integrated Intelligent Information and Analytical System of Management of a Life Cycle of Products of Transport Companies”. In: *Journal of Information Technology Management* 12.3 (2020), pp. 26–33. ISSN: 2008-5893. DOI: 10.22059/jitm.2020.76291. URL: https://jitm.ut.ac.ir/article_76291_0.html.

- [0] Kadam, O. B., Pirayesh, A., and Fatahi Valilai, O. “Technological Insights of Interoperable Models for Integration of CAD/PLM/PDM and ERP Modules in Engineering Change Management”. In: Springer, Cham, 2023, pp. 556–564. doi: 10.1007/978-3-031-17629-6{\textunderscore}58. url: https://link.springer.com/chapter/10.1007/978-3-031-17629-6_58.
- [0] Kappmeyer, G. and Novovic, D. “Production technology research – Building blocks for competitiveness and solution for future challenges in aerospace component manufacturing”. In: 2212-8271 101 (2021), pp. 62–68. issn: 2212-8271. doi: 10.1016/j.procir.2020.09.189. url: <https://www.sciencedirect.com/science/article/pii/s2212827121006570>.
- [0] NX Manufacturing. *Hybrid Additive Manufacturing with NX CAM Overview - NX Manufacturing*: Last access: 30.10.2023. 2015. url: <https://blogs.sw.siemens.com/nx-manufacturing/hybrid-additive-manufacturing-with-nx-cam-overview/>.
- [0] Brecher, C. and Lohse, W. “Evaluation of toolpath quality: User-assisted CAM for complex milling processes”. In: *CIRP Journal of Manufacturing Science and Technology* 6.4 (2013), pp. 233–245. issn: 1755-5817. doi: 10.1016/j.cirpj.2013.07.002. url: <https://www.sciencedirect.com/science/article/pii/s1755581713000539>.
- [0] Xu, T., Chen, Z., Li, J., and Yan, X. “Automatic tool path generation from structuralized machining process integrated with CAD/CAPP/CAM system”. In: *The International Journal of Advanced Manufacturing Technology* 80.5-8 (2015), pp. 1097–1111. issn: 1433-3015. doi: 10.1007/s00170-015-7067-5. url: <https://link.springer.com/article/10.1007/s00170-015-7067-5>.
- [0] Tunc, L. T. and Stoddart, D. “Tool path pattern and feed direction selection in robotic milling for increased chatter-free material removal rate”. In: *The International Journal of Advanced Manufacturing Technology* 89.9-12 (2017), pp. 2907–2918. issn: 1433-3015. doi: 10.1007/s00170-016-9896-2. url: <https://link.springer.com/article/10.1007/s00170-016-9896-2>.
- [0] Liu, C., Li, Y., and Hao, X. “An adaptive machining approach based on in-process inspection of interim machining states for large-scaled and thin-walled complex parts”. In: *The International Journal of Advanced Manufacturing Technology* 90.9-12 (2017), pp. 3119–3128. issn: 1433-3015. doi: 10.1007/s00170-016-9647-4.
- [0] Takeuchi, Y. “Current State of the Art of Multi-Axis Control Machine Tools and CAM System”. In: *Journal of Robotics and Mechatronics* 26.5 (2014), pp. 529–539. issn: 1883-8049. doi: 10.20965/jrm.2014.p0529. url: https://www.jstage.jst.go.jp/article/jrobomech/26/5/26_529/_article/-char/ja/.
- [0] Zhao, H., Zhang, H., Xin, S., Deng, Y., Tu, C., Wang, W., Cohen-Or, D., and Chen, B. “DSCarver”. In: *ACM Transactions on Graphics* 37.4 (2018), pp. 1–14. issn: 0730-0301. doi: 10.1145/3197517.3201338.

- [0] Sivanandam, S. N. and Deepa, S. N. "Genetic Algorithm Optimization Problems". In: *Introduction to genetic algorithms*. Ed. by Sivanandam, S. N. and Deepa, S. N. Berlin u.a.: Springer, 2007, pp. 165–209. ISBN: 978-3-540-73189-4. DOI: 10.1007/978-3-540-73190-0{\textunderscore}7.
- [0] Ruder, S. *An overview of gradient descent optimization algorithms*. 2017.
- [0] Bäck, T. and Schwefel, H.-P. "An Overview of Evolutionary Algorithms for Parameter Optimization". In: *Evolutionary Computation* 1.1 (1993), pp. 1–23. ISSN: 1063-6560. DOI: 10.1162/evco.1993.1.1.1.
- [0] Lambora, A., Gupta, K., and Chopra, K. "Genetic Algorithm- A Literature Review". In: *2019 International Conference on Machine Learning, Big Data, Cloud and Parallel Computing (COMITCon)*. IEEE, 2019. DOI: 10.1109/comitcon.2019.8862255.
- [0] Katoch, S., Chauhan, S. S., and Kumar, V. "A review on genetic algorithm: past, present, and future". In: *Multimedia Tools and Applications* 80.5 (2021), pp. 8091–8126. ISSN: 1573-7721. DOI: 10.1007/s11042-020-10139-6. URL: <https://link.springer.com/article/10.1007/s11042-020-10139-6>.
- [0] Yang, X.-S. "Metaheuristic Optimization: Algorithm Analysis and Open Problems". In: Springer, Berlin, Heidelberg, 2011, pp. 21–32. DOI: 10.1007/978-3-642-20662-7{\textunderscore}2. URL: https://link.springer.com/chapter/10.1007/978-3-642-20662-7_2.
- [0] Huo, L. and Baron, L. "The joint-limits and singularity avoidance in robotic welding". In: *Industrial Robot: An International Journal* 35.5 (2008), pp. 456–464. DOI: 10.1108/01439910810893626. URL: <https://www.emerald.com/insight/content/doi/10.1108/01439910810893626/full/pdf>.
- [0] Cvitanic, T., Nguyen, V., and Melkote, S. N. "Pose optimization in robotic machining using static and dynamic stiffness models". In: *Robotics and Computer-Integrated Manufacturing* 66 (2020), p. 101992. ISSN: 0736-5845. DOI: 10.1016/j.rcim.2020.101992. URL: <https://www.sciencedirect.com/science/article/pii/s0736584520302039>.
- [0] Paryanto, Brossog, M., Bornschlegl, M., and Franke, J. "Reducing the energy consumption of industrial robots in manufacturing systems". In: *The International Journal of Advanced Manufacturing Technology* 78.5-8 (2015), pp. 1315–1328. ISSN: 1433-3015. DOI: 10.1007/s00170-014-6737-z. URL: <https://link.springer.com/article/10.1007/s00170-014-6737-z>.
- [0] Breaz, R. E., Bologa, O., and Racz, S. G. "Selecting industrial robots for milling applications using AHP". In: *1877-0509* 122 (2017), pp. 346–353. ISSN: 1877-0509. DOI: 10.1016/j.procs.2017.11.379. URL: <https://www.sciencedirect.com/science/article/pii/s1877050917326224>.
- [0] Hirzinger, G., Bals, J., Otter, M., and Stelter, J. *The DLR-KUKA Success Story*. Vol. 12. 2005. DOI: 10.1109/MRA.2005.1511865.

- [0] Pham, A.-D. and Ahn, H.-J. "High Precision Reducers for Industrial Robots Driving 4th Industrial Revolution: State of Arts, Analysis, Design, Performance Evaluation and Perspective". In: *International Journal of Precision Engineering and Manufacturing-Green Technology* 5.4 (2018), pp. 519–533. ISSN: 2198-0810. DOI: 10.1007/s40684-018-0058-x. URL: <https://link.springer.com/article/10.1007/s40684-018-0058-x>.
- [0] Halbauer, M., Lehmann, C., Stadter, J. P., Berger, U., and Leali, F. "Milling strategies optimized for industrial robots to machine hard materials". In: *2013 IEEE 18th Conference on Emerging Technologies & Factory Automation (ETFA)*. IEEE, 2013. DOI: 10.1109/etfa.2013.6648124.
- [0] Mecademic Industrial Robotics. *What are Singularities in a Six-Axis Robot Arm? | Mecademic Robotics*: Last access: 02.11.2023. URL: https://www.mecademic.com/academic_articles/singularities-6-axis-robot-arm/.
- [0] Wei, Y., Jian, S., He, S., and Wang, Z. "General approach for inverse kinematics of nR robots". In: *Mechanism and Machine Theory* 75 (2014), pp. 97–106. ISSN: 0094-114X. DOI: 10.1016/j.mechmachtheory.2014.01.008.
- [0] Stevenson, R., Shirinzadeh, B., and Alici, G. "Singularity avoidance and aspect maintenance in redundant manipulators". In: (2002), pp. 857–862. DOI: 10.1109/ICARCV.2002.1238536. URL: <https://ieeexplore.ieee.org/abstract/document/1238536>.
- [0] Bedrossian, N. S. "Classification of singular configurations for redundant manipulators". In: *Proceedings, IEEE International Conference on Robotics and Automation*. New York: IEEE, 2002, pp. 818–823. ISBN: 0-8186-9061-5. DOI: 10.1109/ROBOT.1990.126089.
- [0] Dai, C., Lefebvre, S., Yu, K.-M., Geraedts, J. M. P., and Wang, C. C. L. "Planning Jerk-Optimized Trajectory With Discrete Time Constraints for Redundant Robots". In: *IEEE Transactions on Automation Science and Engineering* 17.4 (2020), pp. 1711–1724. ISSN: 1545-5955. DOI: 10.1109/TASE.2020.2974771.
- [0] Jiang, L., Lu, S., Gu, Y., and Zhao, J. "Time-Jerk Optimal Trajectory Planning for a 7-DOF Redundant Robot Using the Sequential Quadratic Programming Method". In: 2017 (2017), pp. 343–353. DOI: 10.1007/978-3-319-65298-6{\textunderscore}32.
- [0] Wang, L., Liu, Y., Yu, Y., Zhang, J., and Shu, B. "Optimization of redundant degree of freedom in robotic milling considering chatter stability". In: *The International Journal of Advanced Manufacturing Technology* 121.11-12 (2022), pp. 8379–8394. ISSN: 1433-3015. DOI: 10.1007/s00170-022-09889-4.

Disclaimer

I hereby declare that this thesis is entirely the result of my own work except where otherwise indicated. I have only used the resources given in the list of references.

Garching, March 15, 2024

(Signature)